# REPORT DOCUMENTATION PAGE

Form Approved OMB No. 0704-0188

Public reporting burden for this collection of information is estimated to average 1 hour per response, including the time for reviewing instructions, searching existing data sources, gathering and maintaining the data needed, and completing and reviewing the collection of information. Send comments regarding this burden estimate or any other aspect of this collection of information, including suggestions for reducing this burden to Washington Headquarters Services, Directorate for Information Operations and Reports, 1215 Jefferson Davis Highway, Suite 1204, Arlington, VA 22202-4302, and to the Office of Management and Budget, Paperwork Reduction Project (0704-0188), Washington, DC 20503.

| 1. AGENCY USE ONLY (Leave blank) | 2. REPORT DATE | 3. REPORT TYPE AND DATES COVERED |
|---|---|---|
| | 1 March 2002 | Final Technical Report |

4. TITLE AND SUBTITLE

Pressure amplification due to clothing

5. FUNDING NUMBERS

N68171-01-M-5821

6. AUTHOR(S)

S. Bugarin and B.W. Skews

7. PERFORMING ORGANIZATION NAME(S) AND ADDRESS(ES)

School of Mechanical, Industrial, and Aeronautical Engineering, University of the Witwatersrand, PO WITS, 2050, South Africa

9. SPONSORING/MONITORING AGENCY NAME(S) AND ADDRESS(ES

USARDSG-UK, Fiscal Office, Edison House, 223 Old Marylebone Road, London NW1 5th, UK

10. SPONSORING/MONITORING AGENCY REPORT NUMBER

R&D 9096-MS-01

11. SUPPLEMENTARY NOTES

Final Technical Report, Contract No. 68171-01-M-5821, 104 pages.

12a. DISTRIBUTION/AVAILABILITY STATEMENT

Approved for Public Release.

12b. DISTRIBUTION CODE

A

ABSTRACT (Maximum 200 words)

Initial tests of shock wave impact on a surface covered with a layer of textile and positioned a short distance in front of it have shown that the pressure on the surface could be significantly higher than what would be experienced with no covering. The amplification of pressure is a function of textile type. It is suggested that the two mechanisms responsible for this effect are as follows: Firstly, on shock impact with the textile layer, part of the wave is reflected and part is transmitted. The transmitted wave then reflects off the underlying surface and part of this reflected wave is re-reflected back from the textile onto the surface raising the pressure further. A number of such reflections between the textile and the surface can raise the pressure further. Secondly, the textile layer is initially accelerated towards the wall, acting as a piston and pressurizing the gas in the gap through a compression wave.

A comprehensive study of these effects is reported on, using a wide variety of textiles, both for single and multiple layers, and for head-on and inclined shock impact. Amplifications of up to 400 per cent have been recorded, and amplification variations with permeability, specific mass, and number of layers determined. Some tests with a 10 mm backing layer of gelatin have also been conducted in order to obtain information on pressure propagation into this simulated body tissue. Loads due to physical impact of the textile with the surface are not examined.

14. SUBJECT TERMS

US Army Research, South Africa, Blast wave loading, Protective clothing, Pressure amplification

15. NUMBER OF PAGES

16. PRICE CODE

| 17. SECURITY CLASSIFICATION OF REPORT | 18. SECURITY CLASSIFICATION OF THIS PAGE | 19, SECURITY CLASSIFICATION OF ABSTRACT | 20. LIMITATION OF ABSTRACT |
|---|---|---|---|
| Unclassified | Unclassified | Unclassified | Unlimited |



20021202 023

AD

# PRESSURE AMPLIFICATION DUE TO CLOTHING

Final Technical Report
by

S. Bugarin and B.W. Skews
July 2002

United States Army

EUROPEAN RESEARCH OFFICE OF THE U.S. ARMY

London, England

CONTRACT NUMBER: N68171-01-M-5821
R&D 9096-MS-01

School of Mechanical, Aeronautical and Industrial Engineering,
University of The Witwatersrand,
Johannesburg, South Africa.

Approved for Public release; distribution unlimited

AQ F03-01-0150

# Contents


1. Objectives ..... 1
2. Introduction ..... 2
   2.1. Importance of the study ..... 2
   2.2. Primary injuries caused by blast waves ..... 2
   2.3. Clothing effects on shock wave amplification ..... 4
   2.4. Applicable Gas Dynamics ..... 5
      2.4.1. The Geometry of Shock Fronts ..... 5
      2.4.2. Reflection geometry of the shock wave ..... 6
      2.4.3. Refraction geometry of the shock wave ..... 7
      2.4.4. Analysis ..... 8
      2.4.5. Definition of pressure amplification ..... 9
3. Experimental equipment and procedures ..... 10
   3.1. The shock tube ..... 10
      3.1.1. The driver section ..... 11
      3.1.2. The expansion chamber ..... 11
      3.1.3. The test section ..... 13
   3.2. Data Acquisition system and instrumentation ..... 13
      3.2.1. Data acquisition system ..... 13
      3.2.2. Pressure and temperature measurements ..... 14
   3.3. Operation of the shock tube ..... 14
      3.3.1. Testing Procedure ..... 15
   3.4. Tests with perforated plates ..... 15
      3.4.1. Test specimens ..... 15
      3.4.2. Attachment of the test specimens ..... 16
   3.5. Tests with single and multiple layers of textiles ..... 17
      3.5.1. Test specimens ..... 17
   3.6. Tests with gelatin and multiple layers of textile ..... 18
      3.6.1. Textile Properties ..... 18
      3.6.2. Gelatin and textile assembly ..... 19
      3.6.3. Attachment of textile samples ..... 19
   3.7. Tests with textiles placed at an angle ..... 20
      3.7.1. Inclined Plate Assembly ..... 20
      3.7.2. Attachment of Textile Samples for the Inclined Tests ..... 21
      3.7.3. Optical Techniques ..... 22
4. Experimental results and observations ..... 24
   4.1. Perforated plates tests ..... 24
      4.1.1. Test results ..... 26
   4.2. Single and multiple layer textiles test results ..... 30
   4.3. Gelatine Behind Textile Tests ..... 33
   4.4. Inclined Textile Tests ..... 40
5. Discussion ..... 52
   5.1. Perforated plates test ..... 52
   5.2. Multiple layers of textiles ..... 52
   5.3. Gelatin behind textile tests ..... 53
   5.4. Inclined Textile Tests ..... 55
      5.4.1. Investigation of Pressure Amplification Results ..... 58
      5.4.2. Discussion of Pressure Traces ..... 60
   5.5. Discussion of Schlieren Photographs ..... 61
6. Conclusions and Recommendations ..... 70
7. References ..... 71

# List of Figures

Figure 2.1. The reflection of shock waves from a solid interface: (a) Regular reflection by a weak shock from a steep wall; (b) Mach reflection by a strong shock from a gradually sloping wall. ..... 6
Figure 2.2. The refraction of shock waves from an interface: (a) Regular refraction; (b) Irregular refraction. ..... 7
Figure 2.3. Schematic illustration of the Galilean transformation ..... 8
Figure 2.4. Nomenclature for: (a) Regular refraction, (b) Mach refraction. ..... 8
Figure 3.1. Schematic diagram of the shock tube ..... 10
Figure 3.2. Compression chamber, intermediate chamber and part of the expansion chamber ..... 12
Figure 3.3. Expansion chamber and the test section ..... 12
Figure 3.4. Available pressure transducer ports on the back wall, roof and the floor of the test section. ..... 13
Figure 3.5. Data acquisition system ..... 14
Figure 3.6. Positioning of the sample inside the test section ..... 16
Figure 3.7. Attachment of the textile sample to the backing plate ..... 18
Figure 3.8. Gelatin textile assembly ..... 20
Figure 3.9. Inclined plate assembly ..... 21
Figure 3.10. Attachment of the textile sample to the inclined plate assembly ..... 22
Figure 3.11. Schematic of the Schlieren photography set up ..... 23
Figure 4.1. % pressure amplification vs mass of the samples from group 1; Mach no 1.419 and porosity 5.5%. ..... 26
Figure 4.2. % pressure amplification vs mass of the samples from group 2; Mach no 1.415 and porosity 6.7%. ..... 27
Figure 4.3. % Pressure amplification vs mass of the samples from group 3; Mach no 1.415 and porosity 20.5%. ..... 28
Figure 4.4. % Pressure amplification vs mass of the samples from group 4; Mach no 1.41 and porosity 33%. ..... 29
Figure 4.5. Amplification of 1 and 5 layer of textile samples, average Mach no=1.42 ..... 31
Figure 4.6. Amplification of 1 and 5 layers of textile samples, average Mach no=1.34 ..... 32
Figure 4.7. Only gelatin sample 1 M=1.416 ..... 33
Figure 4.8. Only gelatin sample 2 M=1.416 ..... 33
Figure 4.9. Only gelatin sample 3 M=1.421 ..... 34
Figure 4.10. Normal shock (no gelatine) M=1.413 ..... 34
Figure 4.11. Gelatin with 1 layer of satin M=1.421 ..... 35
Figure 4.12. Gelatin with 3 layers of satin M=1.417 ..... 35
Figure 4.13. Gelatin with 5 layers of satin M=1.426 ..... 36
Figure 4.14. Gelatin with 1 layer of polycotton M=1.419 ..... 36
Figure 4.15. Gelatin with 3 layers of polycotton M=1.418 ..... 37
Figure 4.16. Gelatin with 5 layers of polycotton M=1.421 ..... 37
Figure 4.17. Gelatin with 1 layer of muslin M=1.425 ..... 38
Figure 4.18. Gelatin with 3 layers of muslin M=1.419 ..... 38
Figure 4.19. Gelatin with 5 layers of muslin M=1.425 ..... 39
Figure 4.20. Pressure traces with no textile ..... 41
Figure 4.21. Pressure traces with satin ..... 41
Figure 4.22. Pressure traces with polycotton ..... 42
Figure 4.23. Pressure traces with muslin ..... 42
Figure 4.24. Pressure traces with no textile ..... 43
Figure 4.25. Pressure traces with satin ..... 43
Figure 4.26. Pressure traces with polycotton ..... 44
Figure 4.27. Pressure traces with muslin ..... 44
Figure 4.28. Pressure traces with no textile ..... 45
Figure 4.29. Pressure traces with satin ..... 45

Figure 4.30. Pressure traces with polycotton ..... 46
Figure 4.31. Pressure traces with muslin ..... 46
Figure 4.32. Satin, M =1.421, $\theta_w$=60°, T=1650μs ..... 47
Figure 4.33 Polycotton, M =1.415, $\theta_w$=60°, T=1675μs ..... 48
Figure 4.34. Muslin, M =1.424, $\theta_w$=60°, T=1650μs ..... 48
Figure 4.35. Satin, M =1.42, $\theta_w$=35°, T=1585μs ..... 49
Figure 4.36. Polycotton M =1.409, $\theta_w$=35°, T=1670μs ..... 49
Figure 4.37. Muslin M =1.418, $\theta_w$=35°, T=1680μs ..... 50
Figure 4.38. Satin, M =1.438, $\theta_w$=60°, T=1555μs ..... 50
Figure 5.1. Gelatin with satin of 1, 3 and 5 layers ..... 53
Figure 5.2. Gelatin with polycotton of 1, 3 and 5 layers ..... 53
Figure 5.3. Gelatin with muslin of 1, 3 and 5 layers ..... 54
Figure 5.4. Pressure amplification vs number of layers for all 3 textiles ..... 54
Figure 5.5. Pressure traces at $\theta_w$ = 45° ..... 55
Figure 5.6. Pressure traces at $\theta_w$ = 60° ..... 55
Figure 5.7. Pressure traces at $\theta_w$ = 70° ..... 56
Figure 5.8. Pressure traces with satin ..... 56
Figure 5.9. Pressure traces with polycotton ..... 57
Figure 5.10. Pressure traces with muslin ..... 57
Figure 5.11. Pressure amplification versus wall angle ..... 58
Figure 5.12. Pressure amplification versus Permeability ..... 59
Figure 5.13. Pressure amplification versus Mass/Area ..... 59
Figure 5.14. Pressure trace for polycotton at $\theta_w$ = 60° ..... 60
Figure 5.15. Characteristics of the flow through a slit wedge ..... 62
Figure 5.16. Interaction of the shock wave with the textile sample at 60° angle ..... 63
Figure 5.17. Regular reflection over a surface with inflow, in a frame of reference fixed in the point of reflection ..... 64
Figure 5.18. Total deflection of the flow against the permeability of the textile for the incidence angle of 60° ..... 65
Figure 5.19. Flow geometry with velocity triangles connecting the frames of reference ..... 65
Figure 5.20. $V^*_2$ against permeability of textiles for incident angles of 60° and 35° ..... 66
Figure 5.21. ε (Direction of $V^*_2$) against permeability of textiles for incident angles of 60° and 35° ..... 67
Figure 5.22. Predicted pressures of transmitted reflected shock for the textile at 60° angle against the permeability of the textile ..... 68

# List of Tables

Table 3.1. Thickness and mass of 1 layer of sample only ..... 17
Table 3.2. Thickness and mass of samples with 5 layers ..... 17
Table 3.3. Textile Properties ..... 19
Table 4.1 Properties of manufactured samples ..... 24
Table 4.2. Amplification and peak pressure of one layer of textile for average Mach No=1.42 ..... 30
Table 4.3. Amplification and peak pressure of five layers of textile for average Mach No=1.42 ..... 30
Table 4.4. Amplification and peak pressure of one layer of textile for average Mach No=1.34 ..... 31
Table 4.5. Amplification and peak pressure of five layers of textile for average Mach No=1.34 ..... 32
Table 4.6. Test Data Corresponding to Pressure Traces ..... 40
Table 4.7. Test Data Corresponding to the Schlieren Images ..... 41
Table 5.1. Total deflection angle against permeability of textile at 60° incidence angle ..... 64
Table 5.2. $V^*_2$ and ε angle for different textile material and incident angle of 60° ..... 66

Table 5.3. $V^*_2$ and ε angle for different textile material and incident angle of 35° ..... 66
Table 5.4. Pressures of the transmitted reflected shock predicted from the schlieren photographs of textile at 60° angle ..... 67

# List of Appendices

APPENDIX A ..... 72

Figure A 1 Satin, M =1.423, $\theta_w$=60°, T=1550μs ..... 73
Figure A 2 Satin, M =1.415, $\theta_w$=60°, T=1550μs ..... 73
Figure A 3 Satin, M =1.413, $\theta_w$=60°, T=1545μs ..... 74
Figure A 4 Satin, M =1.417, $\theta_w$=60°, T=1545μs ..... 74
Figure A 5 Satin, M =1.438, $\theta_w$=60°, T=1555μs ..... 75
Figure A 6 Satin, M =1.411, $\theta_w$=60°, T=1539μs ..... 76
Figure A 7 Satin, M =1.41, $\theta_w$=60°, T=1559μs ..... 76
Figure A 8 Satin, M =1.409, $\theta_w$=60°, T=1512μs ..... 77
Figure A 9 Satin, M =1.415, $\theta_w$=60°, T=1539μs ..... 77
Figure A 10 Satin, M =1.412, $\theta_w$=60°, T=1559μs ..... 78
Figure A 11 Satin, M =1.42, $\theta_w$=60°, T=1512μs ..... 78
Figure A 12 Polycotton, No backing plate, M =1.422, $\theta_w$=60°, T=1590μs ..... 79
Figure A 13 Polycotton, No backing plate, M =1.424, $\theta_w$=60°, T=1600μs ..... 79
Figure A 14 Polycotton, No backing plate, M =1.422, $\theta_w$=60°, T=1620μs ..... 80
Figure A 15 Polycotton, No backing plate, M =1.413, $\theta_w$=60°, T=1650μs ..... 80
Figure A 16 Polycotton, No backing plate, M =1.412, $\theta_w$=60°, T=1650μs ..... 81
Figure A 17 Polycotton, No backing plate, M =1.415, $\theta_w$=60°, T=1675μs ..... 81
Figure A 18 Satin, No backing plate, M =1.419, $\theta_w$=60°, T=1590μs ..... 82
Figure A 19 Satin, No backing plate, M =1.422, $\theta_w$=60°, T=1600μs ..... 82
Figure A 20 Satin, No backing plate, M =1.416, $\theta_w$=60°, T=1620μs ..... 83
Figure A 21 Satin, No backing plate, M =1.416, $\theta_w$=60°, T=1630μs ..... 83
Figure A 22 Satin, No backing plate, M =1.421, $\theta_w$=60°, T=1650μs ..... 84
Figure A 23 Satin, No backing plate, M =1.424, $\theta_w$=60°, T=1675μs ..... 84
Figure A 24 Muslin, No backing plate, M =1.421, $\theta_w$=60°, T=1590μs ..... 85
Figure A 25 Muslin, No backing plate, M =1.42, $\theta_w$=60°, T=1600μs ..... 85
Figure A 26 Muslin, No backing plate, M =1.424, $\theta_w$=60°, T=1620μs ..... 86
Figure A 27 Muslin, No backing plate, M =1.424, $\theta_w$=60°, T=1650μs ..... 86
Figure A 28 Muslin, No backing plate, M =1.412, $\theta_w$=60°, T=1650μs ..... 87
Figure A 29 Muslin, No backing plate, M =1.413, $\theta_w$=60°, T=1675μs ..... 87
Figure A 30 Satin, No backing plate, M =1.42, $\theta_w$=35°, T=1585μs ..... 88
Figure A 31 Satin, No backing plate, M =1.42, $\theta_w$=35°, T=1585μs ..... 88
Figure A 32 Satin, No backing plate, M =1.413, $\theta_w$=35°, T=1600μs ..... 89
Figure A 33 Satin, No backing plate, M =1.413, $\theta_w$=35°, T=1620μs ..... 89
Figure A 34 Satin, No backing plate, M =1.413, $\theta_w$=35°, T=1620μs ..... 90
Figure A 35 Satin, No backing plate, M =1.413, $\theta_w$=35°, T=1650μs ..... 90
Figure A 36 Satin, No backing plate, M =1.416, $\theta_w$=35°, T=1650μs ..... 91
Figure A 37 Muslin, No backing plate, M =1.414, $\theta_w$=35°, T=1585μs ..... 92
Figure A 38 Muslin, No backing plate, M =1.415, $\theta_w$=35°, T=1610μs ..... 92
Figure A 39 Muslin, No backing plate, M =1.417, $\theta_w$=35°, T=1630μs ..... 93

Figure A 40 Muslin, No backing plate, M =1.413, θw=35°, T=1660μs ..... 93
Figure A 41 Muslin, No backing plate, M =1.418, $\theta_w$=35°, T=1670μs ..... 94
Figure A 42 Muslin, No backing plate, M =1.418, $\theta_w$=35°, T=1680μs ..... 94
Figure A 43 Polycotton, No backing plate, M =1.417, $\theta_w$=35°, T=1585μs ..... 95
Figure A 44 Polycotton, No backing plate, M =1.414, $\theta_w$=35°, T=1600μs ..... 95
Figure A 45 Polycotton, No backing plate, M =1.414, $\theta_w$=35°, T=1620μs ..... 96
Figure A 46 Polycotton, No backing plate, M =1.418, $\theta_w$=35°, T=1650μs ..... 96
Figure A 47 Polycotton, No backing plate, M =1.409, $\theta_w$=35°, T=1670μs ..... 97
Figure A 48 Polycotton, No backing plate, M =1.421, $\theta_w$=35°, T=1680μs ..... 97

APPENDIX B ..... 98

# 1. Objectives

1. Confirm that a shock wave passing through a textile will result in increased pressure on a backing surface.

2. Determine the effect that different textile mass per unit area and porosity has on the pressure amplification.

3. Determine the effect that multiple layers of different textiles have on the pressure amplification.

4. Determine as closely as possible the effect of human tissue on pressure amplification by using a layer of gelatin between the textile and the pressure transducer.

5. Research two-dimensional effects of interaction of shock wave with the textile placed on an inclined wedge.

# 2. Introduction

## 2.1. Importance of the study

Injuries that humans or even animals can experience as a result of exposure to explosions may be classified as primary, secondary or tertiary injuries (Maynard et al. 1989). Primary injuries are caused by the impact of shock or a blast wave that is generated by an explosion. Secondary injuries arise from the impact of explosion fragments with the person. Tertiary injuries include whole body displacement and amputation of body parts by a very strong explosion.

When an explosive device detonates, an intense shock wave is generated in the air surrounding the charge. Primary injuries are considered to result from the impact of this shock wave with the human body. These injuries affect mainly the gas – containing organs of the body i.e. the auditory canals, lungs and abdominal organs but mostly with no external indications of trauma. In the organ such as a lung, the injury is usually revealed by oedema and haemorrhage (Yen et al. 1998). The result is serious and life threatening internal injuries. Occurrence of primary injuries due to blast waves is not a new phenomenon and has been reported in battlefields as far back as the First World War (Zuckerman 1940). First blast effect was described at the battle of Chegre and first research was initiated by F. Rasko (1915). Hoker (1924) was the first to set and prove the hypothesis of the blast injury.

Cases of blast injury are usually under-reported due to complicated multiple-injury scenarios that can occur, thus although the patients suffer from primary injuries, the secondary or tertiary injuries lead to death (Philips et al. 1988).

Other than on the battlefield blast (primary) injuries also occur in crowded urban environments where people are victims of terrorist bombings (Leibovici et al. 1996). An investigation done by him into survivors of an explosion in a bus revealed that 83% of the survivors suffered from lung blast injury, 20% of whom died as a result. Various studies have been completed to determine the mechanism that causes the primary injuries as a result of a blast. The most recent research has proved that when some kind of clothing is worn the severity of injuries can be increased.

## 2.2. Primary injuries caused by blast waves

Two principal effects of detonation are the generation of a supersonic shock wave that propagates through the air and the subsequent outward motion of the gaseous products formed during explosion. The speed and the strength of the shock wave gradually decrease as the wave moves away from the centre of the explosion, thus the effect of blast is most prominent on the personnel in the close vicinity of the explosion (W.E. Baker "Explosions in Air"(1973*)*).

Primary injuries involve most gas-containing organs i.e. lungs, bowel, stomach, ears etc. Blast injuries can frequently be seen on the eardrums. Pressure of only 1.5 kg/cm$^2$ is enough to rupture the eardrum, while other organs would need 4 to 5 times greater pressure to be affected by the blast. The most notable organ affected by blast injury and that has attracted most attention is the lung. Blast-lung is the frequently seen primary injury to the lung. This is the contusion or bruising of the lungs in which the blood contaminates air sacs (alveoli) within the lung. The contusions are most frequently unilateral, being on the side facing the blast, and rarely bilateral. The haemorrhaging contamination that results is followed by haemoptysis

(coughing up blood) and difficulty in breathing as alveoli and airways fill up with blood. The quantity of oxygen carried by the blood reduces and the disease may progress to a life threatening condition known as Acute Respiratory Distress Syndrome (ARDS). Blast lung has been shown to be the result of the sudden impact or pressure applied by the ribs on the lungs. Usually during the compression of the thorax wall (rib cage), just after the impact with the blast wave, multiple fractures of the ribs occur. In some cases the fragments of the broken rib are dislocated towards the lung and lead to the damage of the pleura. The strength and the intensity of the blast or the shock wave greatly effects the lung injury. The intensity of the blast can be described in terms of the overpressure, which is the pressure above atmospheric.

For men, exposed to a single short duration blast, Richard et al. (1968) estimated that lung injury starts occurring at a threshold overpressure of 120 – 185 kPa. Evidence suggests that this threshold overpressure may be lower when multiple exposures to blast wave are considered. Such multiple exposures may arise from muzzle blast that arise when firing artillery. Exact threshold overpressure values for these weaker waves have not yet been quantified.

Reports from Clemendson and Johnsson et al. (1976) suggest that the threshold overpressure for lung injury due to complex blast waves, occurring inside an enclosure, is five times lower than for free – field waves having the same incidence pressure. This is due to complex blast loading that arises due to internal reflection of the waves. Such an enclosure could be a tank, bus or building.

Four suicide bombings resulting from terrorist attacks were investigated by Leibovici et al. (1996). Two of the bombing incidents occurred in the open air and two happened inside public busses. In all four cases the bombs had similar explosive devices and the victim density around the bomb was similar. Observations showed that there was no difference in the incidence of penetrating trauma, burns or traumatic amputations, however the bus accidents resulted in 77.5% of the victims suffering from blast injuries compared to 34.2% victims in the open air explosions. It was postulated that for a brief period of several hundred milliseconds the bus's casing contained the blast, allowing the amplitude of the pressure wave to increase and the overpressure to be sustained.

Huller and Bazini (1970) completed studies into 32 survivors who were exposed to an under water explosion caused by a missile. Injuries were similar to aforementioned air blast injuries (pulmonary lesions and abdominal trauma), however, intra-abdominal injuries were more prominent than the lung injuries. The injuries included heart (myocardial) damage and tears or haemorrhaging of bowel walls.

Studies done by van Bree and Fairlie (1999) show that when a projectile is stopped by protective armour, the impact causes compression waves to be formed behind the armour that propagate into the human tissue. The injury inflicted to the personnel wearing the armour upon projectile impact is termed blunt trauma.

Studies involving animals (Zuckerman 1940) indicated that lung haemorrhages caused by blast lung tended to follow the line of the ribs. Most of the damage inflicted on the animal was localised to the side that faced the explosion. The cause of the organ damage was concluded to be due to the impact of the blast or shock wave with the chest walls and not, as previously thought, due to the lowering of the intrathoracic pressure as a result of the suction wave acting through the respiratory passages.

Cooper and Taylor (1989) showed, by means of photographs, that the body wall has a very slow rebound velocity, which indicates that it is highly damped or viscous. It was concluded that the displacement of the body wall is rate dependent i.e. the faster it is deformed, the stiffer it becomes. The experiments also confirmed that rapid but small displacements caused the worst injury.

## 2.3. CLOTHING EFFECTS ON SHOCK WAVE AMPLIFICATION

Fibrous body armour and cloth ballistic vests (CBVs) are worn by soldiers to protect them from the most common battlefield threat, which is fragmenting munitions from small-arm fire. There is however evidence that the soldiers wearing fibrous body armour are more vulnerable to injury from blast waves than the personnel not wearing the armour. It has been found that permeable protective layers amplify the shock wave pressure on impact and hence increase the risk of lung injury.

Numerous studies have been performed to determine the effect the protective clothing has on primary injuries on both humans and animals and the mechanism of impact with the blast wave.

Philips et al. (1988) conducted an experiment to evaluate the effect of cloth ballistic vests (CBV) on blast injury level in animals. 58 sheep were exposed to nominal blast levels of 115, 230 and 420 kPa peak pressure with half of the sheep wearing CBV's. Intrathoracic pressure was shown to be higher in the case of CBV's. 83% of the sheep wearing the CBV's died while only 27% of the sheep not wearing CBV's died. It was believed that the cause was due to increase in surface area as a result of wearing the protective clothing, which subsequently increased the force applied to the body.

Studies were performed on ten healthy young male volunteers (Young et al. 1985) to evaluate the effects of four clothing ensembles on peak intrathoracic pressure exposed to low-level short duration air blast. Each subject was exposed to air blast while standing face-on in five different clothing ensembles. Clothing ensembles included 1) military fatigues used as a control condition; 2) fatigues with field jacket (2.9 kg Kevlar vest); 3) fatigues with ballistic armour vest; 4) fatigues with ceramic vest (6.4 kg); 5) fatigues with ceramic vest over the ballistic vest. Results showed that, when the vests were worn over the fatigues, greater values of ITP resulted than in the case of the fatigues alone. These results indicate that protective clothing may not offer protection against air blast lung injury.

Von Gierke (1968) estimated that, at least for steady-state noise, maximum resonance of the thorax is between 40 and 60 Hz and therefore, maximum energy transfer will occur in these frequencies. Therefore, when the predominant frequency of the incident shock wave most closely matches the resonance of the thorax, it is probable that the resulting deformation and oscillation of intrathoracic structures would be greatest.

Gibson (1995) conducted tests on multiple layers (4-20) of various materials including Kevlar, polyurethane foam, ballistic nylon and cotton/nylon cloth. He found that the compressible and porous textile materials have tended to amplify the reflected peak pressure of the air shock wave. The degree of amplification was found to be related to the apparent bulk modulus of the materials, with the materials of low bulk density (low solid mass fraction) having the greatest tendency to produce very high shock pressures. He suggests that the speed of sound in the material and the rate at which the material compresses as the compression waves move through it, dictates whether or not the compression waves will coalesce to form a shock wave.

The studies mentioned above all provide evidence that both the lung damage and ITP due to air blast are increased when some form of protective clothing is used. These tests, however, have been approached from a medical perspective and focus on the damage to the internal organs and very little on the physical process responsible for the pressure amplification.

Research done in the year 2000 (Hattingh and Skews 2001) at the University of Witwatersrand on impact of shock waves on different textiles supported previous observations that the pressures are amplified when a textile is placed in front of a surface. The studies, however, mainly focused on the actual mechanism that leads to the pressure amplification. Three different textile materials were tested in a shock tube, namely polycotton, muslin and satin. The tests showed that, for the same shock Mach number the peak pressure

increased as the air permeability of the textile decreased. The maximum pressure amplification increased with increasing Mach number and the initial air gap width, up to a critical width after which the amplification decreased.

It was concluded that the amplification of the pressure was caused by two mechanisms, both being dependent on the textile properties. The first mechanism is the reflection of the transmitted wave in the air gap between the textile and the tube back wall. The second mechanism is the compression waves that are generated by the piston like motion of the textile towards the back wall of the tube. The textile position could not be tracked properly due to lack of a suitable measuring device. The studies concentrated on conventional (civilian) textiles.
The effects of the different material air permeability and masses per unit area on pressure amplification were not fully quantified.

## 2.4. Applicable Gas Dynamics

The following section outlines the gas dynamic principles that will be employed in the analysis of the physical processes. The theory was extracted from John (1969).

The Mach number is used to express the speed of waves generated in a gas relative to the speed of sound ahead of the wave. For a compressible gas, the speed of sound in the gas, c, is calculated as follows:

$$c = \sqrt{\gamma RT}$$

Where: $\gamma$ = ratio of specific heats of the gas used
R = gas constant
T = temperature of the gas

The Mach number, M, is a dimensionless parameter and is defined as the ratio of the fluid velocity, V, to the local sonic velocity:

$$M = \frac{V}{c}$$

If a particle travels slower than the local speed of sound, the gas ahead of the particle is able to adjust smoothly. This is the subsonic case, where $M < 1$. In the supersonic case, where $M > 1$, there will be a discontinuous adjustment of fluid properties (pressure, temperature and density). This adjustment takes place by means of a shock wave.

### 2.4.1. The Geometry of Shock Fronts

Shock wave reflection phenomena have been examined for over a century, with Ernst Mach first reporting the reflection of shock waves as early as 1878, intensive research, though, only began in the 1940's (Ben-Dor 1992). Shock interactions for many situations are thus well documented and understood. There are many large areas, however, that are still to be fully investigated.

Shock waves adjust the fluid properties instantaneously and are thus very thin. This makes the description of how shocks propagate relatively simple, since the propagation can be formulated entirely in terms of the geometry of the fronts. The most important feature of the non-linear propagation of shock waves is that the overtaking of shock fronts by waves from behind can dramatically alter the geometry of the fronts. In particular, compressive waves overtaking obliquely from behind the front may pile up by non-linear steepening to cause a sharp kink on the front. The consequences of the kink are that the incident shock is in effect split into two parts, and the splitting is possible only if a third shock is formed at the kink. This process happens in shock reflection and refraction, which are important when shock waves propagate through non-uniform media such as textiles.

### 2.4.2. Reflection geometry of the shock wave

Shock waves reflect from hard material in one of two different configurations. If non-linearity is relatively weak, as with weak shock waves and when the interface is relatively steep, the reflection is *regular* and the reflected shock joins the incident shock at the surface. For very weak shocks in regular reflection, the angle of incidence is equal to the angle of reflection, as in optics or acoustics. On the other hand, when the shock is strong, or the slope of the wall is gradual, the reflection is *irregular* and is called Mach reflection.

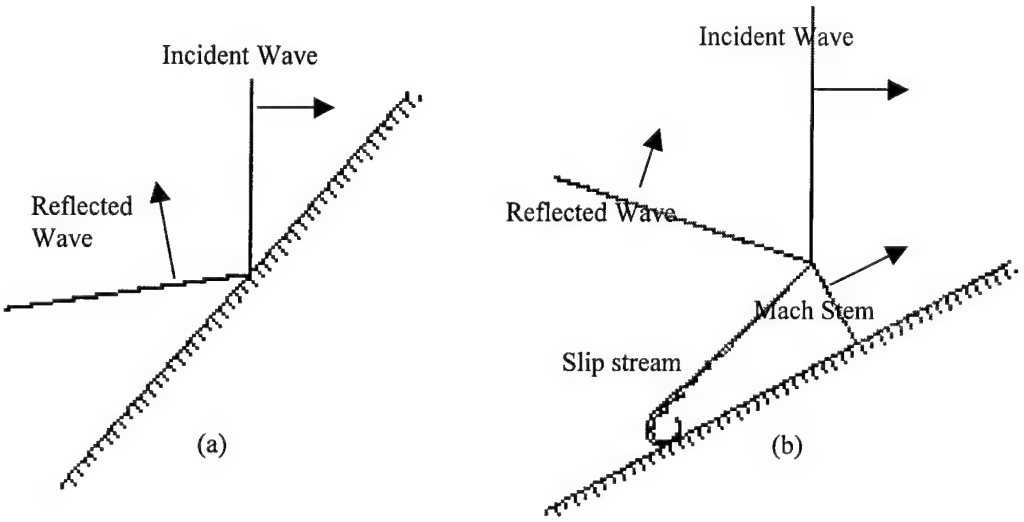


Figure 2.1. The reflection of shock waves from a solid interface: (a) Regular reflection by a weak shock from a steep wall; (b) Mach reflection by a strong shock from a gradually sloping wall.

Because in Mach reflection all three shock waves are of different strength and orientation, a slipstream divides two of the regions, as shown in Figure 2.1 above. The point at which the three shock waves intersect is known as the triple point.

### 2.4.3. Refraction geometry of the shock wave

Bending of waves by irregularities in materials and at interfaces is called refraction. In general, when a wave refracts reflection also occurs, resulting in a configuration as shown in Figure 2.2 below.

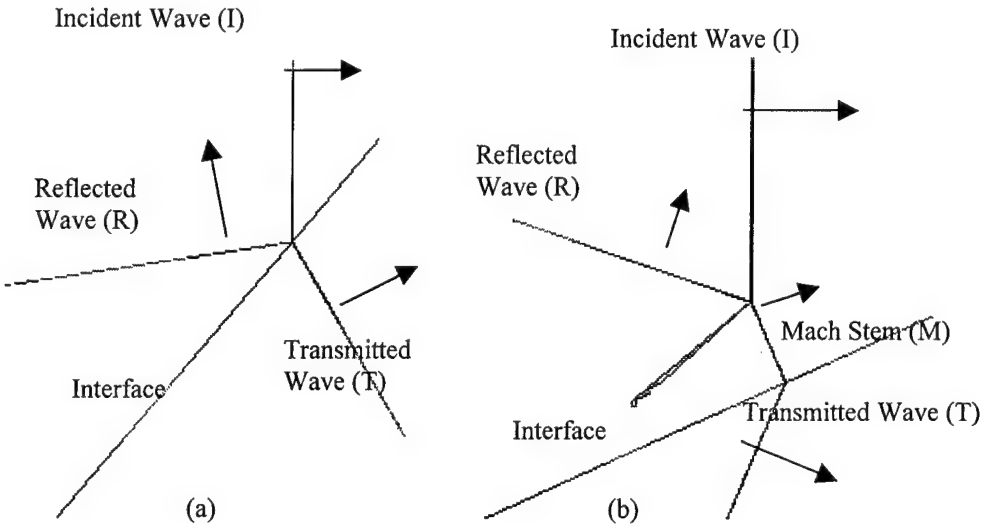


Figure 2.2. The refraction of shock waves from an interface: (a) Regular refraction; (b) Irregular refraction.

Again, both regular and irregular refraction may occur, depending on the shock strength and the interface properties. Irregular refraction is also known as Mach refraction. The direction in which the shock front bends at the material interface depends on the speed of sound in the two materials. When the interaction is slow-fast, the transmitted shock bends upstream of the incident shock. A shock, which refracts into a solid, generates not only compressive stress waves in the solid but also shear stress waves and surface waves by `mode conversion'.

Shock waves having constant velocities with respect to an inertial frame of reference can be investigated using steady flow concepts by attaching a frame of reference to the shock wave. In such a frame of reference, the shock is stationary and the entire flow field is known as pseudo-stationary or pseudo-steady. The transformation, known as a Galilean transformation, is shown schematically in Figure 2.3 (Ben-Dor 1992).

In Figure 2.3 (a), a constant velocity shock wave, having a velocity $V_s$, propagates towards a flow having velocity $V_1$, and inducing behind it a flow velocity $V_j$. Figure 2.3 (b) shows the adjusted velocities, now with the frame of reference attached to the shock wave.

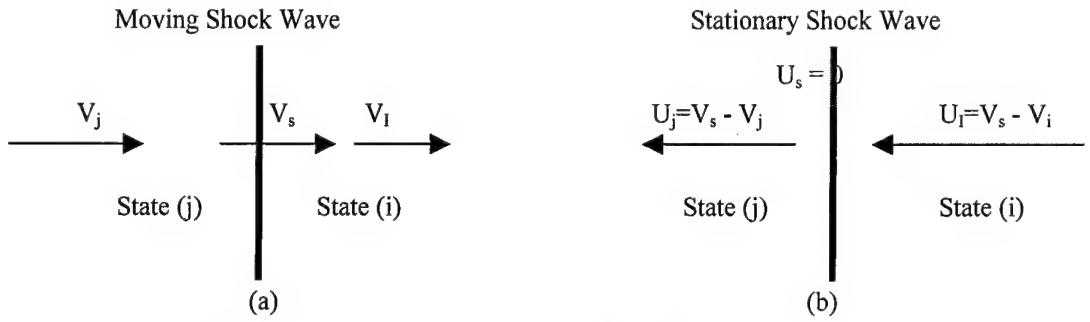


Figure 2.3. Schematic illustration of the Galilean transformation

### 2.4.4. Analysis

**Definition of Shock Interaction Angles**

The following figure illustrates the conventions used in this paper to present the results for both types of shock interactions outlined in section 2.4.2.

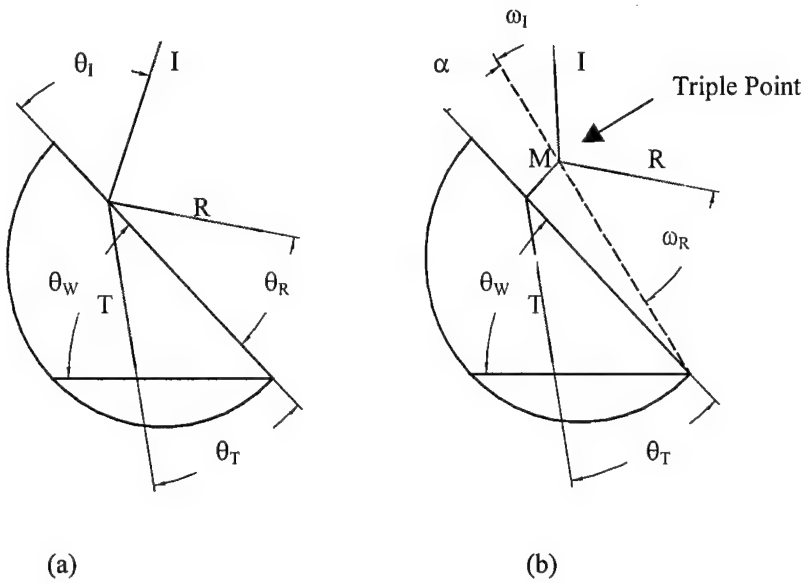


Figure 2.4. Nomenclature for: (a) Regular refraction, (b) Mach refraction.

Where: $\theta_W$ = reflecting wall angle
$\theta_I$ = angle of incidence
$\theta_R$ = angle of reflection
$\theta_T$ = angle of transmission
$\alpha$ = angle between direction of motion of the triple point and the wall

$\omega_I$ = angle between direction of motion of the slipstream and the incident shock
$\omega_R$ = angle between direction of motion of the slipstream and the reflected shock

### 2.4.5. Definition of pressure amplification

The percentage pressure amplification, $P_{amp}$, is defined as the increase in peak pressure, due to the presence of the textile (as compared to the peak pressure with no textile). The amplification is expressed as a percentage and calculated as follows:

$$P_{amp} = \frac{P_{tex} - P_{none}}{P_{none}} \times 100$$

Where:
$P_{tex}$ = average peak pressure when a textile is present
$P_{none}$ = average peak pressure when no textile is present

# 3. Experimental equipment and procedures

This section outlines the experimental equipment used for testing and its operation.

## 3.1. The shock tube

All tests were conducted in a fully automated shock tube in the Mechanical Engineering Laboratories at the University of the Witwatersrand.
The shock tube consists of three chambers; the driver section (the compression chamber and the intermediate chamber) and the expansion chamber with the test section at the end as sketched in the Figure 3.1 below.

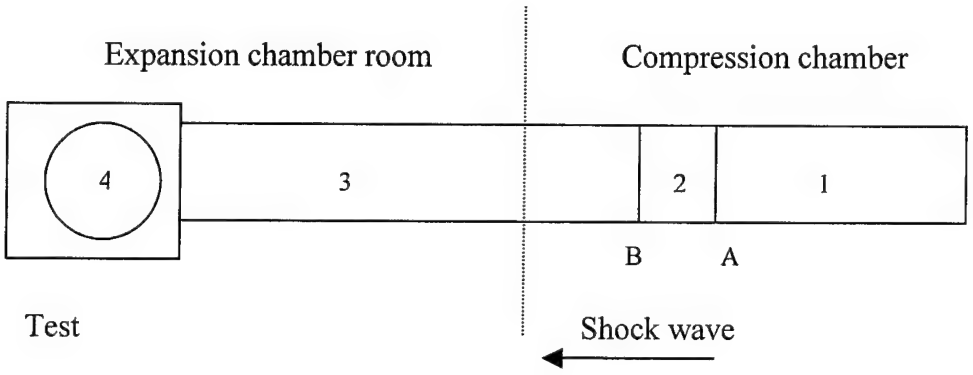


Figure 3.1. Schematic diagram of the shock tube

Referring to the figure 3.1 above:
1 – Compression Chamber
2 – Intermediate Chamber
3 – Expansion Chamber
4 – Test section
A & B – Diaphragm positions

The shock tube is located in two rooms that will be referred to as the compression chamber and the expansion chamber rooms. The compression chamber room holds the compression chamber, intermediate chamber and part of the expansion chamber.
The rest of the expansion chamber and the test section are situated in the expansion chamber room together with the control console.
The shock tube is a 6.3 m long and is calibrated to attain Mach numbers in the range between 1.23 and 1.57 using atmospheric pressure as the expansion chamber pressure. (Higher Mach numbers can be achieved if the expansion chamber is evacuated).

### 3.1.1. The driver section

The compression chamber and the intermediate chamber constitute the driver section. The driver section is 2 m long with an internal diameter of 260 mm and has a safe operating pressure of 20 bar.
Diaphragms of different thickness are placed between the compression chamber and the intermediate chamber and between the intermediate chamber and the expansion chamber (Refer to Figure 3.1).
Thickness of the diaphragm plastics depend on the required Mach number and are determined by the shock tube software system once a Mach number is selected.

Two reductions of area occur at the intermediate section. The first reduction in area occurs just before the first diaphragm where the circular section of the compression chamber (diameter 260 mm) transforms in to a square cross – section (180 mm x 180 mm). The second reduction occurs across the intermediate chamber where the square cross – section (180 x 180) transforms into a rectangular cross – section (180 x 76.2 mm). This transformation in area is to increase the Mach number of an incident shock for a fixed pressure and to smooth out irregularities.
A hydraulic cylinder located at the rear of the shock tube assembly is used to separate and close together all of the three chambers. This arrangement allows the diaphragm material to be clamped between the flanges of the driver sections and seal the chamber. The hydraulic actuator is fully automated and is controlled by the computer in the expansion chamber room. The compression chamber and the intermediate chamber are supplied with high – pressure air from an air receiver situated in the Mechanical Engineering Laboratory. Once the test is initiated the hydraulic arrangement closes the driver section and the compression and the intermediate chambers are pressurized. The intermediate chamber is then vented, thus bursting the diaphragms and sending the shock wave down the expansion chamber. Figure 3.2 overleaf shows the driver section.

### 3.1.2. The expansion chamber

The expansion chamber is constructed from cast iron sections; it is 6 m in length and has a height of 180 mm and the width of 76.2 mm. The cast iron has superior vibration damping properties compared to other metals (like steel or aluminum) and reduces wall vibrations that can negatively affect the readings of the sensitive pressure transducers.
Several ports are available for positioning the pressure transducers along the expansion chamber and are situated 450 mm apart and can be seen in Figure 3.3. Two of these ports closest to the test section are fitted with the pressure transducer used for calculating the actual Mach numbers of the tests and for initiating the recordings of the transducers in the test section.

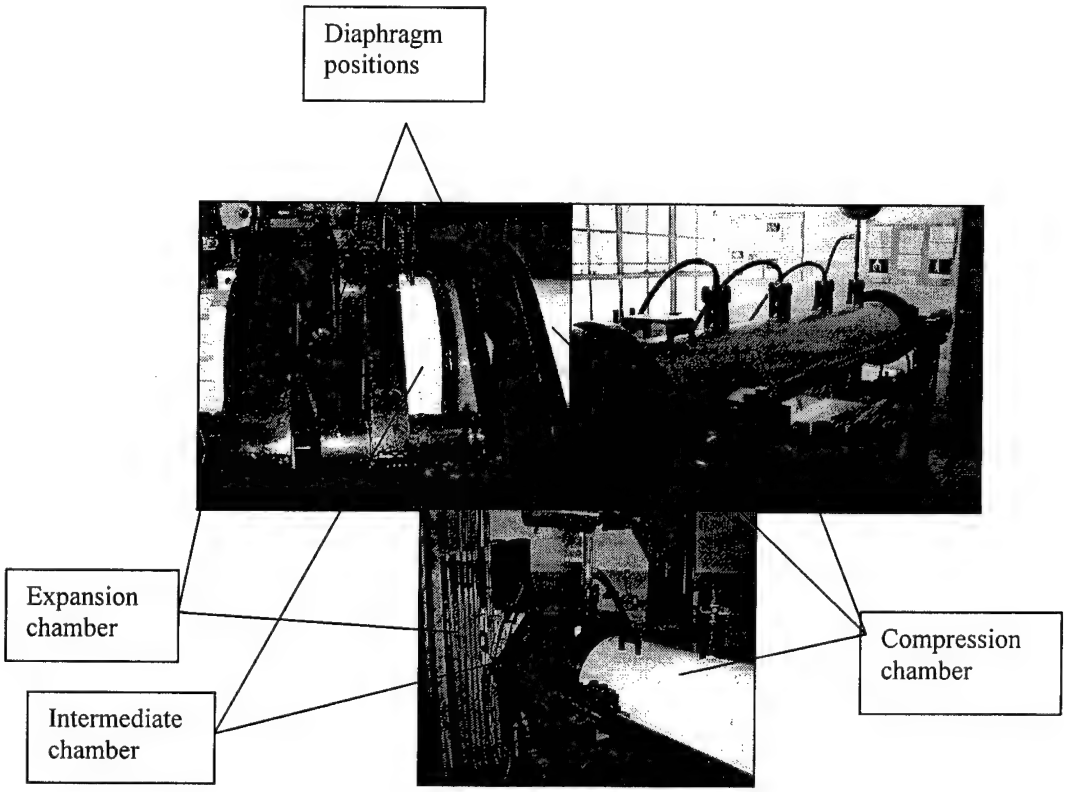


Figure 3.2. Compression chamber, intermediate chamber and part of the expansion chamber

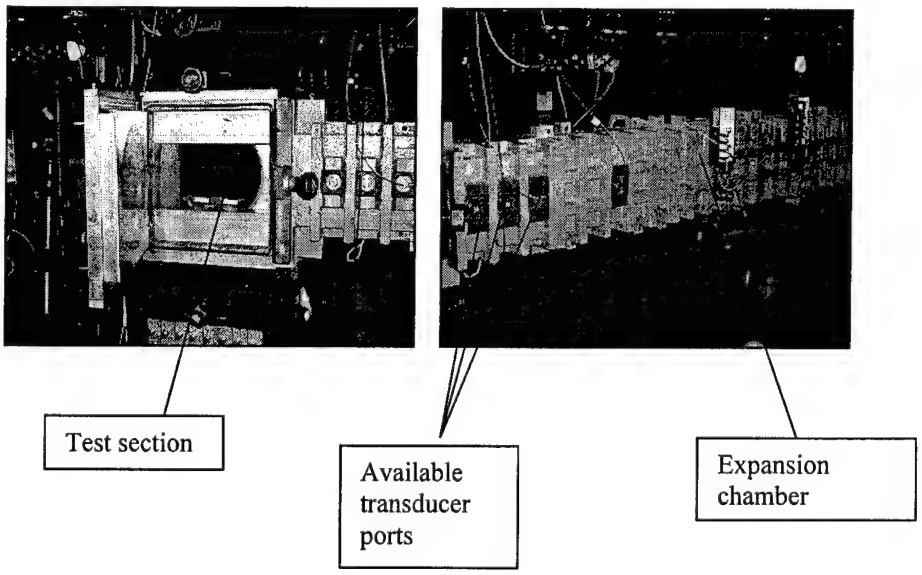


Figure 3.3. Expansion chamber and the test section

### 3.1.3. The test section

Figure 3.3 shows the test section and part of the expansion chamber.
The end of the expansion chamber extends into the test section that is 303 mm in length. The wall at the very end of the test section is a solid block 80 mm in length.
Two large doors, 500 x 470 mm, enclose the tests section. Two large, 55 mm thick and 260 mm diameter, circular glass windows are placed in the two doors thereby allowing the complete view of the test section. Total viewing area of the test section is 180 x 180 mm. The two doors are hinged and can be opened between tests to allow for the positioning of the sample and cleaning of the test section. Transducer ports are located on the floor, roof and the back wall of the test section. There are total of 24 transducer ports in the test section with eight on each side. Transducers on the floor and the roof are positioned along the midline of the tube and are 30 mm apart. Location of these ports is shown in Figure 3.4 below.

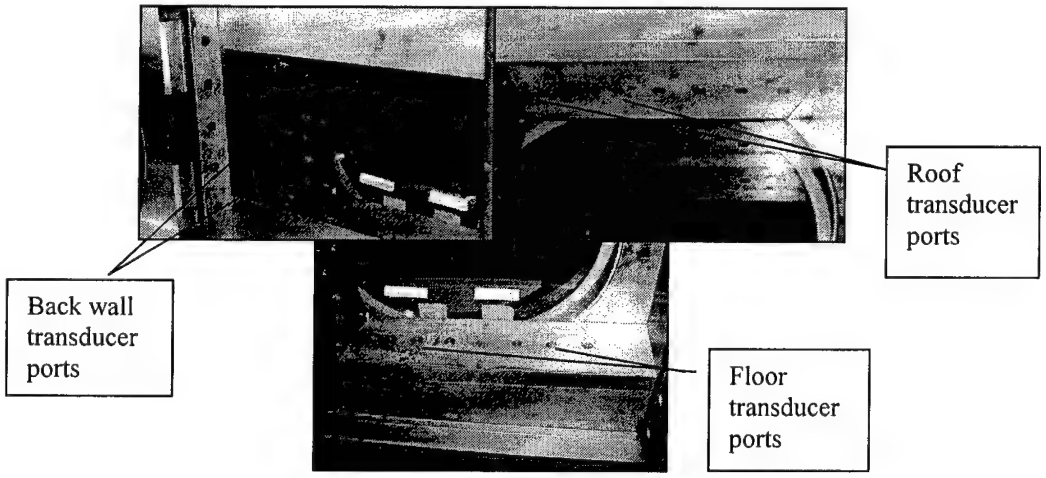


Figure 3.4. Available pressure transducer ports on the back wall, roof and the floor of the test section.

## 3.2. Data Acquisition system and instrumentation

### 3.2.1. Data acquisition system

The data acquisition system is situated in the expansion chamber room and consists of a personal computer and two A to D converters. Two 12 bit, 167 kHz, eight port Analogue to Digital (ADC) converters were used to receive and store outputs from all measuring devices (Refer to Figure 3.5 overleaf). Screen cables were used to transfer signals from the measuring devices to the ADC.
The ADC used was a Rene Mauer ADAM (Analogue Data Acquisition Memory) with 2MHz sampling frequency and eight separate channels. Every channel uses 64 Kb input buffers to store digital data captured from the transducers. The digitized signals received were accessed by a 486 DX 33 MHz personal computer. Software was used to convert the voltage signals from the transducers to pressure data.

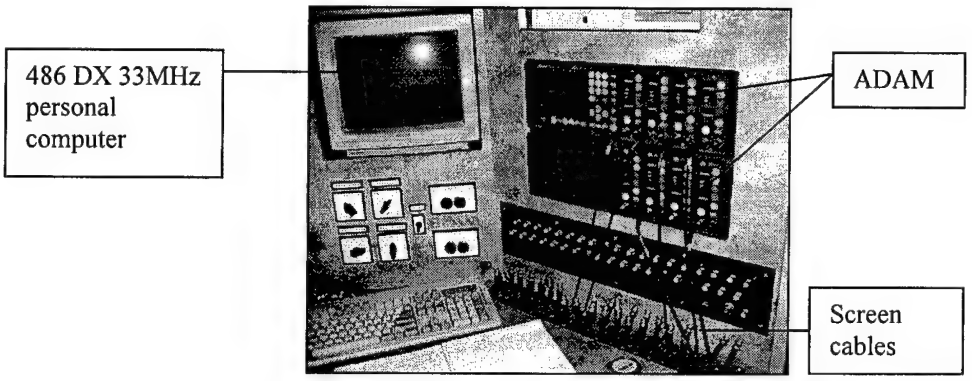


Figure 3.5. Data acquisition system

### 3.2.2. Pressure and temperature measurements

**Static pressure and temperature measurement**

Ambient temperature measurements were done by LM35DZ integrated temperature sensors with accuracy of 0.25 °C. The expansion chamber barometric pressure was measured using a Barotek B1000 pressure transducer with the resolution of 0.4 millibars and a range of 800 – 1000 millibars.

**Driver section pressure measurement**

A SCHAEVITZ P1041 high-pressure transducer with a measuring range of 0 – 20 bar gauge measured the pressure in the compression chamber and intermediate chamber. This transducer is designed to withstand any rapid pressure changes such as those caused by a diaphragm burst.

**High – speed pressure measurement**

All the pressure measurements inside the shock tube are measured using fast response PCB (model113A21), piezo – electric pressure transducers. The signals from these transducers are amplified by PCB line power units (model 482A) and received by the ADC.

## 3.3. Operation of the shock tube

The testing begins with the hydraulic ram closing the intermediate and compression chambers. The hydraulic pump is actuated by the software routine.

The intermediate and compression chambers are pressurized simultaneously to avoid overloading the diaphragm. The final pressure in the intermediate chamber is lower than in the compression chamber. The intermediate chamber is then vented increasing the pressure difference between it and compression chamber thus causing the diaphragm to burst. This sets the shock wave down the expansion chamber. Once the shock wave has impacted with the back wall of the test section, the shock tube is then vented to the atmosphere. When the pressure in the shock tube has reached atmospheric pressure, the chambers are opened.

The shock tube needs to be cleaned after every test to remove any diaphragm fragments left over, by blowing compressed air down the expansion and compression chambers.

### 3.3.1. Testing Procedure

The following steps outline the procedure followed for each test:

1. All the instrumentation had to be switched on and allowed sufficient time to reach operating conditions before the testing commences (approximately 30 minutes).
2. The supply pressure from the air receiver was checked to be sufficient for the required Mach number (above 600 kPa).
3. The compression chamber and the expansion chamber had to be blown down using high-pressure air to remove any fragments of diaphragm remaining from previous tests.
4. The expansion chamber had to be vacuum cleaned from inside to remove any diaphragm fragments that were not blown out by the high-pressure air. This was done by inserting a ordinary vacuum cleaner hose through the test section of the shock tube down the expansion chamber.
5. The correct sample was than placed in the test section at the desired distance from the back wall. If the sample was strong enough to support its own weight without buckling, it was only slightly supported with Prestik to the top and the bottom ends of the test section, otherwise two pins were used.
6. The hinged door of the test section was then closed securely.
7. A value of Mach number was then entered in to the personal computer. The computer then displays the correct thickness of the diaphragm material to produce the desired Mach number.
8. The plastic diaphragms with the correct thickness were placed between the compression chamber and the intermediate chamber and between the intermediate chamber and the expansion chamber.
9. A check was done to ensure that all the valves used for the shock tube were in correct position and by following the instructions on the computer the test is initiated automatically.

## 3.4. Tests with perforated plates

### 3.4.1. Test specimens

The experimental conditions require that the mass and the air permeability effects of the textiles on the shock wave pressure amplification be researched separately. This means that the samples of different mass and same porosity are tested to find the effects of one variable separately from the other and vice versa. As it was not possible to obtain textiles that satisfied this condition, special specimens were made from plastic sheet material and perforated with holes. These results would then be correlated with the textile specimens. Test specimens were made from plastic samples of different thickness and porosity. Plastic sheets were bought, cut to size and then perforated by drilling holes of different sizes and spacing for different specimens to attain different porosity. To vary mass of the samples a range of thickness were used from the same material. This method was suggested in order to attain different masses and porosity in a controllable range.

PVC and Polycarbonate plastic sheet materials were used for the specimens, as they are hard plastics with enough elasticity. Samples were perforated using a high-speed drill (22000 rpm) to attain smooth holes without drawing any material during drilling.

Several groups of textiles were manufactured each with the same porosity and different mass per unit area. Air permeability tests for the samples were done by SABS (South African Bureau of Standards).

### 3.4.2. Attachment of the test specimens

The plastics were cut into 76 x 180 mm samples so that they would fit the dimensions of the shock tube. The attachment of the samples thick enough and strong enough to support their own weight without buckling was done simply. A small piece of Prestik was placed at the bottom and the top walls of the test section and the sample was then positioned between the back wall of the test section and the Prestik. The sample was pressed very gently against the Prestik so that with a very small force of one's finger it could be removed (See Figure 3.6 below). This arrangement allowed for the sample to be completely free of any obstructions during its motion towards the back wall after the impact with the shock wave. Spacing between the back wall and the sample, which will be referred to as the air gap, was set to 3 mm for every test. A small 3 mm thick metal bar was used to set the samples distance from the back wall.

The samples that were too thin and buckled when placed upright had to be supported on two pins positioned at the two upper corners of the back wall. The pins consisted of 0.5 mm diameter, 40 mm long drill bit inserted inside a 5 mm threaded rod. The rods are then screwed in to the two threaded holes on the upper corners of the back wall. The sample then hangs freely on the two drill bits that act as a guide pins.

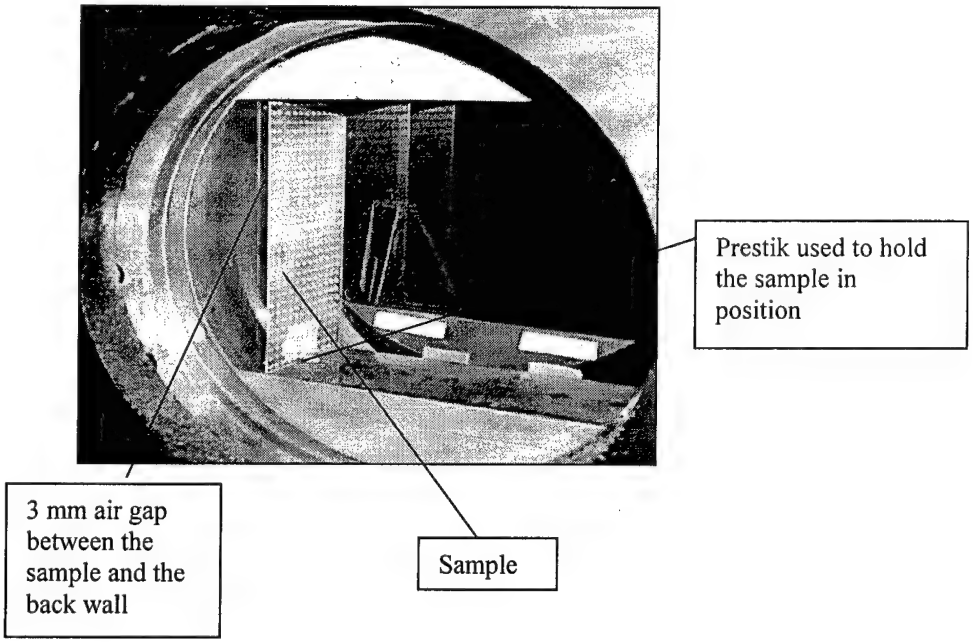


Figure 3.6. Positioning of the sample inside the test section

## 3.5. Tests with single and multiple layers of textiles

### 3.5.1. Test specimens

The backing plate with the transducers necessary for testing was already built into the shock tube and no special equipment was needed for the testing. Cloth specimens were chosen from variety of textile material. Air permeability of the majority of samples was too low to be measured under standard conditions. Five layers of these samples are totally impermeable under standard conditions, and for this reason it was decided that air permeability is not an important variable but rather only the weight of the samples. Mass and thickness properties of the textiles tested are shown in the Tables 1 and 2 below. Kevlar was chosen for the sample 5 in the one layer (Table 3.1) case and sample 4 in 5 layers case (Table 3.2).

The textiles were cut into 76 × 180 mm samples (completely covering the test cross-sectional area) and fixed in place by double-sided tape (3 mm thick) at the upper and lower corners of the backing plate as shown in Figure 3.7.

The textile samples were gently pressed against the double-sided tape so that they are just held in place and free to move easily towards the backing plate in the 3 mm air gap set by the double-sided tapes. This was assured by gently pressing the textile sample by hand against the backing plate. If the sample deflected without resistance the test was carried out, otherwise the sample was adjusted until it was loosely held by the double-sided tape.

The thickness of the textiles could not be measured with screw micrometers, as they are compressible. Thickness was measured by placing each textile between two parallel plates and then applying and maintaining a slight load between the plates. Each of the samples was weighed on a very sensitive scale. Five layers of the same textile were made using a very small amount of textile glue around the edges of each layer. This assured that the layers would not separate during the testing. Multiple layers were tested in the same manner and under the same conditions as single layers. Samples of the textiles used for the experimentation are provided in the Appendix B.

Table 3.1. Thickness and mass of 1 layer of sample only

| Sample | Thickness (mm) | Mass (grams) |
|---|---|---|
| 1 | 0.3 | 1.58 |
| 2 | 0.25 | 2.04 |
| 3 | 0.4 | 2.98 |
| 4 | 1.3 | 3.35 |
| 5 | 0.5 | 3.74 |
| 6 | 0.7 | 4.04 |
| 7 | 1.1 | 6.15 |

Table 3.2. Thickness and mass of samples with 5 layers

| Sample | Thickness (mm) | Mass (grams) |
|---|---|---|
| 1 | 1.5 | 8.07 |
| 2 | 1.2 | 10.37 |
| 3 | 2 | 15.83 |
| 4 | 2.4 | 19.83 |
| 5 | 5.3 | 19.93 |
| 6 | 2.9 | 20.51 |
| 7 | 2.5 | 31.67 |

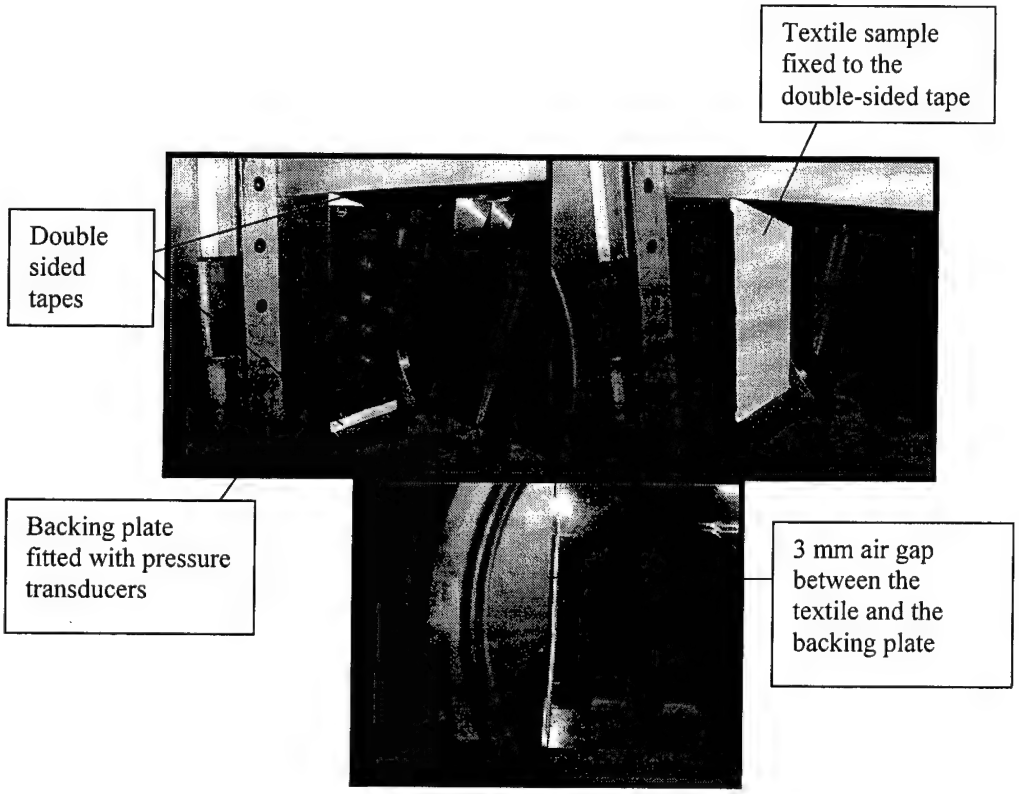


Figure 3.7. Attachment of the textile sample to the backing plate

## 3.6. Tests with gelatin and multiple layers of textile

### 3.6.1. Textile Properties

Three textile materials were tested for this part of the investigation, namely satin, polycotton and muslin due to their difference in porosity and weight. In each case, un-patterned material was used to ensure uniformity. Irregularities (due to patterns) in the materials were undesirable, as they would complicate the analysis of results. The textile properties were measured by the South African Bureau of Standards. Five samples of each textile were measured and the average values obtained. All measurements were performed under controlled laboratory conditions at standard atmospheric pressure.

The thickness of the textiles were measured in the same manner as described in section 3.5 above. Air permeability was determined by measuring the flow rate of air through a given area of a sample when a pressure drop equivalent to 0.5 inches of water is applied across the sample. The properties of the various textiles are shown below in Table 3.3.

Table 3.3. Textile Properties

| | Satin | Polycotton | Muslin |
|---|---|---|---|
| Mass/Area ($g / m^2$) | 134 | 104 | 95 |
| Permeability ($m^3 / m^2 / min$) | 6.0 | 32.9 | 153.6 |
| Thickness (mm) | 0.2 | 0.19 | 0.28 |

### 3.6.2. Gelatin and textile assembly

Gelatin was prepared to try and mimic the elasticity of the skin as close – as possible. After making a few gelatin samples with different weight ratios of gelatin to water it was decided that the ratio of 0.3 and a thickness of 10 mm would be used for the testing.

Tests conducted with gelatin did not require any additional equipment to be made. Once the gelatin was prepared it was simply stuck to the backing plate inside the test section using a very thin layer of vacuum grease at the corners. Since the gelatin already possessed some stickiness a very small amount of grease was used so that it would not interfere with the results. The backing plate was already fitted with the pressure transducers. The gelatin specimen was slightly smaller than the backing plate to allow for the double-sided tape to be placed just above and below the gelatin for securing the textile specimens. By placing the right width of the double-sided tape the air gap between the textile and the gelatin was set to 5 mm. (See Figure 3.8 overleaf).

### 3.6.3. Attachment of textile samples

The textiles were cut into 76 × 180 mm samples to ensure that they completely cover the cross section of the test section. The textiles were attached to the double-sided tape placed just above and bellow the gelatin sample.

Multiple layer samples were prepared by using a small amount of superglue at the corners of the sample, in order to hold them together.

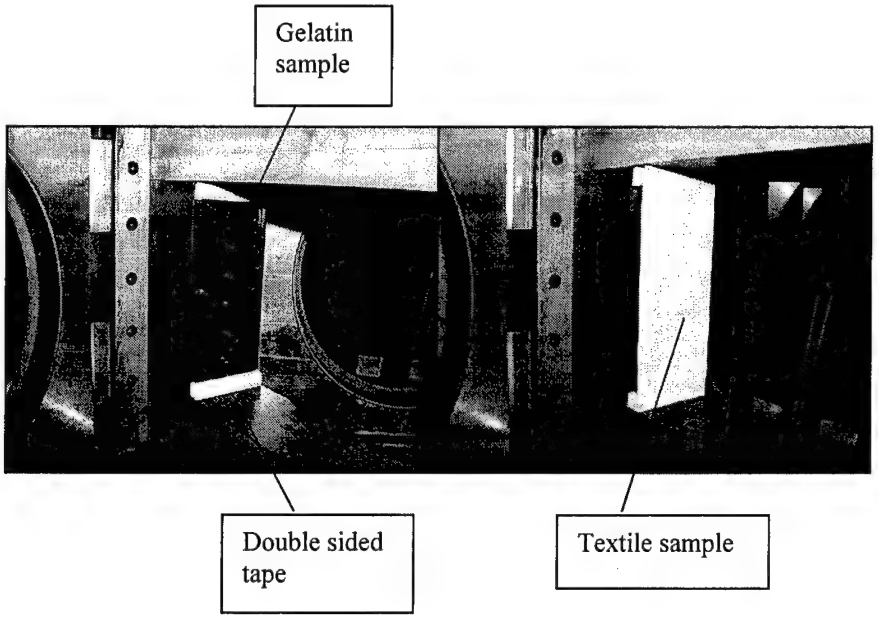


Figure 3.8. Gelatin textile assembly

## 3.7. Tests with textiles placed at an angle

The textile samples used were the same as in the tests with gelatine described in section 3.6 using single layer of textiles only.

### 3.7.1. Inclined Plate Assembly

In order to investigate the impact of the shock waves on the textiles at different angles (known as the reflecting wedge angle, $\theta_w$), it was required to design and construct an attachment for the shock tube. An "Inclined Plate Assembly", shown below in Figure 3.9, was thus designed and manufactured.

The assembly consists of three mild steel parts connected by screws. Detailed drawings of the individual parts are given in Appendix B. The back wall attachment was screwed into the back wall of the shock tube. Three pressure transducers were fed through the existing ports in the back wall and positioned in the inclined plate when pressure traces were desired. The three transducers each yield pressure traces, which will later be referred to as 'Top Trace', 'Bottom Trace' and Middle Trace'. These correspond to the inclined plate ports A, B and C respectively, as shown in Figure 3.9.

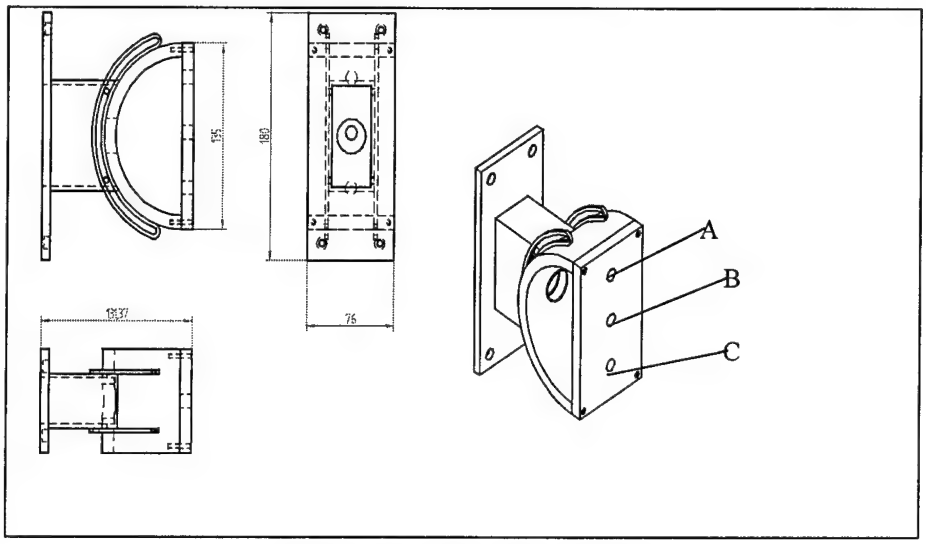


Figure 3.9. Inclined plate assembly

### 3.7.2. Attachment of Textile Samples for the Inclined Tests

The textiles were cut into 76 × 180 mm samples and attached to the inclined backing plate using double-sided tape (see Figure 3.10). Two 76 × 10 mm strips of tape were placed at the top of the inclined plate as well as at the bottom of the inclined plate. This arrangement ensures that the textile is a uniform distance from the inclined plate. When tests were to be conducted without the backing plate, the textiles were attached to the semi-circular plate in the same configuration as described above.

The double-sided tape used was approximately 2.5 mm thick. In order to facilitate analysis of the schlieren and shadowgraph images, two strips of tape were placed between the textiles and the inclined plate thus yielding a 5 mm gap.

Since the textiles were required to simulate clothing, they had to be able to move when impacted by the shock waves. For this reason, the textiles were loosely attached to the double-sided tape. Observations showed that the textiles do in fact move and even completely detach themselves from the assembly after being impacted by the shock wave, thus the tape was deemed satisfactory.

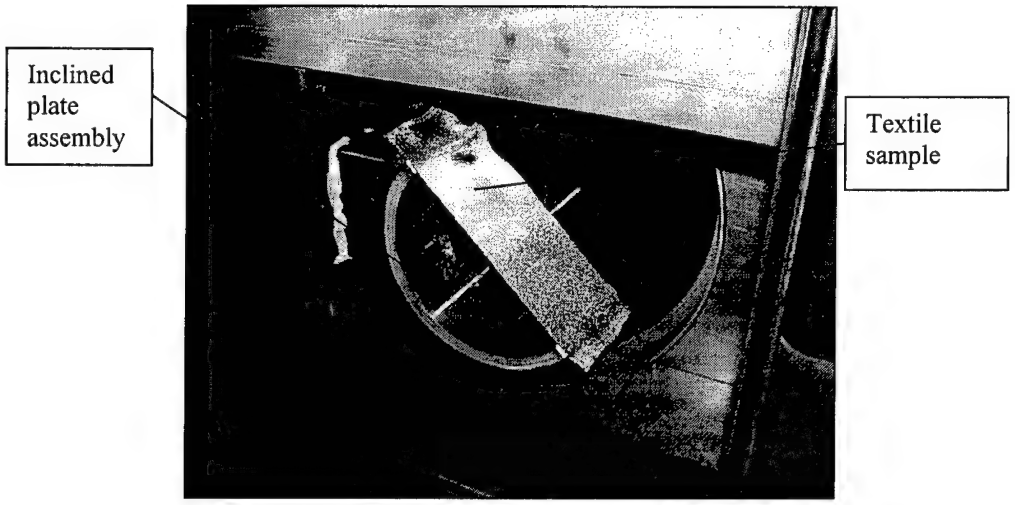


Figure 3.10. Attachment of the textile sample to the inclined plate assembly

### 3.7.3. Optical Techniques

The optical system for flow visualization was set up to produce schlieren images. A schlieren instrument records changes in the refractive index distribution of transparent media such as airflow. The refractive index distribution can then be related to density, temperature, or pressure distributions within the flow.

A white light source is usually used. The source is passed through a thin slit, and then made parallel (collimated) by either a mirror or a lens. A Xenon flash lamp was used as the light source and parabolic mirrors were used to collimate the light. Figure 3.11 shows a schematic of the schlieren photography setup.

The parallel light is passed through the flow and then brought to a focus. The camera is arranged so that the test section of the shock tube is in focus. A knife-edge placed at the focus is positioned so that it blocks roughly half of the light. If the flow is uniform, then the image behind the knife-edge will be uniformly bright. If the flow has refractive index variations that cause some of the light that would have passed by the knife-edge to instead be blocked by it, then the image has dark areas. Conversely, if the flow causes some light rays to pass the knife-edge that would otherwise have been blocked, then the image has light areas.

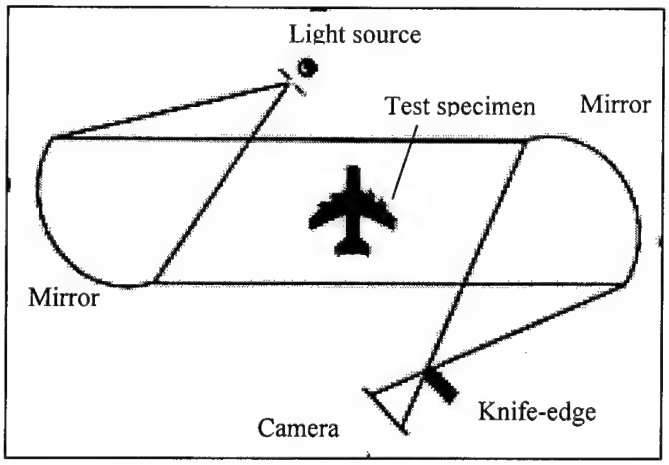


Figure 3.11. Schematic of the Schlieren photography set up

The optical system outlined above is easily adapted to produce shadowgraph images. All that is required is to remove the knife-edge. As mentioned above, strong density gradients give rise to appreciable light deviations. A uniform density gradient would not affect the light on the photographic film since all the light would be bent through the same angle. The shadowgraph method is sensitive only to changes in this angle of deflection so that the light intensity falling on the photographic film is non-uniform.

# 4. Experimental results and observations

## 4.1. Perforated plates tests

For the perforated plates test the porosity (void fraction) serves as a measure of the permeability. Unfortunately actual permeability values were not obtainable from the Bureau of Standards. Table 4.1 below shows the samples that were manufactured and their properties.
Porosity of the samples were calculated as follows:

$$Porosity = 100 * \left( \frac{A*T - \frac{M}{D}}{A*T} \right) \%$$

where: A = longitudinal area of the sample 180 x 76
T = thickness of the sample
M = mass of the sample in grams
D = density of the sample in g/mm$^3$

Table 4.1 Properties of manufactured samples

| Sample No | Thickness (mm) | Mass (g) | Porosity (%) |
|---|---|---|---|
| 1 | 1 | 10.15 | 35.35 |
| 2 | 1.5 | 14.5 | 32.56 |
| 3 | 2 | 22.19 | 31.2 |
| 4 | 1 | 12.56 | 22.55 |
| 5 | 1.5 | 19.56 | 19.06 |
| 6 | 2 | 29.13 | 18.59 |
| 7 | 1 | 15.97 | 4.2 |
| 8 | 1.5 | 22.48 | 6.97 |
| 9 | 2 | 34.05 | 6.17 |
| 10 | 1 | 15.38 | 4 |
| 11 | 1.5 | 23.18 | 3.54 |
| 12 | 2 | 33.78 | 5.43 |
| 13 | 0.05 | 0.71 | 18.36 |
| 14 | 0.01 | 2.17 | 23.46 |
| 15 | 0.3 | 3.83 | 21.06 |
| 16 | 0.05 | 0.71 | 7.85 |
| 17 | 0.01 | 2.25 | 8.52 |
| 18 | 0.3 | 4.5 | 6.37 |
| 19 | 0.05 | 0.65 | 5.03 |
| 20 | 0.01 | 1.83 | 8.02 |
| 21 | 0.3 | 4.58 | 4.7 |

Samples were collected into four groups of similar sample porosity and different weight to evaluate the mass effect on the pressure amplification:

Group 1:

| Sample No | Thickness (mm) | Hole diameter (mm) | Porosity (%) | Mass (g) |
|---|---|---|---|---|
| 12 | 2 | 0.8 | 5.43 | 33.78 |
| 11 | 1.5 | 0.8 | 3.54 | 23.18 |
| 10 | 1 | 0.8 | 4 | 15.38 |
| 21 | 0.03 | 0.8 | 4.7 | 4.58 |
| 20 | 0.1 | 0.8 | 7.3 | 1.83 |
| 19 | 0.05 | 0.8 | 8.3 | 0.65 |

Group 2:

| Sample No | Thickness (mm) | Hole diameter (mm) | Porosity (%) | Mass (g) |
|---|---|---|---|---|
| 9 | 2 | 1 | 6.17 | 34.05 |
| 8 | 1.5 | 1 | 6.97 | 22.48 |
| 7 | 1 | 1 | 4.2 | 15.97 |
| 18 | 0.3 | 1 | 6.37 | 4.5 |
| 17 | 0.1 | 1 | 8.52 | 2.25 |
| 16 | 0.05 | 1 | 7.85 | 0.071 |

Group 3:

| Sample No | Thickness (mm) | Hole diameter (mm) | Porosity (%) | Mass (g) |
|---|---|---|---|---|
| 6 | 2 | 1.5 | 18.59 | 29.13 |
| 5 | 1.5 | 1.5 | 19.06 | 19.56 |
| 4 | 1 | 1.5 | 22.55 | 12.56 |
| 15 | 0.3 | 1.5 | 21.06 | 3.83 |
| 14 | 0.1 | 1.5 | 23.46 | 2.17 |
| 13 | 0.05 | 1.5 | 18.36 | 0.17 |

Group 4:

| Sample No | Thickness (mm) | Hole diameter (mm) | Porosity (%) | Mass (g) |
|---|---|---|---|---|
| 3 | 2 | 2 | 35.35 | 22.19 |
| 2 | 1.5 | 2 | 32.56 | 14.5 |
| 1 | 1 | 2 | 31.2 | 10.15 |

### 4.1.1. Test results

All the tests were performed with a Mach number of 1.42. Although the actual Mach numbers tended to deviate slightly from the specified value they were very close, ranging from 1.415 – 1.421.
The highest pressures obtained with the sample placed 3 mm in front of the back wall and without the sample were compared and the percentage amplification due to the sample was calculated.
Figures 4.1, 4.2, 4.3 & 4.4 that follow show the test results:

Test results:

Group 1:

| Sample No | Porosity (%) | Mass (g) | % amplification |
|---|---|---|---|
| 12 | 5.43 | 33.78 | -12.9 |
| 11 | 3.54 | 23.18 | -11.4 |
| 10 | 4 | 15.38 | -3.0 |
| 21 | 4.7 | 4.58 | 26.0 |
| 20 | 7.3 | 1.83 | 70.0 |
| 19 | 8.3 | 0.65 | 122.4 |

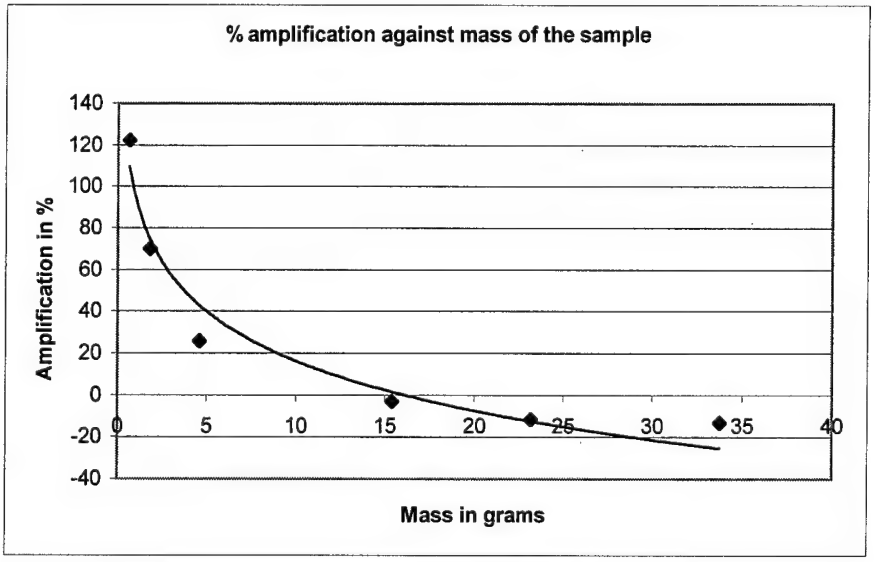


Figure 4.1. % pressure amplification vs mass of the samples from group 1; Mach no 1.419 and porosity 5.5%.

Group 2:

| Sample No | Porosity (%) | Mass (g) | % amplification |
|---|---|---|---|
| 9 | 6.17 | 34.05 | -19.8 |
| 8 | 6.97 | 22.48 | -16.0 |
| 7 | 4.2 | 15.97 | -14.7 |
| 18 | 6.37 | 4.5 | 21.7 |
| 17 | 8.52 | 2.25 | 67.9 |
| 16 | 7.85 | 0.071 | 90.6 |

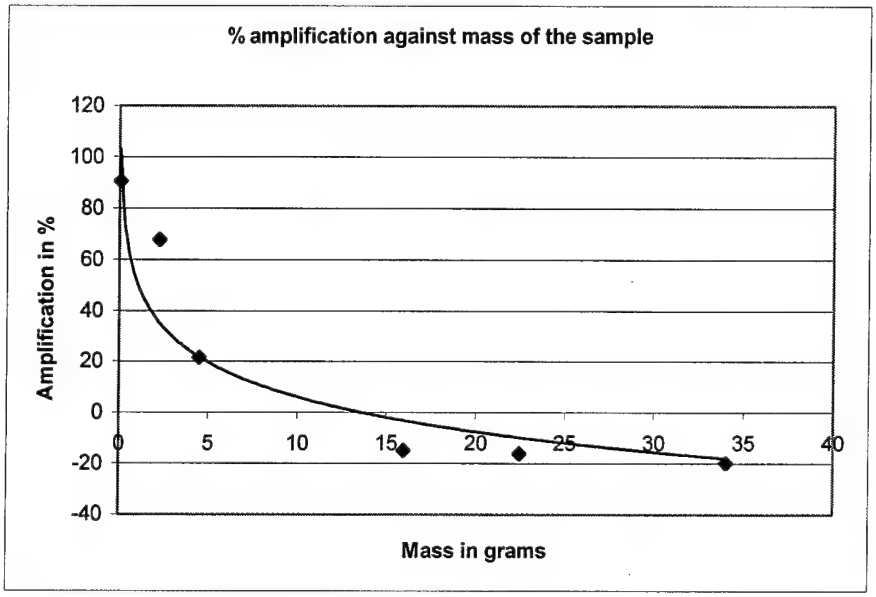


Figure 4.2. % pressure amplification vs mass of the samples from group 2; Mach no 1.415 and porosity 6.7%.

Group 3:

| Sample No | Porosity (%) | Mass (g) | % amplification |
|---|---|---|---|
| 6 | 18.59 | 29.13 | -31.51 |
| 5 | 19.06 | 19.56 | -26.51 |
| 4 | 22.55 | 12.56 | -22.92 |
| 15 | 21.06 | 3.83 | -12.06 |
| 14 | 23.46 | 2.17 | -4.28 |
| 13 | 18.36 | 0.17 | 7.61 |

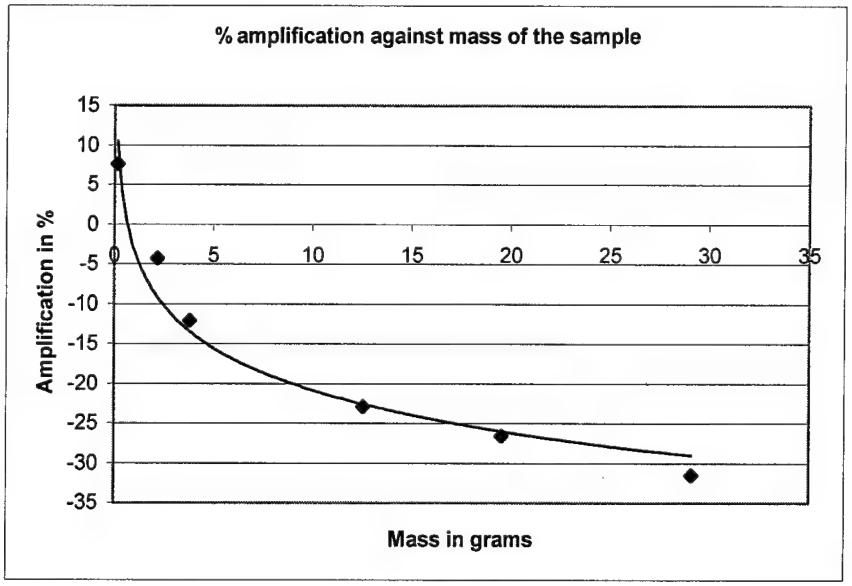


Figure 4.3. % Pressure amplification vs mass of the samples from group 3; Mach no 1.415 and porosity 20.5%.

Group 4:

| Sample No | Porosity (%) | Mass (g) | %amplification |
|---|---|---|---|
| 3 | 35.35 | 22.19 | -14.7 |
| 2 | 32.56 | 14.5 | -11.2 |
| 1 | 31.2 | 10.15 | 2.6 |

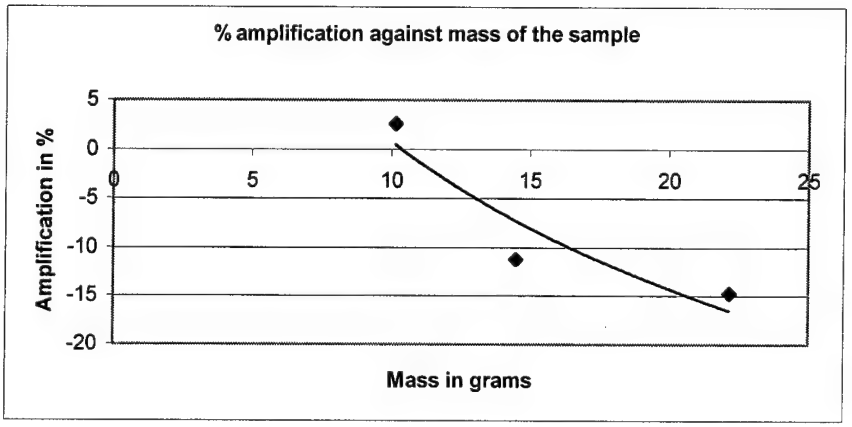


Figure 4.4. % Pressure amplification vs mass of the samples from group 4; Mach no 1.41 and porosity 33%.

## 4.2. Single and multiple layer textiles test results

Tables 4.2, 4.3, 4.4 and 4.5 below display the test specimen mass, number of layers, Mach number achieved and peak pressure for each group of tests. The graph for each group of tests (Figures 4.5 and 4.6) is provided under every table. All the samples were tested with two Mach numbers: 1.42 and 1.35.

Table 4.2. Amplification and peak pressure of one layer of textile for average Mach No=1.42

| Sample | Thickness (mm) | Mass (grams) | % amplification | Mach No | Peak pressure (bar) |
|---|---|---|---|---|---|
| 1 | 0.3 | 1.58 | 88 | 1.425 | 5.5 |
| 2 | 0.25 | 2.04 | 63 | 1.416 | 4.8 |
| 3 | 0.4 | 2.98 | 168 | 1.418 | 7.8 |
| 4 | 1.3 | 3.35 | 250 | 1.423 | 10.2 |
| 5 | 0.5 | 3.74 | 361 | 1.415 | 13.5 |
| 6 | 0.7 | 4.04 | 61 | 1.42 | 4.7 |
| 7 | 1.1 | 6.15 | 50 | 1.418 | 4.4 |

Table 4.3. Amplification and peak pressure of five layers of textile for average Mach No=1.42

| Sample | Thickness (mm) | Mass (grams) | % amplification | Mach No | Peak pressure (bar) |
|---|---|---|---|---|---|
| 1 | 1.5 | 8.07 | 29 | 1.425 | 3.8 |
| 2 | 1.2 | 10.37 | 86 | 1.418 | 5.4 |
| 3 | 2 | 15.83 | 108 | 1.423 | 6.1 |
| 4 | 2.4 | 19.83 | 392 | 1.423 | 14.4 |
| 5 | 5.3 | 19.93 | 250 | 1.423 | 10.2 |
| 6 | 2.9 | 20.51 | 187 | 1.419 | 8.4 |
| 7 | 2.5 | 31.67 | 96 | 1.42 | 5.7 |

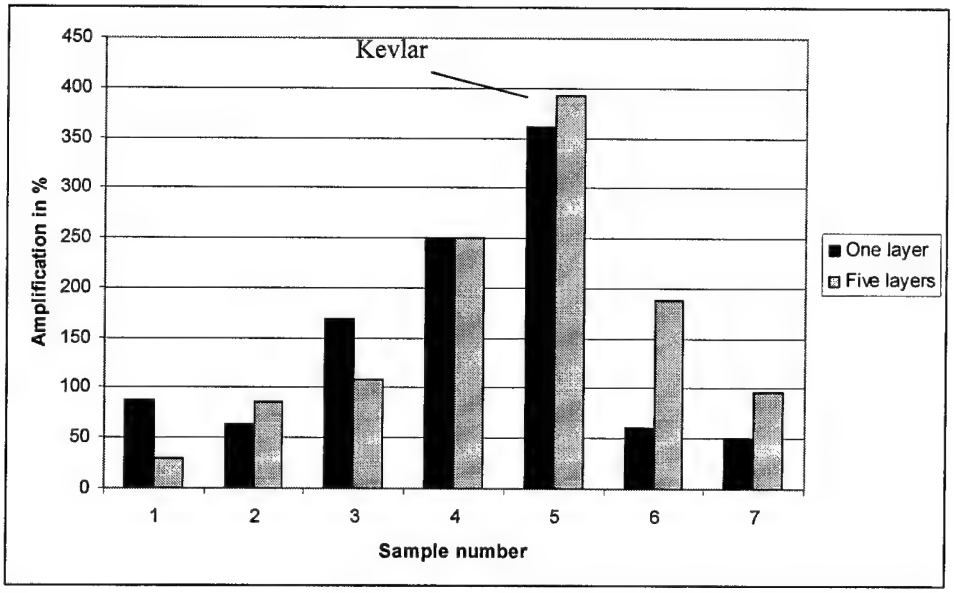


Figure 4.5. Amplification of 1 and 5 layer of textile samples, average Mach no=1.42

Table 4.4. Amplification and peak pressure of one layer of textile for average Mach No=1.34

| Sample | Thickness (mm) | Mass (grams) | % amplification | Mach No | Peak pressure (bar) |
|---|---|---|---|---|---|
| 1 | 0.3 | 1.58 | 34 | 1.336 | 2.3 |
| 2 | 0.25 | 2.04 | 18 | 1.345 | 3.4 |
| 3 | 0.4 | 2.98 | 94 | 1.344 | 5.7 |
| 4 | 1.3 | 3.35 | 121 | 1.342 | 6.4 |
| 5 | 0.5 | 3.74 | 143 | 1.339 | 7.1 |
| 6 | 0.7 | 4.04 | 25 | 1.348 | 3.6 |
| 7 | 1.1 | 6.15 | 6 | 1.342 | 3.1 |

Table 4.5. Amplification and peak pressure of five layers of textile for average Mach No=1.34

| Sample | Thickness (mm) | Mass (grams) | % amplification | Mach No | Peak pressure (bar) |
|---|---|---|---|---|---|
| 1 | 1.5 | 8.07 | 34 | 1.34 | 2.9 |
| 2 | 1.2 | 10.37 | 45 | 1.339 | 3.1 |
| 3 | 2 | 15.83 | 83 | 1.34 | 3.9 |
| 4 | 2.4 | 19.83 | 159 | 1.343 | 5.5 |
| 5 | 5.3 | 19.93 | 179 | 1.346 | 6.0 |
| 6 | 2.9 | 20.51 | 83 | 1.348 | 3.9 |
| 7 | 2.5 | 31.67 | 90 | 1.345 | 4.1 |

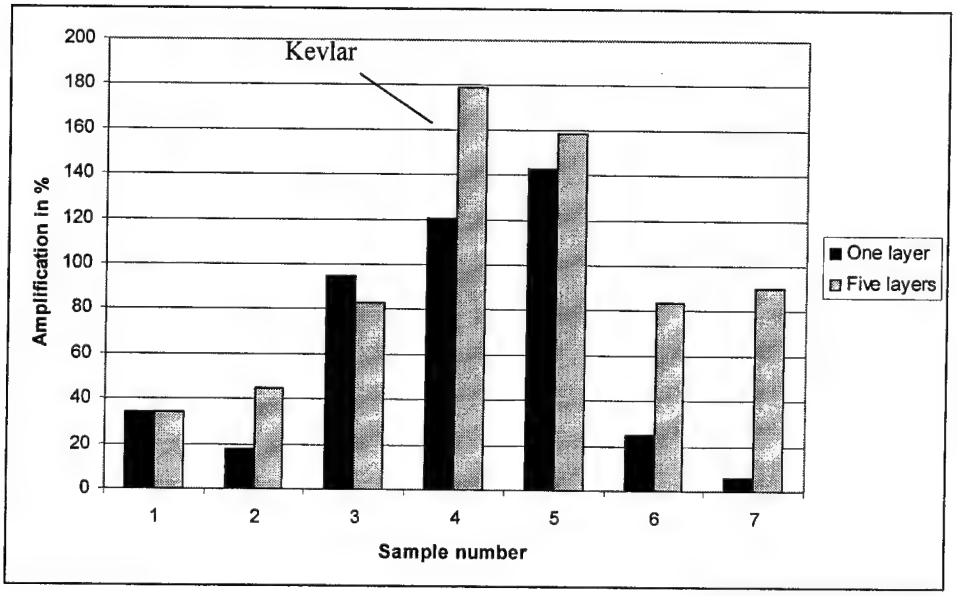


Figure 4.6. Amplification of 1 and 5 layers of textile samples, average Mach no=1.34

## 4.3. Gelatine Behind Textile Tests

Three gelatin samples, with the same size, thickness (10 mm) and gelatin to water weight ratio (0.3) were tested separately for comparative reasons. Pressure traces of those tests are shown on the graphs below (Figures 4.7, 4.8, 4.9 and 4.10). Pressure values on the graphs indicate the pressure above atmospheric (ambient). Ambient pressure recorded during tests was 0.83 bar.
Gelatin sample 1 was then used for testing with different number of textile layers.

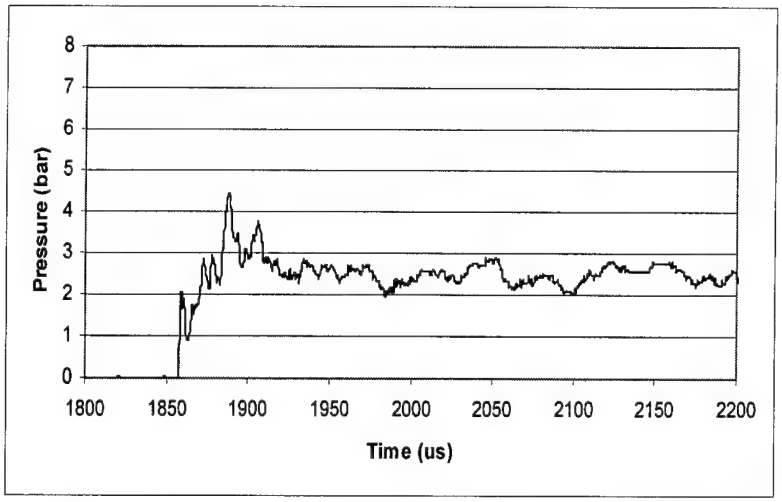


Figure 4.7. Only gelatin sample 1 M=1.416

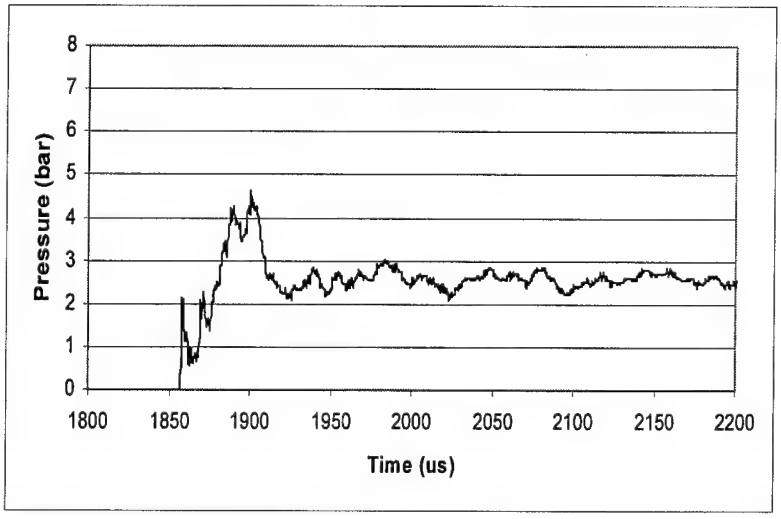


Figure 4.8. Only gelatin sample 2 M=1.416

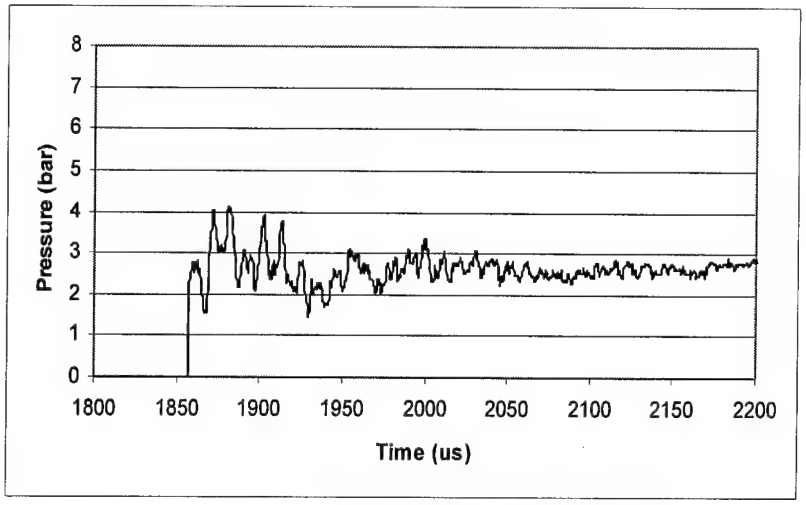


Figure 4.9. Only gelatin sample 3 M=1.421

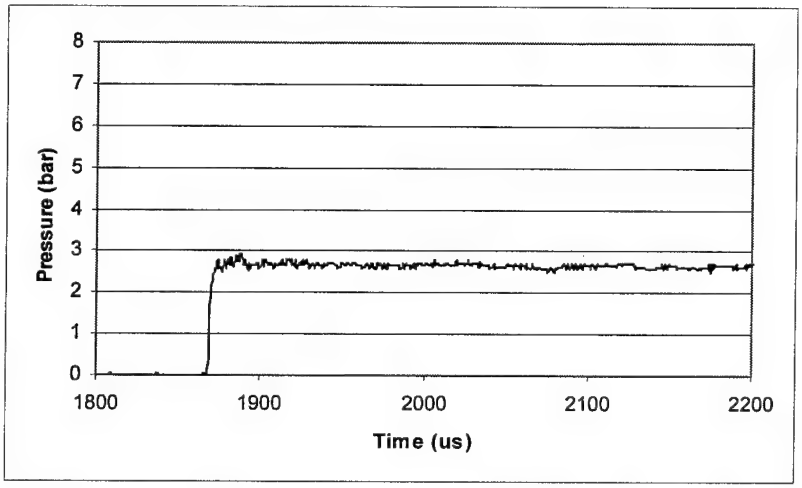


Figure 4.10. Normal shock (no gelatine) M=1.413

Graphs below (Figures 4.11 to 4.19) show the pressure trace with the gelatin behind the textiles with 1, 3 and 5 layers.

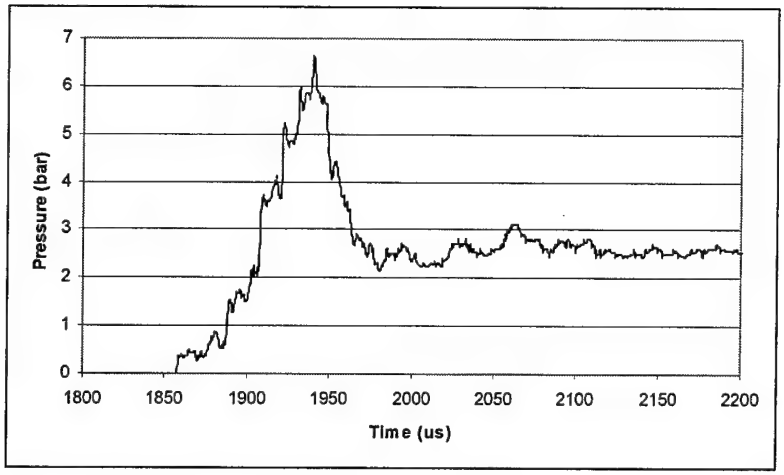


Figure 4.11. Gelatin with 1 layer of satin M=1.421

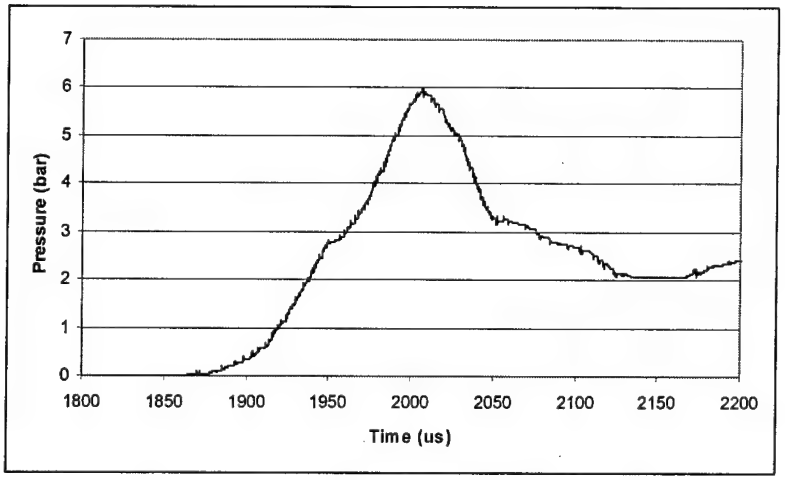


Figure 4.12. Gelatin with 3 layers of satin M=1.417

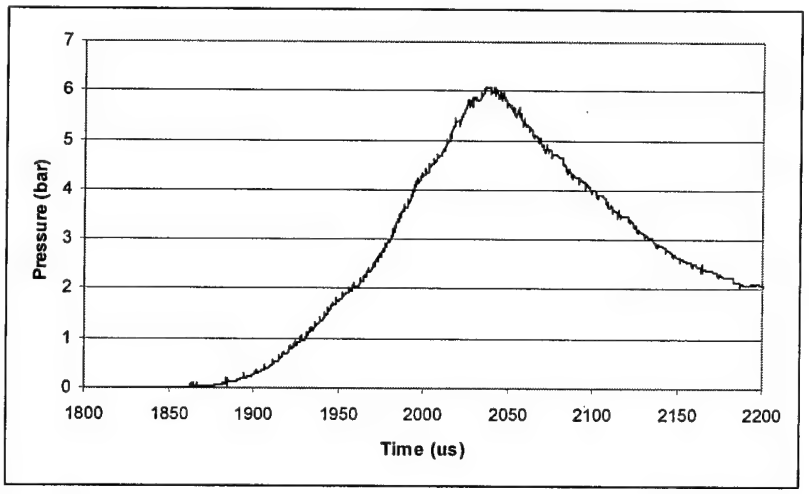


Figure 4.13. Gelatin with 5 layers of satin M=1.426

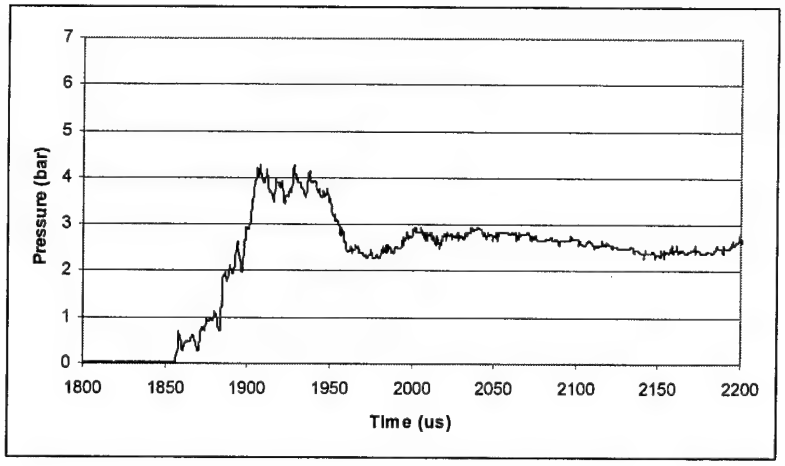


Figure 4.14. Gelatin with 1 layer of polycotton M=1.419

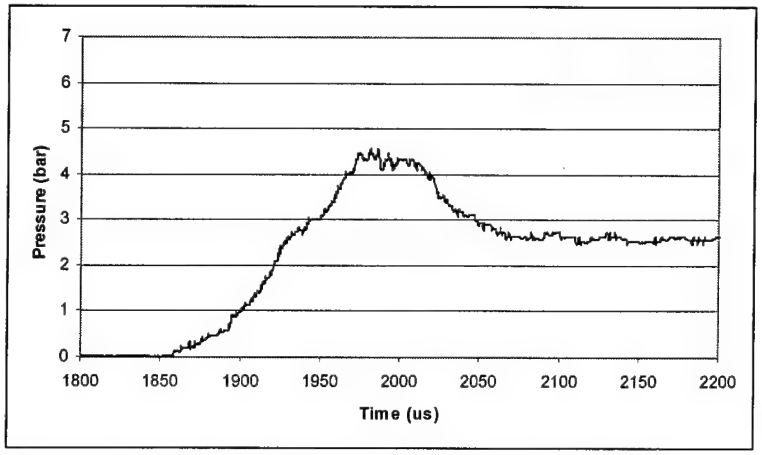


Figure 4.15. Gelatin with 3 layers of polycotton M=1.418

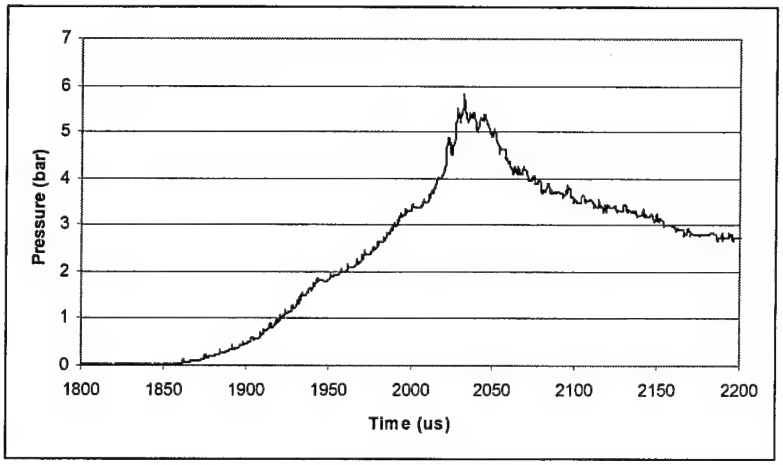


Figure 4.16. Gelatin with 5 layers of polycotton M=1.421

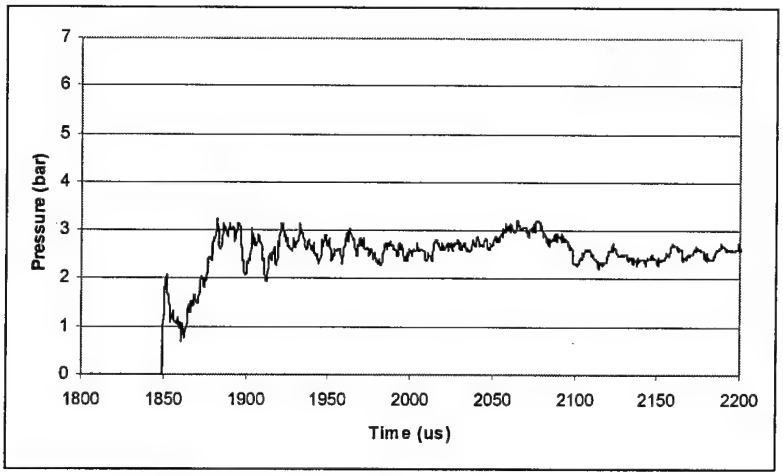


Figure 4.17. Gelatin with 1 layer of muslin M=1.425

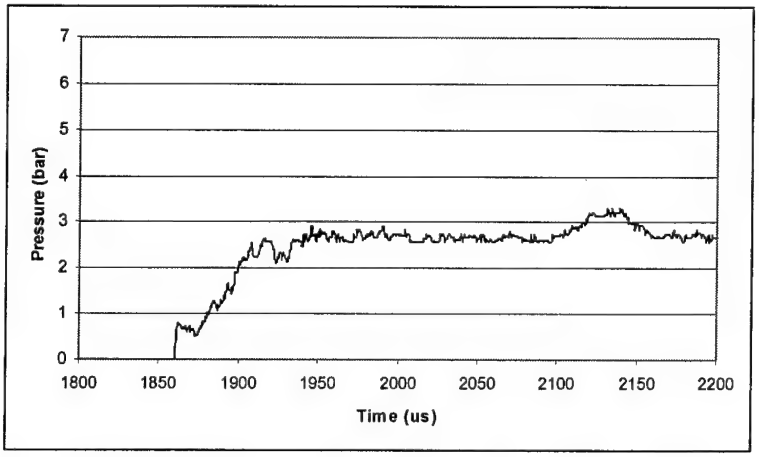


Figure 4.18. Gelatin with 3 layers of muslin M=1.419

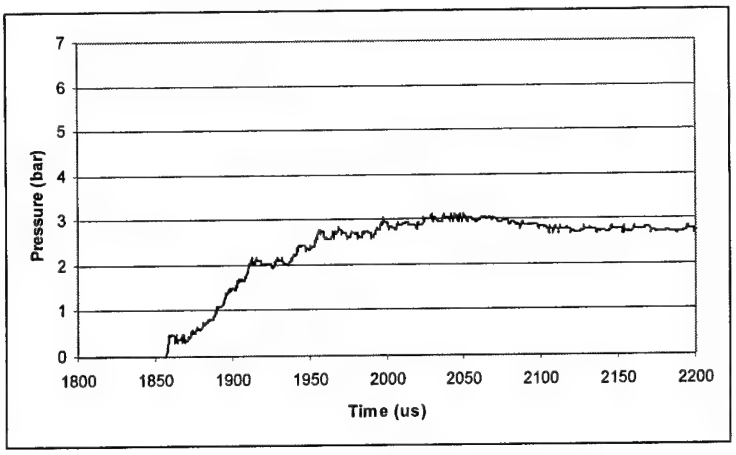


Figure 4.19. Gelatin with 5 layers of muslin M=1.425

## 4.4. Inclined Textile Tests

Table 4.6 below displays the test specimen, reflecting wall angle, Mach number achieved and peak pressure for each test where pressure traces were recorded. The peak pressure was obtained by averaging the peak pressures from the bottom, middle and the top transducer. The pressure traces recorded by each of the three transducers located in the inclined plate are also shown in this section in Figures 4.20 to 4.31. It is important to note that the pressure traces shown are values of pressures above atmospheric.

Table 4.6. Test Data Corresponding to Pressure Traces

| Textile | Wall Angle | Mach Number | Peak Pressure (bar) |
|---|---|---|---|
| None | 45° | 1.417 | 2.62 |
| Satin | 45° | 1.420 | 3.41 |
| Polycotton | 45° | 1.423 | 2.45 |
| Muslin | 45° | 1.415 | 2.02 |
| None | 60° | 1.423 | 2.58 |
| Satin | 60° | 1.421 | 3.96 |
| Polycotton | 60° | 1.421 | 3.26 |
| Muslin | 60° | 1.420 | 2.60 |
| None | 70° | 1.424 | 2.78 |
| Satin | 70° | 1.418 | 4.69 |
| Polycotton | 70° | 1.416 | 3.89 |
| Muslin | 70° | 1.420 | 2.68 |

The Table 4.7 overleaf shows the textiles used for each set of schlieren images captured, with the corresponding shock angles. The angles in the table are explained in section 2.4.4. It is important to note that measurement of the angles from the Schlieren images was difficult and thus the values tabulated are only estimates. This was not deemed problematic since the qualitative assessment of the images is adequate for the current study.

The schlieren photographs that are shown in this section were selected from each set of tests conducted. A full display of all the photographs obtained during testing is available. The 'T' labeled below each photograph refers to the flash time of the Xenon light source, measured from the pressure transducer situated just before the test section on the floor of the shock tube.

Table 4.7. Test Data Corresponding to the Schlieren Images

| Textile | $\theta_W$ | $\theta_I$ | $\theta_T$ | $\theta_R$ | $\alpha$ | $\omega_I$ | $\omega_R$ |
|---|---|---|---|---|---|---|---|
| Satin | 35 | 55 | 36 | - | 10 | 48 | 72 |
| Polycotton | 35 | 55 | 40 | - | 10 | 40 | 70 |
| Muslin | 35 | 55 | 48 | 60 | - | - | - |
| Satin | 60 | 30 | 25 | 28 | - | - | - |
| Polycotton | 60 | 30 | 25 | 25 | - | - | - |
| Muslin | 60 | 30 | 30 | 22 | - | - | - |

Pressure Traces at $\theta_w = 45°$

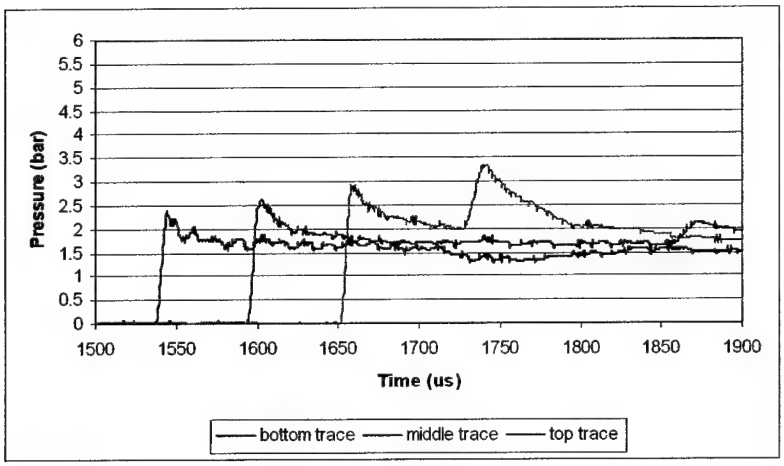


Figure 4.20. Pressure traces with no textile

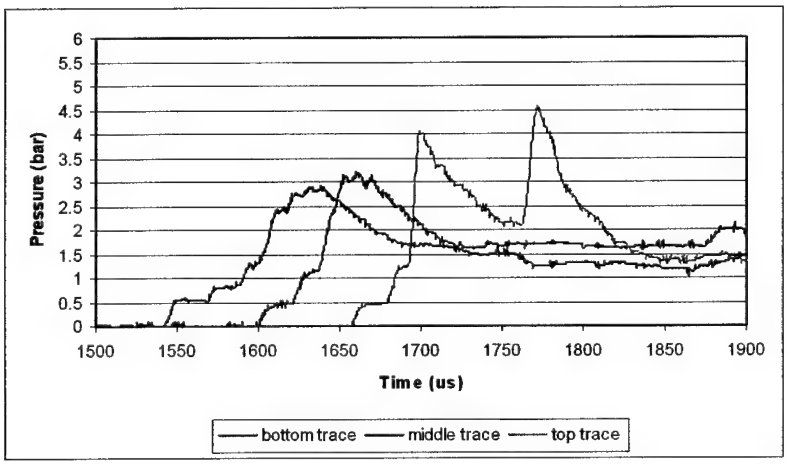


Figure 4.21. Pressure traces with satin

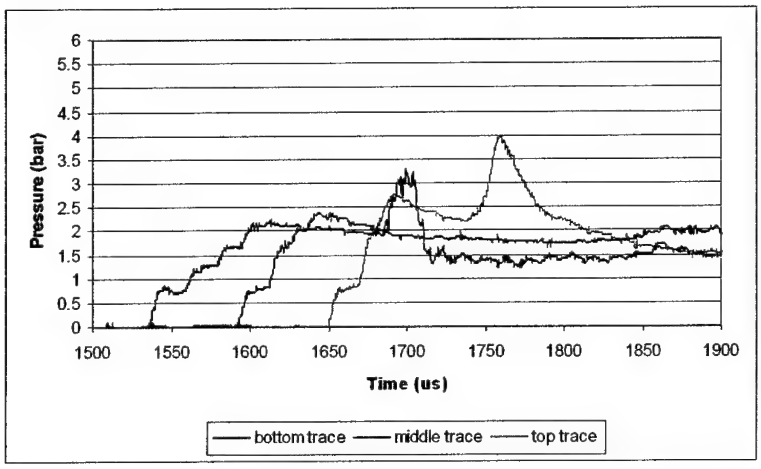


Figure 4.22. Pressure traces with polycotton

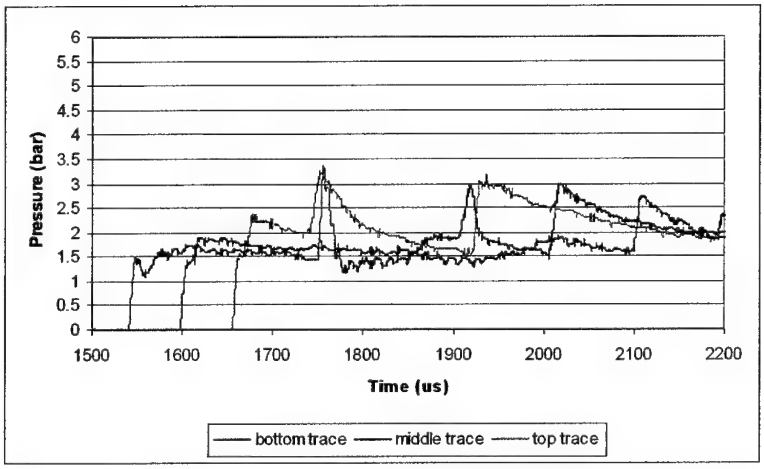


Figure 4.23. Pressure traces with muslin

Pressure Traces at $\theta_w = 60°$

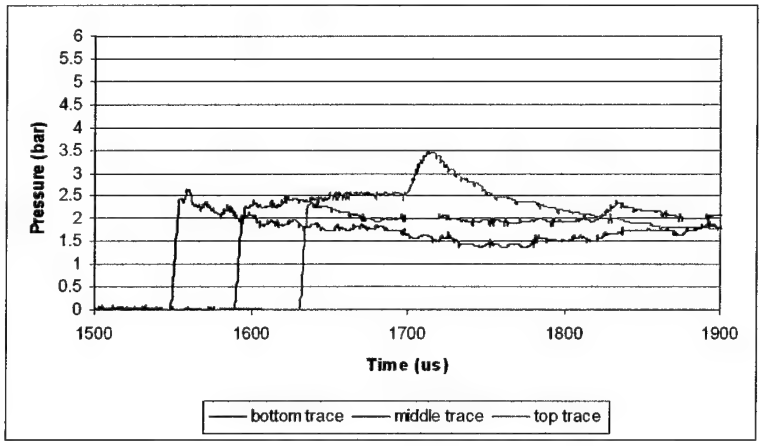


Figure 4.24. Pressure traces with no textile

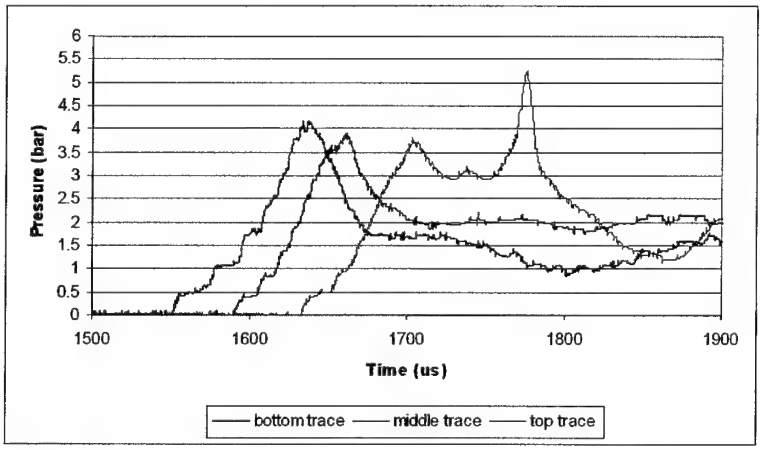


Figure 4.25. Pressure traces with satin

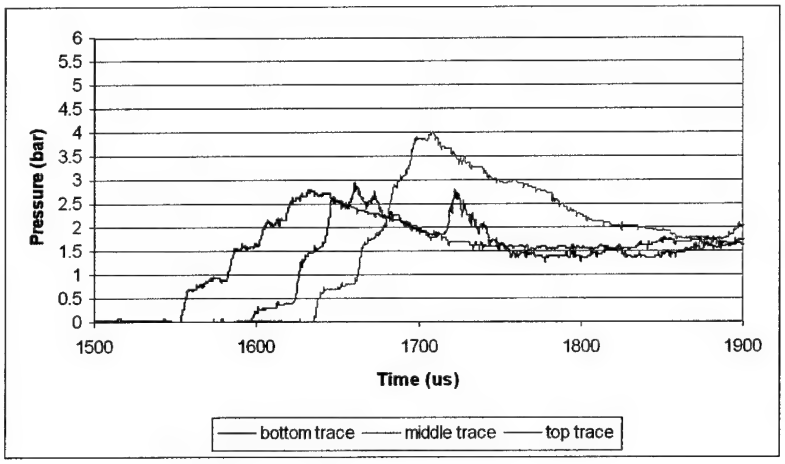


Figure 4.26. Pressure traces with polycotton

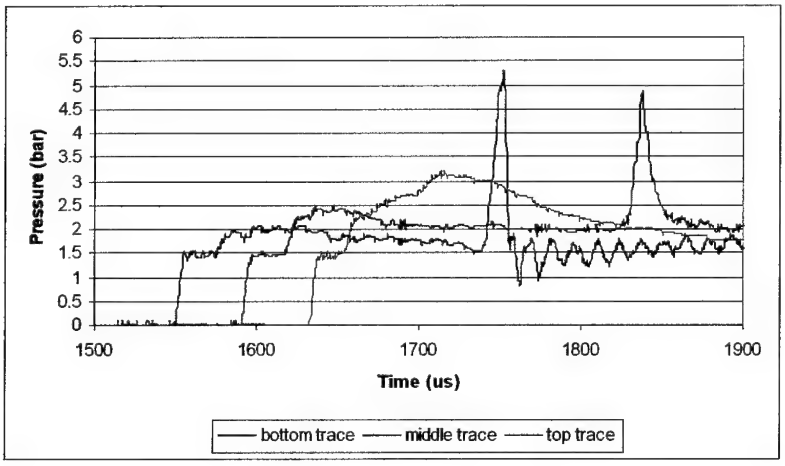


Figure 4.27. Pressure traces with muslin

Pressure Traces at $\theta_w = 70°$

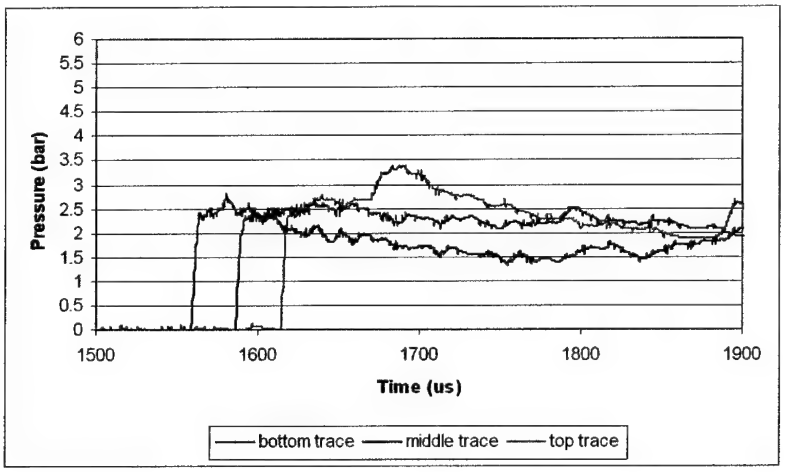


Figure 4.28. Pressure traces with no textile

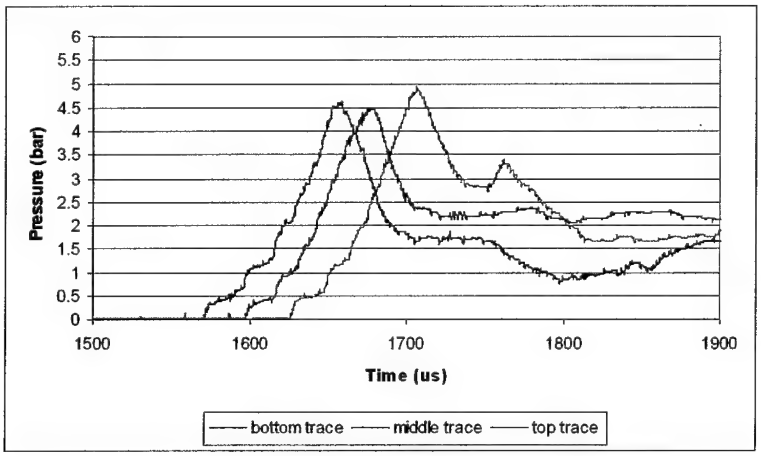


Figure 4.29. Pressure traces with satin

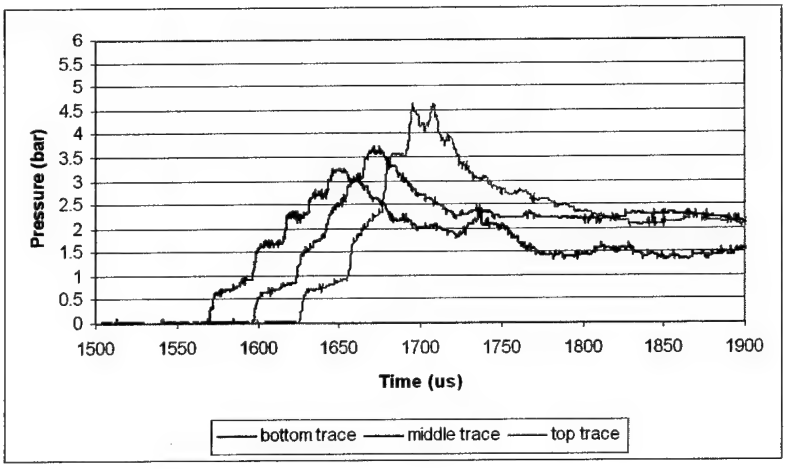


Figure 4.30. Pressure traces with polycotton

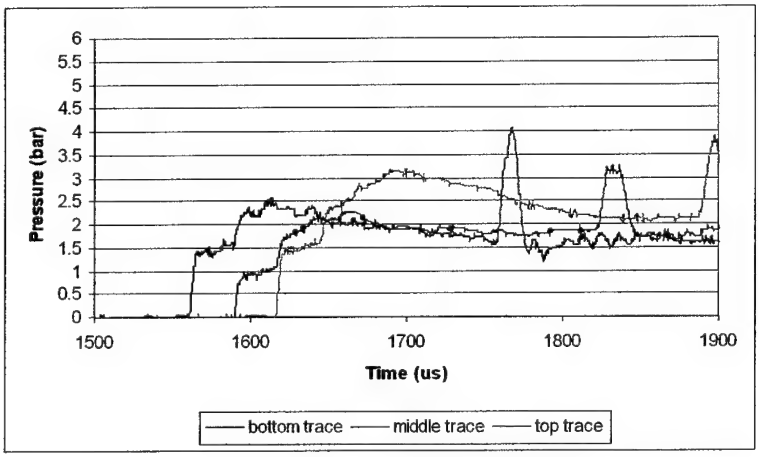


Figure 4.31. Pressure traces with muslin

The sudden high peaks in pressure as seen on the Figures 4.23, 4.27 and 4.31 are due to the direct textile impact with the pressure transducer and are not related to the peak gas pressures given in the graphs above. Graphs indicate that the pressure in the gap between the textile and the plate increases towards the back of the textile.

The majority of the schlieren photographs shown next (Figures 4.32 to 4.38) were conducted without the backing plate, as it is not feasible to measure wave angles and contact surface behavior in the narrow gap between textile and the backing plate. The tests without a backing plate will allow the strength of the transmitted wave and the gas flow through the textile to be determined. For this analysis an Excel spreadsheet was designed that made use of the oblique shock equations. Where the backing plate is present the transmitted wave will reflect as indicated in Figure 4.38. If the strength of the transmitted wave is known the pressure behind this wave once it is reflected can be estimated. Six photographs were made of each textile at a specific angle with the shock wave at different positions along the textile; these are available in the Appendix.

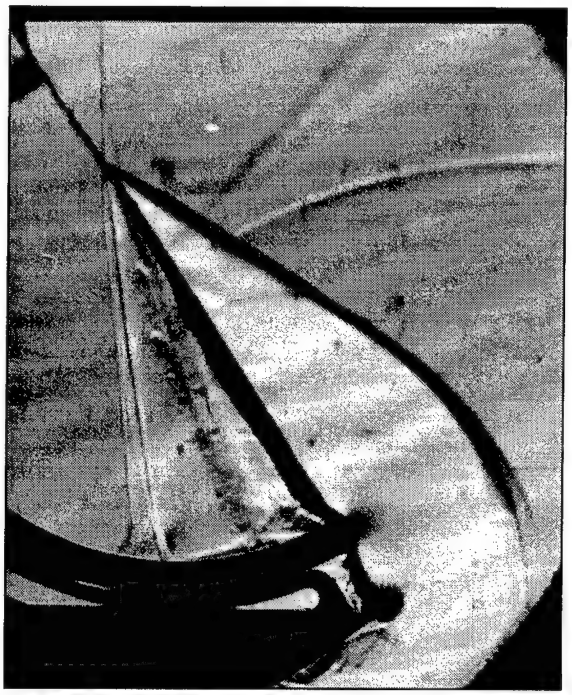

Figure 4.32. Satin, M =1.421, $\theta_w$=60°, T=1650μs

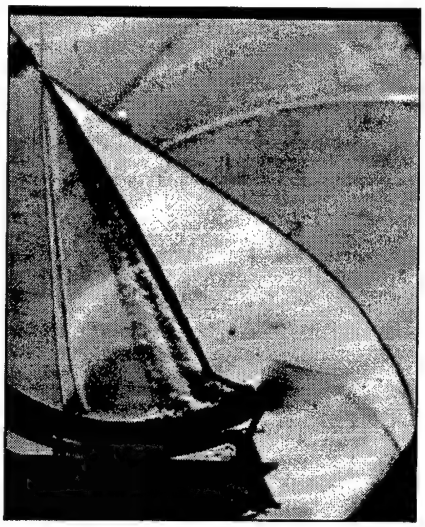

Figure 4.33 Polycotton, M =1.415, $\theta_w$=60°, T=1675μs

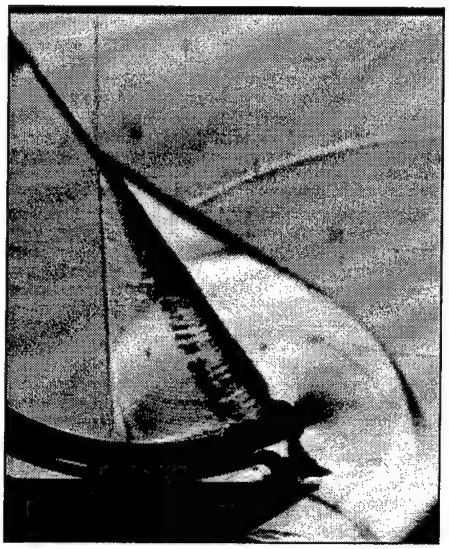

Figure 4.34. Muslin, M =1.424, $\theta_w$=60°, T=1650μs

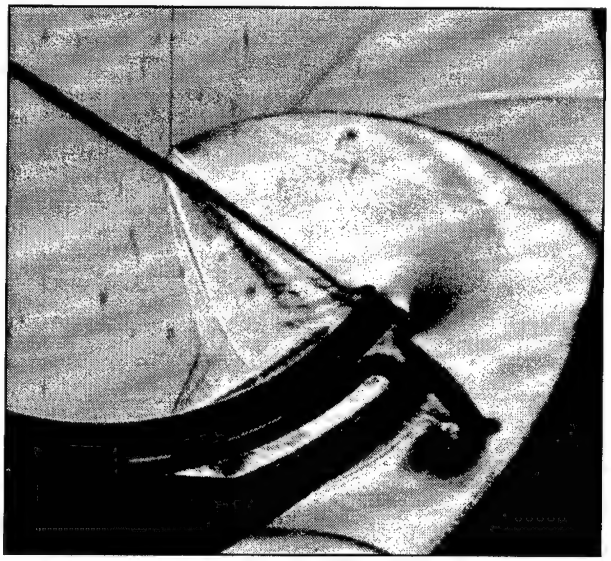

Figure 4.35. Satin, M =1.42, $\theta_w$=35°, T=1585μs

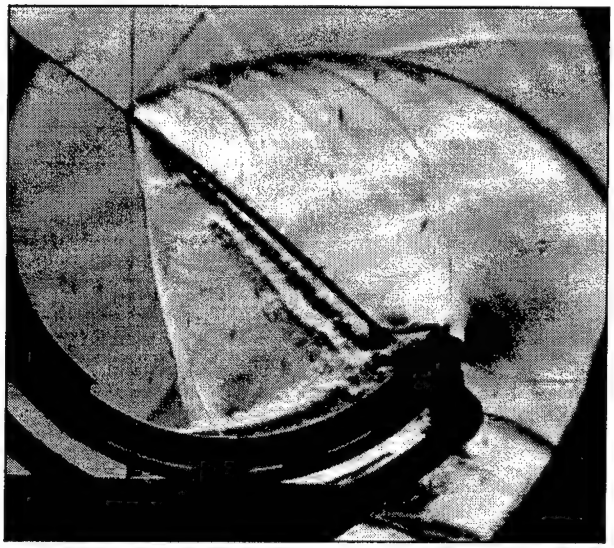

Figure 4.36. Polycotton M =1.409, $\theta_w$=35°, T=1670μs

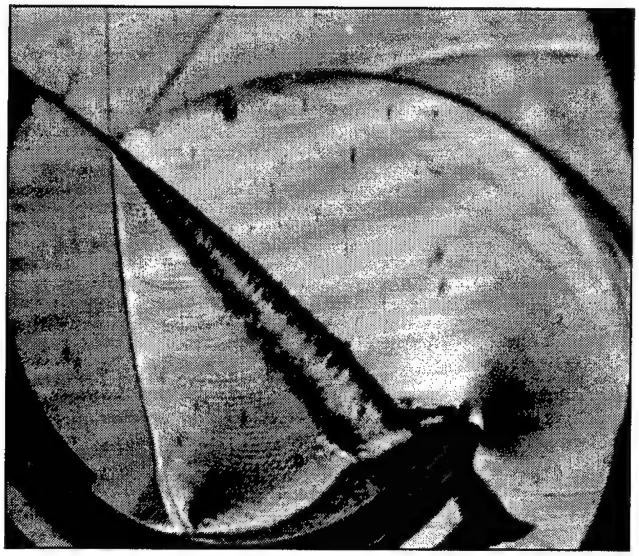

Figure 4.37. Muslin M =1.418, $\theta_w$=35°, T=1680μs

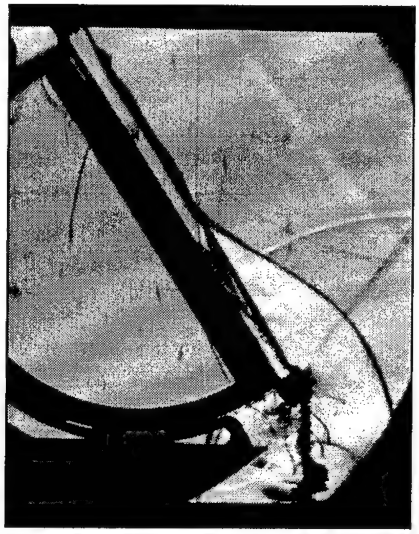

Figure 4.38. Satin with backing plate, M =1.438, $\theta_w$=60°, T=1555μs

Schematic below describes the geometry shown in the Figure 4.38 above.

I – incident shock
R – reflected shock
T – transmitted shock
T-R – transmitted - reflected shock
C – contact surface

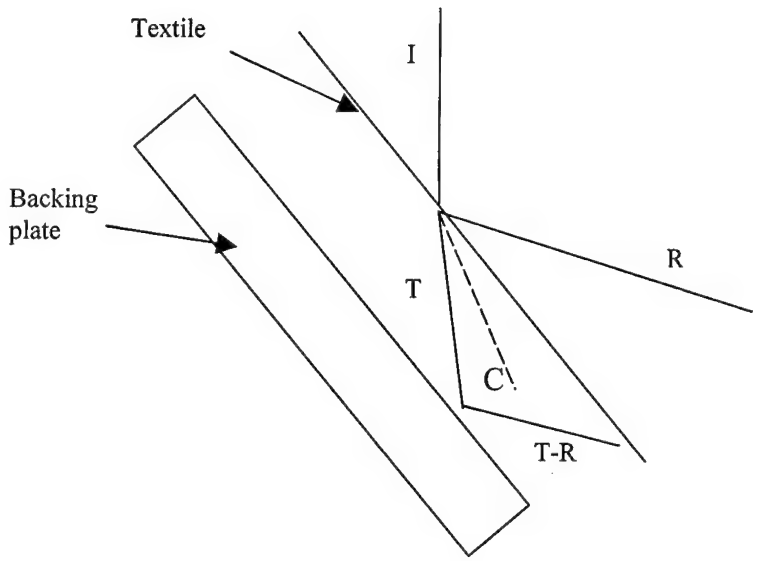

# 5. DISCUSSION

## 5.1. PERFORATED PLATES TEST

All the graphs for these tests (Figures 4.1 to 4.4) follow the same pattern and indicate that amplification reduces as the mass of the sample increases. One can deduce that increase in the mass of the sample, for the same pressure of the shock wave, results in lower acceleration of the sample and therefore, the time to reach the back wall is greater compared to the lighter samples. This increase in time for the sample to reach the back wall, allows the shock wave that is reflected in the air gap between the sample and the back wall, to continuously lose its intensity due to a lesser piston effect and reverse leakage.

Effects of the porosity change on the amplification can be seen by comparing Figures 4.1, 4.2 and 4.3. The higher porosity samples show lower amplification
Increased porosity of the sample indicates that the intensity of the reflected shock wave in the air gap reduces even more once a portion of it is transmitted back through the sample.

The graphs that follow show pressure traces of the individual samples for the four groups against the pressure trace of the shock wave without the sample present.

The graphs show that for the samples with greater mass the highest pressure occurs later than in the case of lighter samples. This indicates that the heavier samples take longer time to reach the back wall of the test section.

## 5.2. MULTIPLE LAYERS OF TEXTILES

From figures 4.5 and 4.6, sample 5 (Kevlar) results in the highest amplification with exception for the five layers at lower Mach number where the sample 4 results in the greatest amplification. All the samples tested resulted in positive amplification that decreased with decreasing Mach number. It is possible that apart from mass, the flexibility of the textile plays a role in amplification. The difference in flexibility of the samples could alter 3D effects of pressure distribution and the air leakage around the sample that occurs during the impact. Kevlar possesses the lowest flexibility amongst the samples tested.

## 5.3. GELATIN BEHIND TEXTILE TESTS

Graphs below compare different number of layers of each textile with the same gelatin used for all tests.

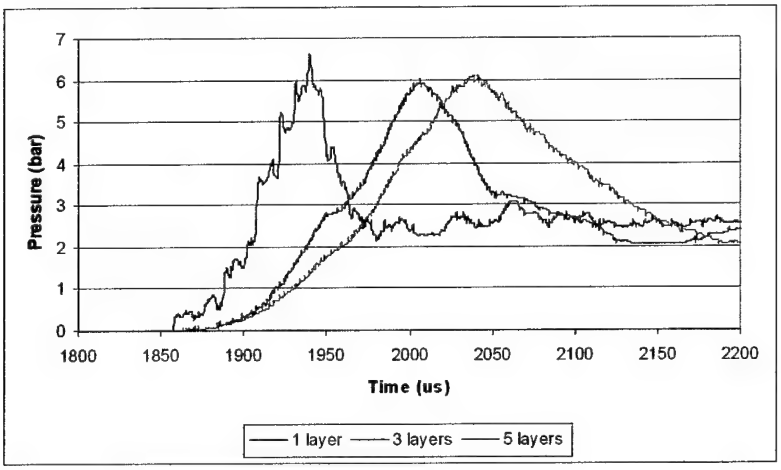


Figure 5.1. Gelatin with satin of 1, 3 and 5 layers

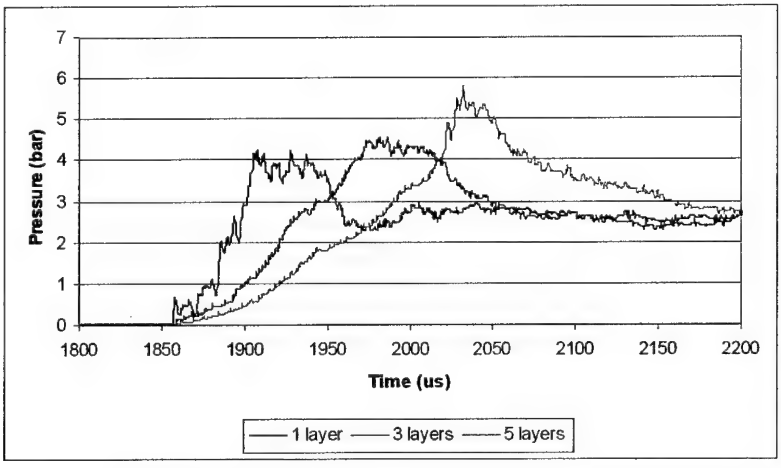


Figure 5.2. Gelatin with polycotton of 1, 3 and 5 layers

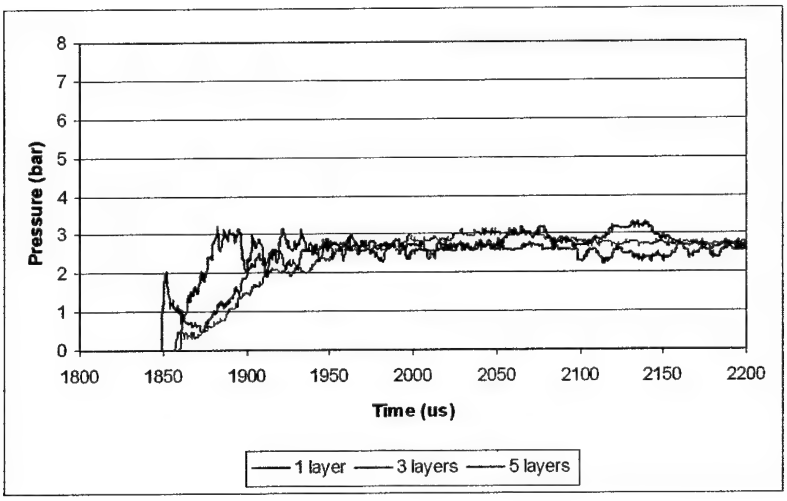


Figure 5.3. Gelatin with muslin of 1, 3 and 5 layers

The presence of gelatin amplifies the peak pressure of the shock by approximately 50%. Figures 4.7 through 4.9 show three samples of gelatin with same size, thickness (10 mm) and gel to water ratio (0.3). Although there is no significant difference in the peak pressure obtained, the overall trace proves that one can not exactly replicate the properties of every sample made. For this reason only one sample was used for tests with the textiles. It should be noted that the gelatin layer does not properly represent the wave penetrating into a layer of body tissue since the test is still backed up with a rigid wall. Any wave propagating through the gelatin is thus reflected raising the pressure. It may have relevance to wave reflection of underlying bone.

Peak pressure in the case of multiple layers does not differ except in the case of the polycotton where greater number of layers amplify the peak pressure. In all the ceases, the use of more layers delays the peak pressure time and prolongs the time for which the overpressure occurs. This can be attributed to the fact that multi-layered textile arrangement is heavier and therefore approaches the wall at the slower speed. Although an addition of layers decreases the permeability, it does not suggest any difference in the cases of satin and muslin. Increase in the peak pressure of polycotton as more layers are added can imply that its permeability approaches the one of satin with a greater number of layers.

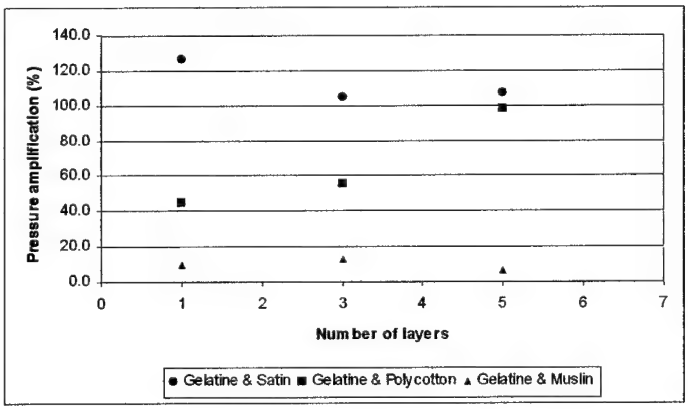


Figure 5.4. Pressure amplification vs number of layers for all 3 textiles

## 5.4. INCLINED TEXTILE TESTS

The pressure traces shown in section 4.4 have been manipulated below to facilitate the analysis of the various factors being investigated. The figures in this section have been produced using only one transducer each, as this is sufficient to show any relevant trends.

Comparisons Between Textiles (Middle Transducer)

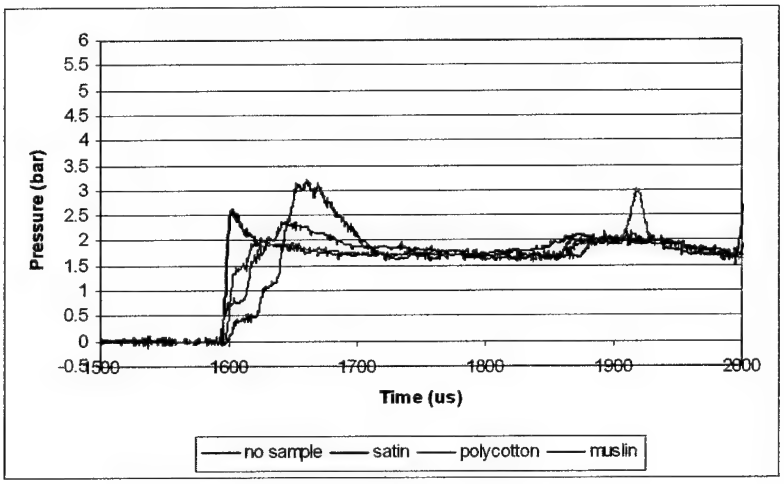


Figure 5.5. Pressure traces at $\theta_w = 45°$

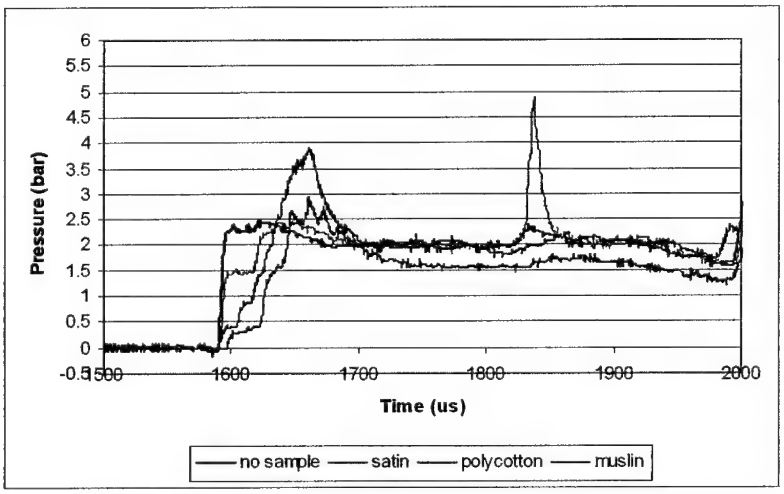


Figure 5.6. Pressure traces at $\theta_w = 60°$

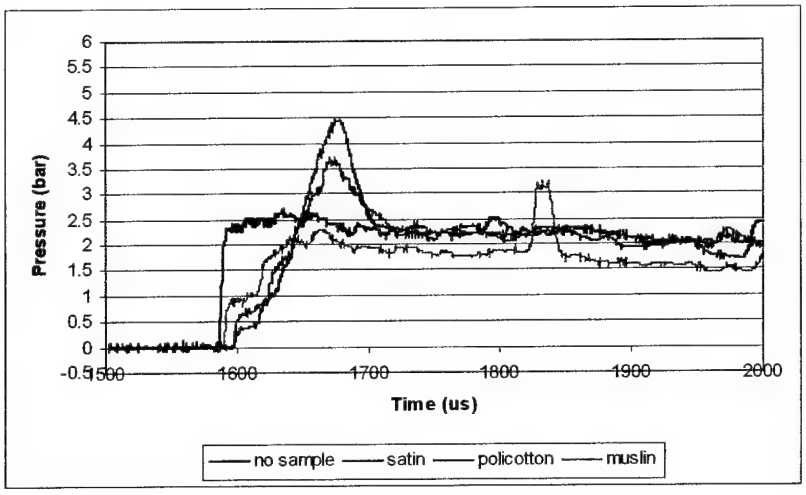


Figure 5.7. Pressure traces at $\theta_w = 70°$

Comparisons Between Angles (Bottom Transducer)

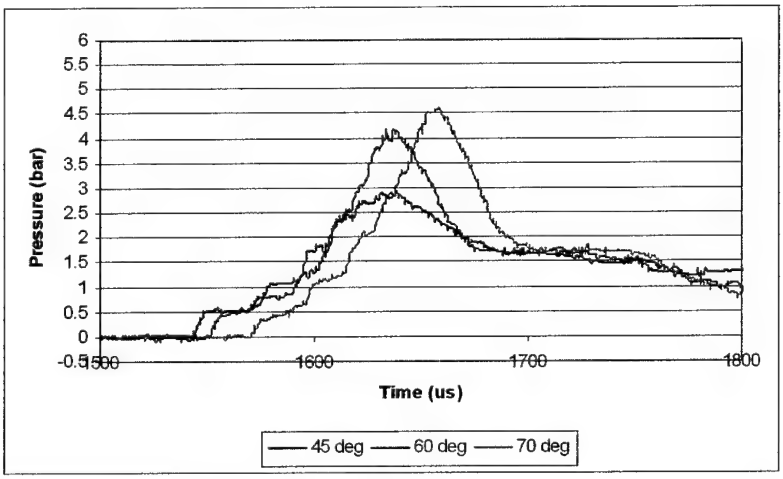


Figure 5.8. Pressure traces with satin

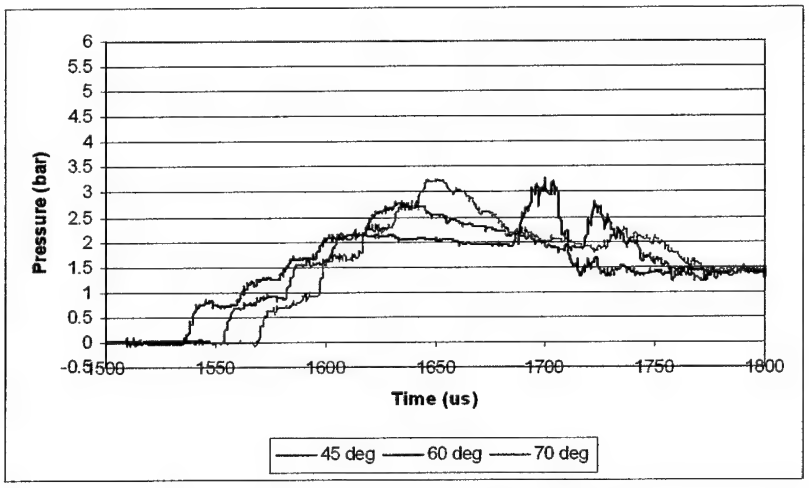


Figure 5.9. Pressure traces with polycotton

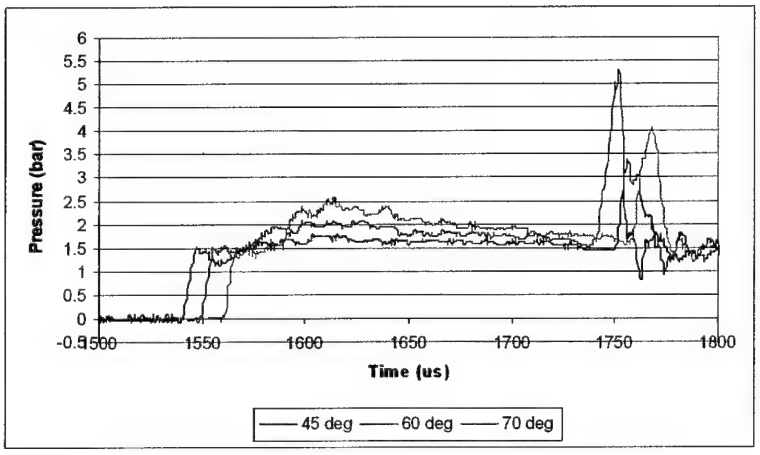


Figure 5.10. Pressure traces with muslin

### 5.4.1. Investigation of Pressure Amplification Results

At each reflecting wall angle, tests were run with each textile attached as well as with no textile attached. This enabled a comparison between each situation to be established.

For each test, there were three active transducers in the inclined plate. This was to ensure that the peak pressure investigated would represent the entire textile. An average of the peak pressure readings from each transducer was then obtained. A further reason for this procedure was to identify any anomalies in the readings. The 90° data was obtained from tests of Hattingh and Skews (2001).

The percentage pressure amplification, $P_{amp}$, is defined as the increase in peak pressure, due to the presence of the textile (as compared to the peak pressure with no textile). The amplification is expressed as a percentage and calculated as follows:

$$P_{amp} = \frac{P_{tex} - P_{none}}{P_{none}} \times 100$$

Where: $P_{tex}$= average peak pressure when a textile is present
$P_{none}$= average peak pressure when no textile is present

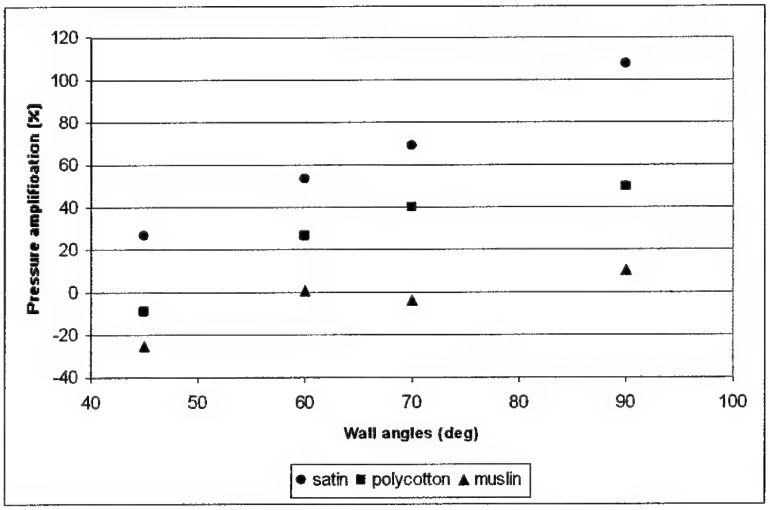


Figure 5.11. Pressure amplification versus wall angle

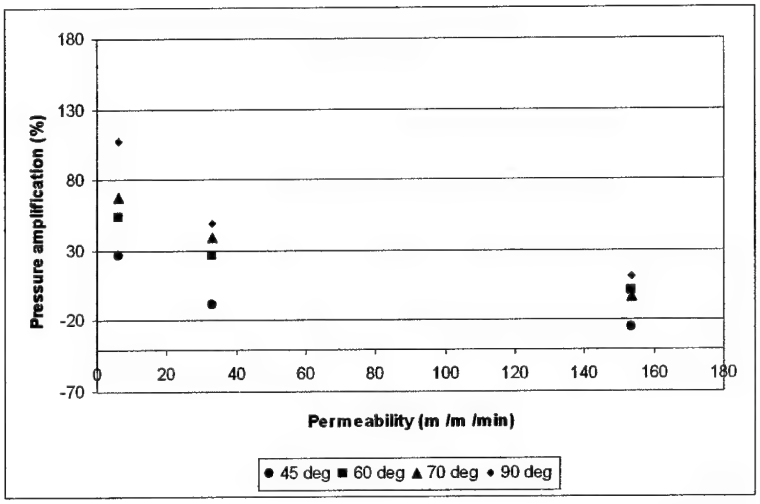


Figure 5.12. Pressure amplification versus Permeability

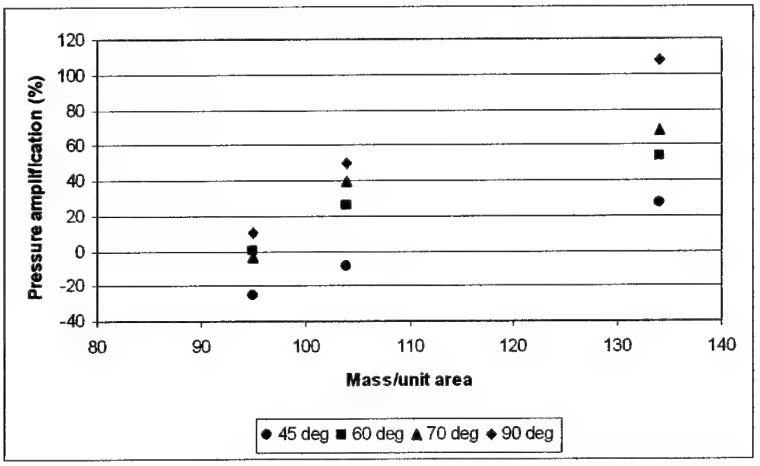


Figure 5.13. Pressure amplification versus Mass/Area

### 5.4.2. Discussion of Pressure Traces

The profiles of the individual pressure traces experienced by the inclined backing plate during testing were analyzed to determine the physical processes that occur when a shock wave interacts with a textile.

Figures 4.20 through 4.31 show the pressure traces recorded by the computer. These figures each show the traces obtained from the bottom, middle and top transducers located in the inclined backing plate. The three traces in each figure all follow similar trends being shifted along the time axis showing that the shock wave impacts the bottom transducer first followed by the middle and then top transducer.

At a reflecting wall angle ($\theta_w$) of 45° as well as in the few cases of higher angles the peak pressures for each textile increase from the bottom trace to the top trace indicating that the transmitted shock wave gains strength as it moves up the inclined wall. As the shock wave is propagating further along the textile it accelerates the textile towards the back wall. The motion of the textile creates the compression waves that propagate towards the back wall. These compression waves gain strength further down the back plate and aid the intensity of the transmitted wave towards the end of the backing plate.

The traces exhibit a stepped profile which resembles the mechanism of the shock wave impact with the textile in the vertical position ($\theta_w = 90°$) described by Hattingh and Skews (2000). The stepped pressure rise is due to the transmitted shock wave reflecting off the plate and the textile in the gap between the two.

The explanation of the phenomenon described above is illustrated in Figure 5.14. This Figure shows the bottom pressure trace with polycotton attached at $\theta_w = 60°$. The stepped profile can be seen for all textiles although muslin displays a noticeably less staggered profile than satin and polycotton. Muslin possesses a greater permeability than other two textiles which results in fewer reflections in the textile-wall gap. As the shock wave re-reflects off the textile more that once a greater portion of the shock is transmitted through the textile resulting in a constant decrease of the strength of the reflecting shock.

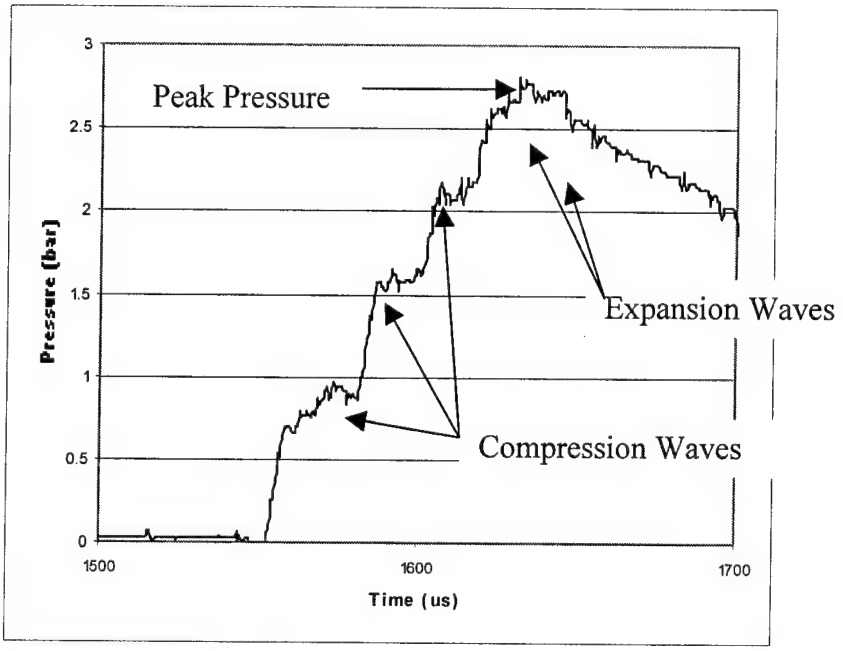


Figure 5.14. Pressure trace for polycotton at $\theta_w = 60°$

When the incident shock wave impacts the textile, part of it is reflected back upstream and part is transmitted through the textile. The first step on the pressure trace is thus the transmitted wave hitting the inclined plate. This transmitted wave then reflects back upstream towards the textile whereupon part is again reflected and transmitted. These reflections give rise to the stepped appearance of the pressure traces.

While these reflections are taking place, the textile begins moving towards the backing plate as it is being accelerated by the shock impact, creating compression waves (refer to Figure 5.14) that propagate in the direction of the backing plate. The movement of the textile can be seen in the schlieren photographs. The time between successive pressure steps decreases thus confirming the movement of the textile due to the shortening gap between it and the plate. The increase in strength of each successive shock wave decreases until a peak pressure is reached.

Figures 5.5 through 5.7 show comparisons between the pressure traces of each textile at the three reflecting wall angles. It is evident from these pressure traces that the transmitted shock strengths vary significantly for the three different textiles and that the peak pressure increases with increasing wall angle. Satin shows the strongest shock wave and muslin the weakest.
Figures 5.8 through 5.10 show that the peak pressure increases as the reflecting wall angle increases.

Pressure amplification decreases as the permeability increases and increases as the mass/area increases as shown in Figures 5.12 and 5.13. The effect of permeability is expected since an infinite permeability corresponds to a situation where no material is present, whereby clearly no amplification exists.
The amplification is greatest for satin followed by polycotton and then muslin. At $\theta_w$=45° the percentage amplifications for satin, polycotton and muslin are respectively 27%, -9% and –25%. This amplifications increases at higher angles, so that at $\theta_w$=70° they are 68%, 40% and -4%and for the head on tests ($\theta_w$=90°) they are 107%, 50% and 10%. Muslin thus actually attenuates the shock strength.

## 5.5. Discussion of Schlieren Photographs

At a wall angle of 60,° the shock wave interactions with all three textiles correspond to regular reflection and for angles of 35° correspond to Mach reflection, as is the case with a solid incidence surface. At an angle of 60° the angle of the transmitted shock increases as the permeability increases. This is expected since increase in permeability offers less resistance to the movement of the shock through the textile; this result correlates with results obtained by Skews and Takayama (1995) in their study on shock interactions with inclined grids. This relationship is also evident for a wall angle of 35°.
At a wall angle of 35° satin and polycotton reveal that Mach refraction has been achieved, as is the case with a solid surface. The Mach reflection of the polycotton is not as strong as that of the satin. Muslin however, does not reveal the Mach reflection at all. This is to be expected due to the larger gas inflow through the surface. Transition between regular and Mach refraction is clearly dependent on permeability of the incident material. The transition between the regular and the Mach reflection usually occurs below 45°

The schlieren photographs of muslin at both reflecting wall angles show lines of vortices between the textile and the transmitted and reflected shock waves. The vortices are visible in the muslin images, as the permeability is highest. These vortices correspond to those obtained by Skews and Takayama (1995) in the interaction of shock wave with perforated surface as shown in Figure 5.15 below.

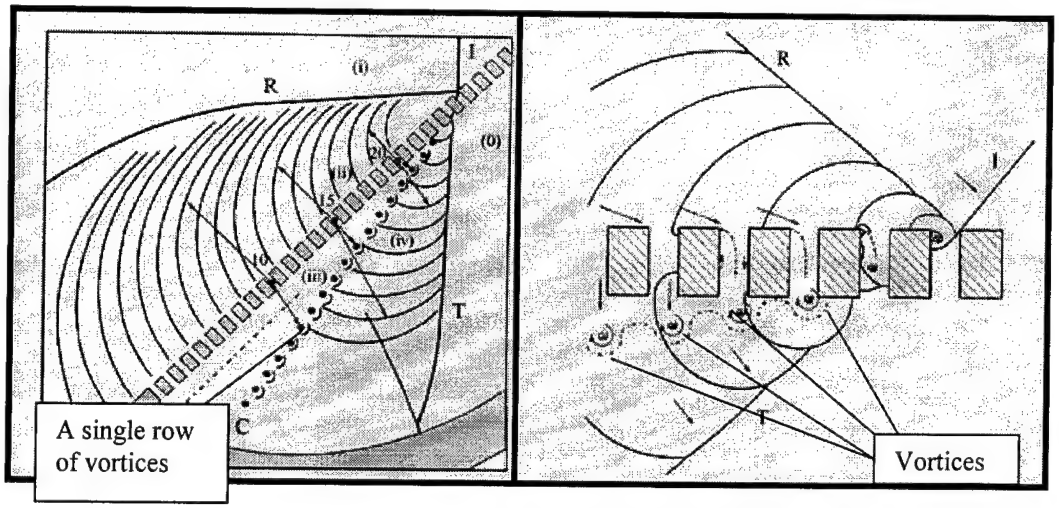


Figure 5.15. Characteristics of the flow through a slit wedge

Six photographs were made of every textile at the specific angle each with different position of the incident shock along the textile. Using equations for oblique shock waves an Excel spreadsheet was designed to calculate all the relevant flow states and the Mach numbers. The measurements of angles of all six photos were entered in to the spreadsheet and once the relevant data were obtained they were averaged for a particular case. The spreadsheet was also designed to calculate the strength and the pressure of the transmitted shock once it reflects off the back surface.

From measurements of angles the second row of vortices (see Figure 5.16 overleaf) are very close to the deflection angles obtained from the spreadsheet of the flow after transmitted shock. This would indicate that the second row of vortices represents the flow through the textile.

The first row of vortices can then be attributed to the edge effects being the flow passing around the edge of the textile (between the textile and window of the test section).

The motion of the textile that can be seen from the schlieren photos complicates matters. The calculations follow the scheme given by Skews and Takayama (1995), which assumes a rigid plate. Measurements of textile movements would be needed in order to refine the calculations.

One could try and suppress the edge effect by suspending the textile on the frame and block the shock from passing around the edge of the textile, however this would not be a realistic representation, as the frame would limit textile movement. Figure 5.16 overleaf describes the interaction between the textile and the shock wave at an angle.

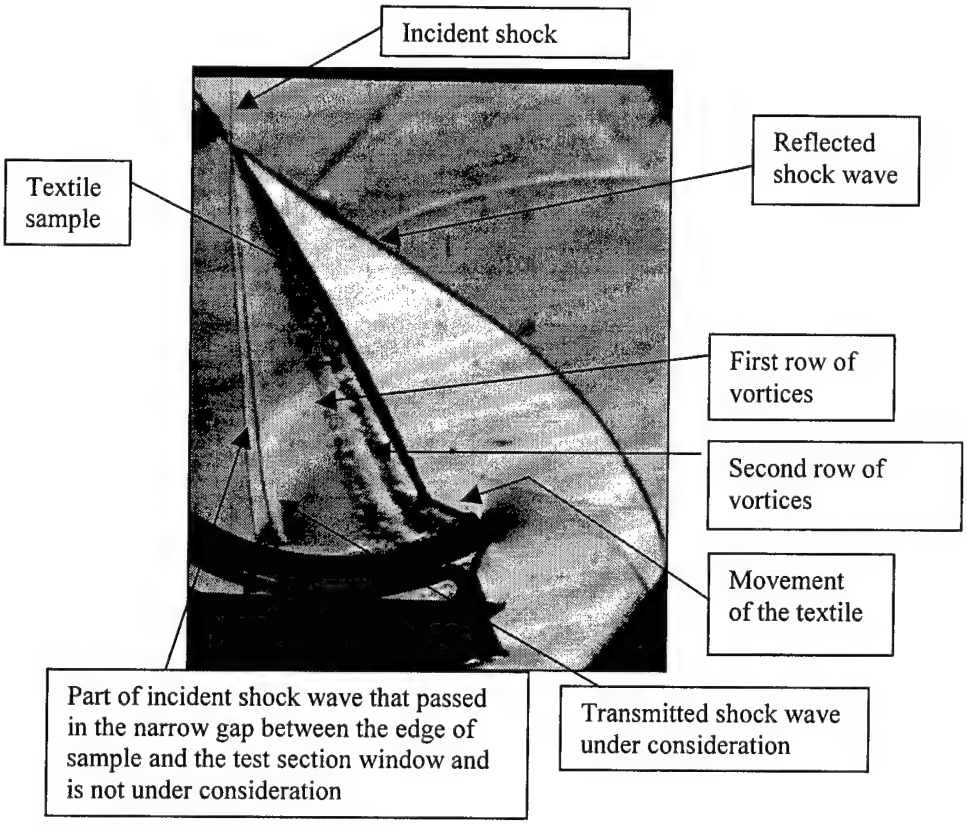


Figure 5.16. Interaction of the shock wave with the textile sample at 60° angle

The Figure 5.17 below closely describes the pseudo steady flow through the shock as the incident shock reflects off the textile.

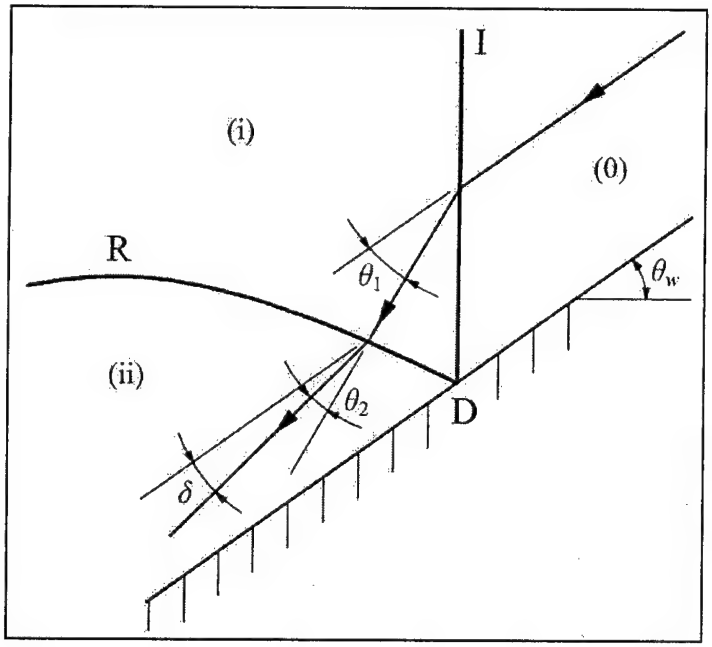


Figure 5.17. Regular reflection over a surface with inflow, in a frame of reference fixed in the point of reflection

In the case of an impermeable material the total deflection angle labeled δ on the Figure 5.17 above would be zero as the reflected shock deflects the flow to be parallel to the reflecting surface. In the case of the permeable material some flow is allowed to pass through the surface and the deflection angle is not zero but a greater number depending on the permeability of the surface. The results obtained from the schlieren photographs support this mode. Table 5.1 below and the Figure 5.18 overleaf show the total deflection angle against the permeability of the textile for the 60° angle.

Table 5.1. Total flow deflection angle against permeability of textile at 60° incidence angle

| Textile material | Permeability [m^3/m^2/min] | Total deflection angle [deg] |
|---|---|---|
| SATIN | 6 | 0.883 |
| POLYCOTTON | 32.9 | 2.293 |
| MUSLIN | 153.6 | 4.405 |

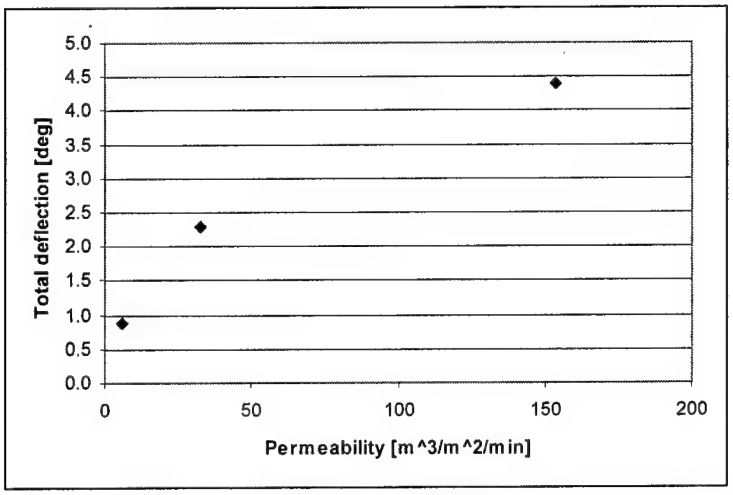


Figure 5.18. Total deflection of the flow against the permeability of the textile for the incidence angle of 60°

Figure 5.19 below describes the flow on both sides of the textile. Velocities with asterisks are in a frame fixed in the laboratory frame of reference, and the corresponding velocities without asterisks in a frame fixed in the point D, which is the point of contact of the incident shock and the textile. $V_D$ is the velocity of the point of reflection, D, relative to the plate.

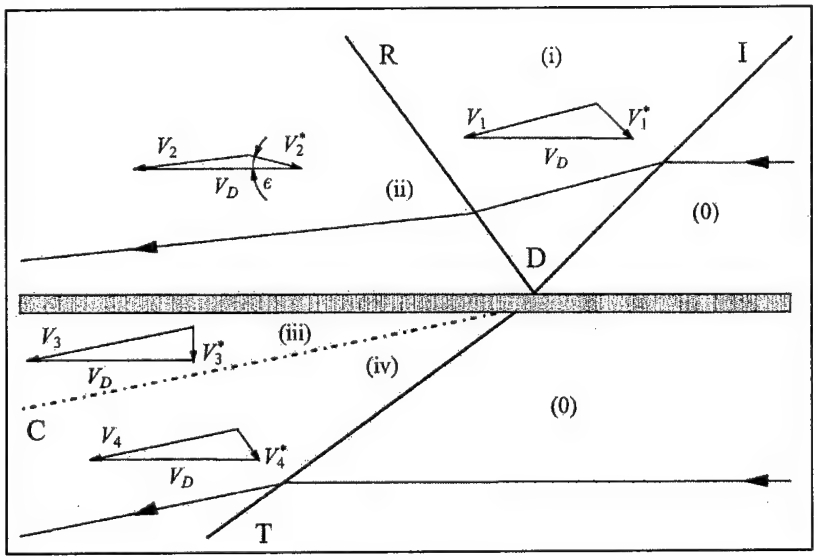


Figure 5.19. Flow geometry with velocity triangles connecting the frames of reference

$V^*_1$ and $V^*_4$ are normal to the incident and transmitted shocks, being the induced velocity behind a plane wave moving into ambient air. The magnitude and direction (ε) of $V^*_2$ are the main parameters to be determined from the experimental results as they quantify the inflow in to the textile. The above Figure 5.19 describes the velocity $V^*_3$ to be perpendicular to the perforated surface which is the case of the Skews and Takayama (1995) analysis. In that case the perforated surface did not move relative to the test section and it can be assumed that the flow was guided through the slits in the surface.
However in the case of the flow through a textile one can not assume that velocity $V^*_3$ is perpendicular to the textile due to its movement and a more elaborate analysis based on further measurements would be required.

Tables 5.2 and 5.3 and Figures 5.20 and 5.21 show the values of the $V^*_2$ and the angle ε for varying textile air permeability.

Table 5.2. $V^*_2$ and ε angle for different textile material and incident angle of 60°

| Textile material | Permeability [m^3/m^2/min] | Epsilon angle [deg] | V*2 [m/s] |
|---|---|---|---|
| SATIN | 6 | 4.136 | 173.284 |
| POLYCOTTON | 32.9 | 8.875 | 174.736 |
| MUSLIN | 153.6 | 14.662 | 163.600 |

Table 5.3. $V^*_2$ and ε angle for different textile material and incident angle of 35°

| Textile material | Permeability [m^3/m^2/min] | Epsilon angle [deg] | V*2 [m/s] |
|---|---|---|---|
| SATIN | 6 | 19.795 | 243.684 |
| POLYCOTTON | 32.9 | 21.567 | 237.610 |
| MUSLIN | 153.6 | 23.016 | 229.118 |

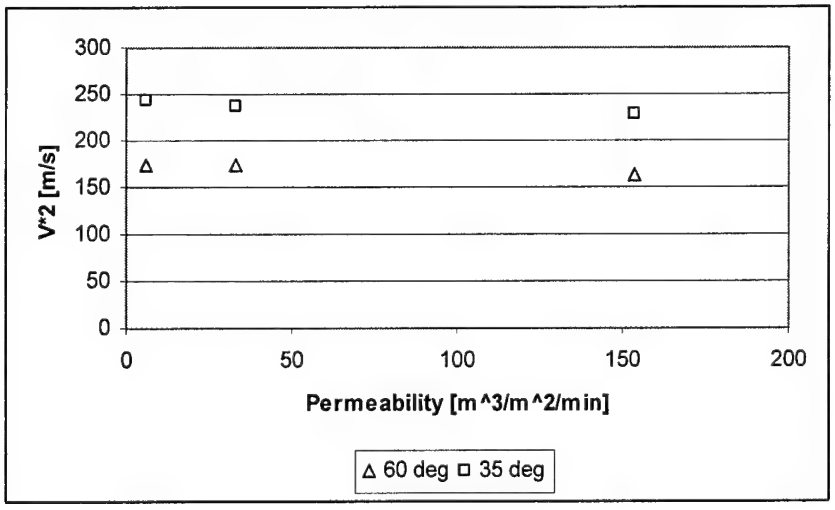


Figure 5.20. $V^*_2$ against permeability of textiles for incident angles of 60° and 35°

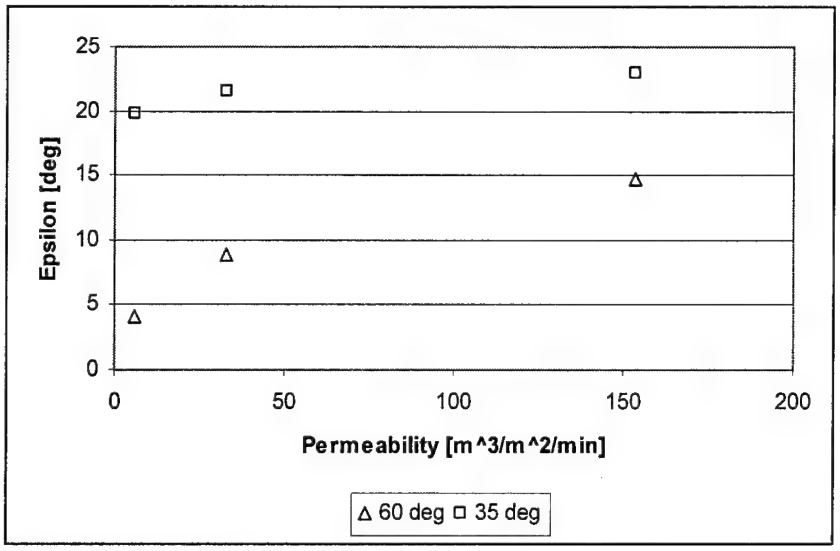


Figure 5.21. ε (Direction of $V^*_2$) against permeability of textiles for incident angles of 60° and 35°

$V^*_2$ does not change significantly with the permeability but ε increases with permeability proving that the inflow is greater for higher permeable textiles, as expected.

Table 5.4 below and the Figure 5.22 overleaf present the predicted pressures that would occur once the transmitted shock reflects of the impermeable plate as is the case of the pressure traces obtained from an experiments done with textile and shock interaction at an angle.

Table 5.4. Pressures of the transmitted reflected shock predicted from the schlieren photographs of textile at 60° angle

| Textile material | Permeability [m^3/m^2/min] | Pressure above atmospheric [bar] |
|---|---|---|
| SATIN | 6 | 0.584 |
| POLYCOTTON | 32.9 | 0.843 |
| MUSLIN | 153.6 | 1.680 |

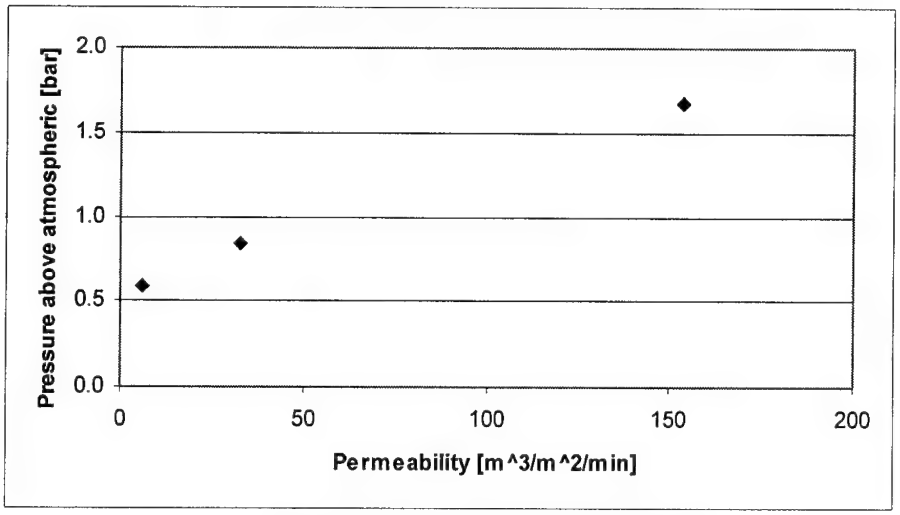


Figure 5.22. Predicted pressures of transmitted reflected shock for the textile at 60° angle against the permeability of the textile

Schematic below describes the geometry

I – incident shock
R – reflected shock
T – transmitted shock
T-R – transmitted - reflected shock
C – contact surface

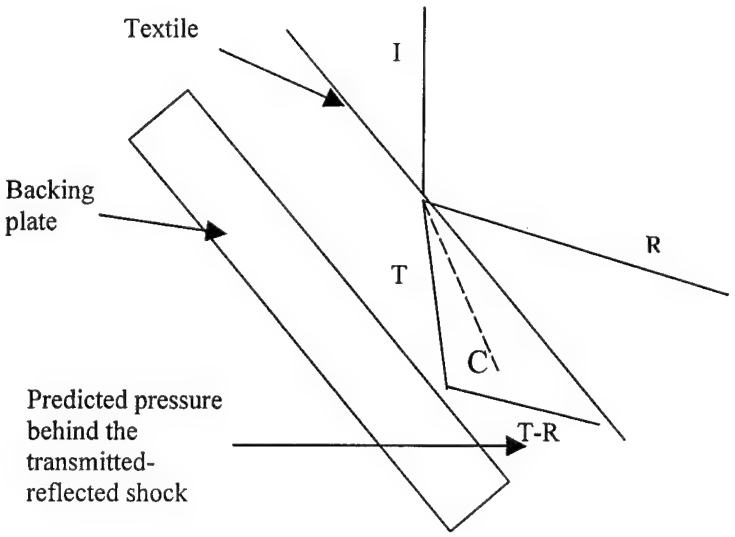

Comparing Table 5.4 and Figure 5.22 with Figures 5.8 to 5.10, the pressure values that were predicted using the spreadsheet and the measured shock angles from the schlieren photos compare well with the measured values. These pressures occur once the transmitted shock wave reflects off the impermeable plate. In the case of muslin at an incident angle of 35° the transmitted shock is of too high a value for regular reflection to take place and Mach reflection must occur on the backing plate. However this case is complicated to analyze and the pressure values are not available.

The Figure 5.22 clearly shows that the pressure increases with the increase in permeability of the textile, however this is only the first increase in pressure after the reflection of the transmitted shock. Further interactions of the transmitted reflected shock that weakens due to constant interaction with the textile and the textile movement towards the back wall complicates matter and makes it very difficult to predict the total pressure rise.

# 6. Conclusions and Recommendations

Heavier impermeable textiles increase pressure amplification due to a shock wave as their mass increases. Pressure amplifications up to 400% can be expected. However if the heavier textile materials posses a higher air permeability as in the case of the perforated plates the peak pressure will significantly drop.
Greater number of layers of the same textile behave in similar manner as one layer. Although the results show significant difference between one and five layers of a particular textile, the pattern of peak pressure increase with increase in mass of five layers is similar as in the case of one layer.
Three-dimensional effects such as the air leakages around the textile edges as well as the shape that the textile acquires up on impact can greatly affect the results as discussed in the previous section. Restraining the textiles fully in the test section would not however result in a real life case.

In comparison with the results obtained by Hattingh and Skews (2001) the gelatin does not significantly alter the pressure values. Different number of layers of the same textile still results in the same peak pressure. The presents of more layers delays the peak pressure time as well as prolonging the time for which the overpressure occurs.
Since the test with gelatin backed up by a rigid wall does not properly represent the wave penetrating into a layer of body tissue other methods could be used such as suspending a layer of gelatin freely in the test section with a pressure transducer fixed in it. However there is a risk of damaging the transducer, as it would not be restrained.

Form the interaction of shock wave with the textile at an angle it is clear that the head on case will result in a highest pressure. The pressure rise having a stepped profile for the textile at an angle to the incident shock resembles the one from the head on case.
Due to a significant difficulty in identifying the transmitted shock through the textile due to a leakage affects a better means of fixing the textile sample to its stationery frame is recommended although one must be careful as it could lead to a three dimensional case.

# 7. References


Cooper, G.J. and Taylor, D.E.M. (1989) Biophysics of impact injury to the chest and abdomen, *Journal of the Royal Army Medical Corps.*

Epps, H.H. and Leonas, K.K. (1997) The relationship between porosity and air permeability of woven textile fabrics, *Journal of Testing and Evaluation,* vol. 25, no 1.

Fung, Y.C. Yen, R.T., Tao, Z.L. and Liu, S.Q. (1988) A hypothesis on the mechanism of trauma of lung tissue subjected to impact load, *Journal of Biomechanical Engineering,* vol. 110.

Gibson, P.W. (1995) Amplification of air shock waves by textile materials, *Journal of the Textile Institute,* vol. 86, no. 1.

Huller, T., Bazini, Y. (1970) Blast injuries of the chest and abdomen, *Archives of Surgery,* vol. 100.

Philips, M.D., Mundie, T.G., Yelverton, J.T., Richmond, D.R. (1988) Cloth ballistic vest alters response to blast, *The Journal of Trauma,* vol. 28, no. 1.

Yen, R.T., Fung, Y.C. and Liu, S.Q. (1988) Trauma of lung due to impact load, *Journal of Biomechanics,* vol. 21., no. 9.

Young, A.J., Jaeger, J.J., Phillips, Y.Y., Yelverton, J.T. and Richmond, D.R. (1985) The influence of clothing on human intrathoracic pressure during airblast, *Aviation, Space and Environmental Medicine,* vol. 56.

Van Bree, J.L.M.J. and Fairlie, G. (1999) Compression wave experimental and numerical studies in gelatin behind armor, *Proceedings of the 18$^{th}$ International Symposium on Ballistics.*

Zuckerman, S., Krohn, P.L. and Whitteridge, D. (1942) Physiological effects of blast, *The Lancet.*

Hattingh, T.S. and Skews, B.W. (2001) Experimental investigation of the interaction of shock waves with textiles, *Proceedings of the 22$^{nd}$ International Symposium on Shock Waves.*

Ben-Dor, G. (1992) Shock Wave Reflection Phenomena, Springer-Verlag, New York.

Skews, B.W. and Takayama, K. (1996) Flow through a perforated surface due to shock-wave impact, Journal of Fluid Mechanics, vol. 314, pp. 27-52

# APPENDIX A

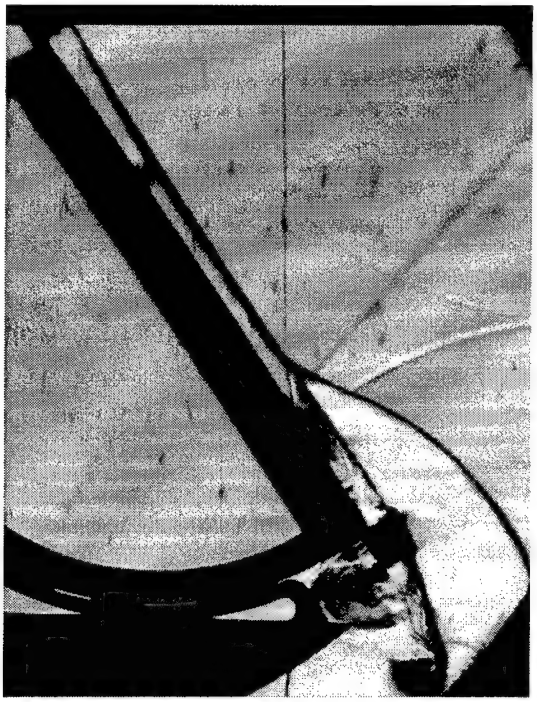

Figure A 1 Satin, M =1.423, $\theta_w$=60°, T=1550μs

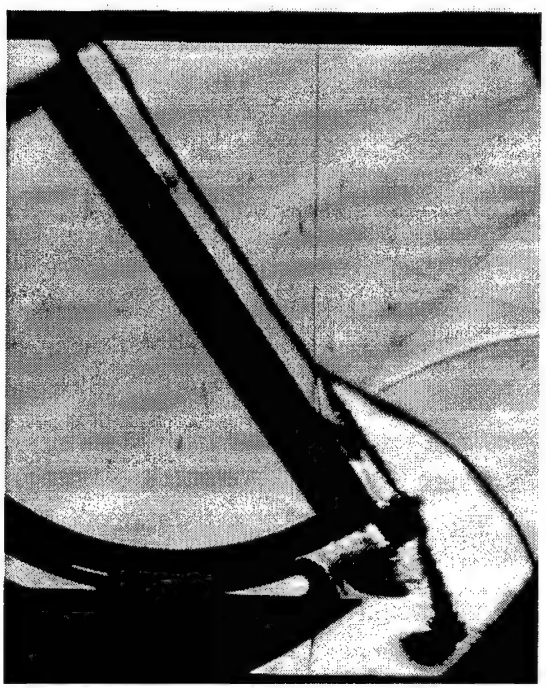

Figure A 2 Satin, M =1.415, $\theta_w$=60°, T=1550μs

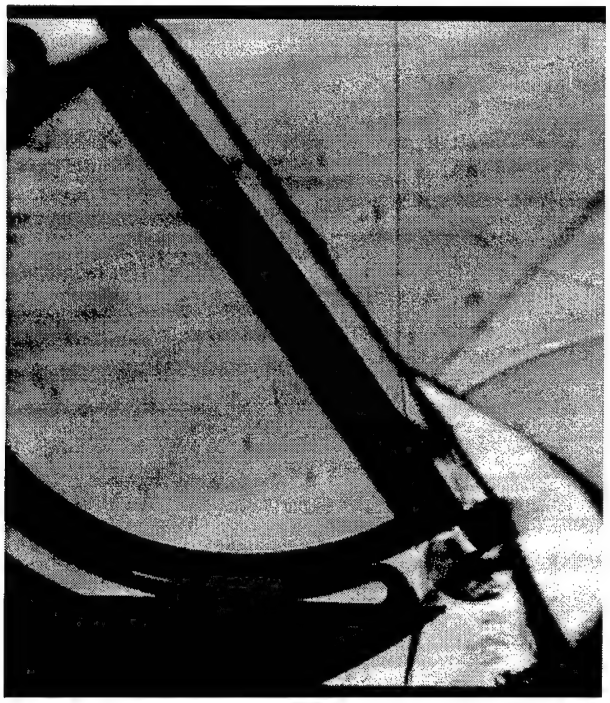

Figure A 3 Satin, M =1.413, $\theta_w$=60°, T=1545μs

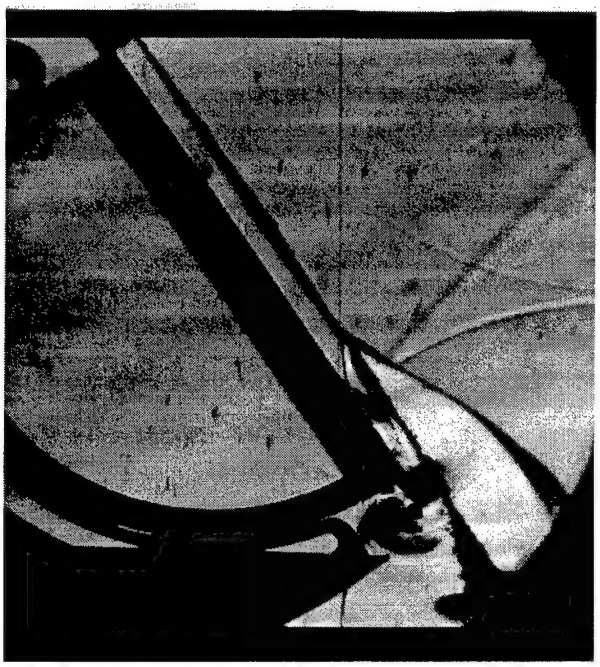

Figure A 4 Satin, M =1.417, $\theta_w$=60°, T=1545μs

Figure A 5 Satin, M =1.438, $\theta_w$=60°, T=1555μs

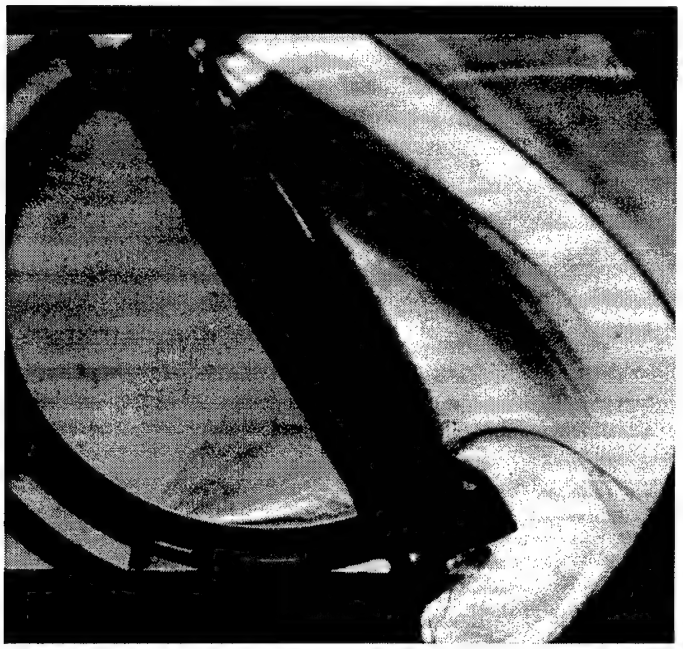

Figure A 6 Satin, M =1.411, $\theta_w$=60°, T=1539μs

Figure A 7 Satin, M =1.41, $\theta_w$=60°, T=1559μs

Figure A 8 Satin, M =1.409, $\theta_w$=60°, T=1512μs

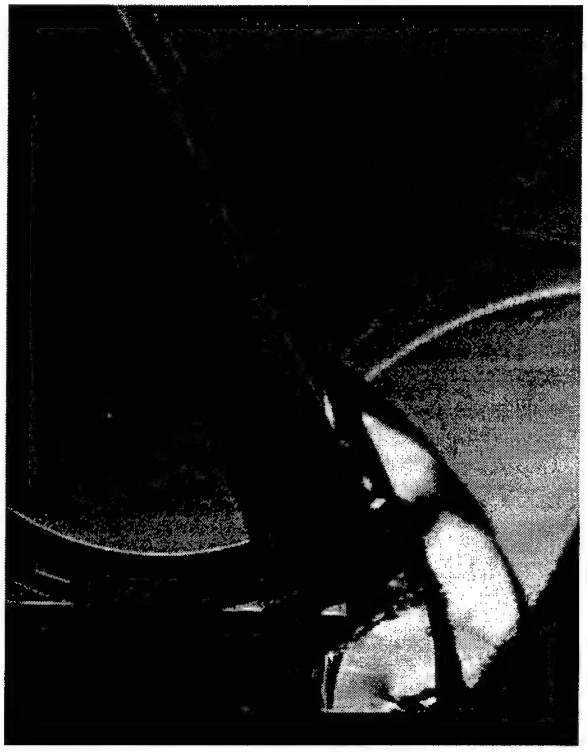

Figure A 9 Satin, M =1.415, $\theta_w$=60°, T=1539μs

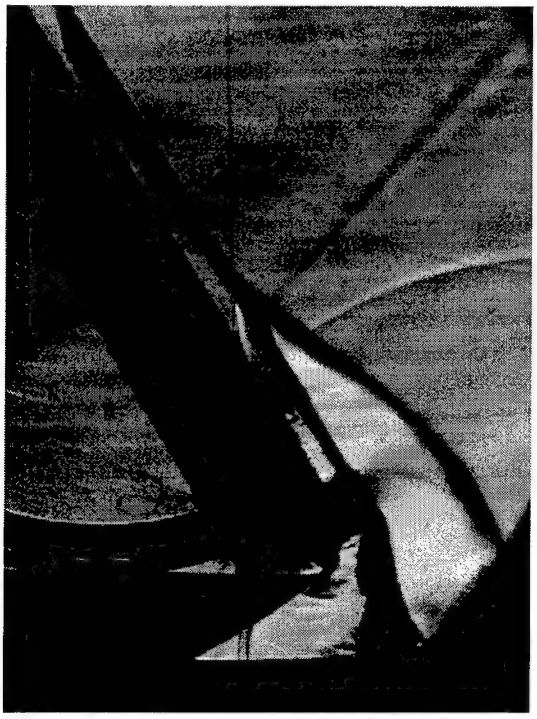

Figure A 10 Satin, M =1.412, $\theta_w$=60°, T=1559μs

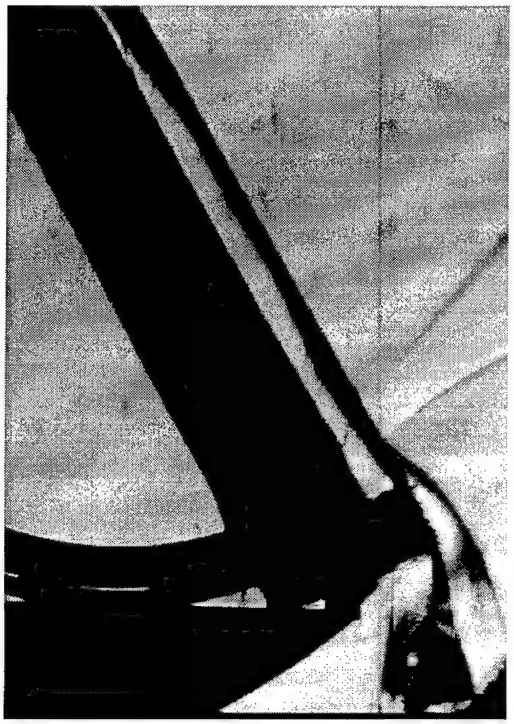

Figure A 11 Satin, M =1.42, $\theta_w$=60°, T=1512μs

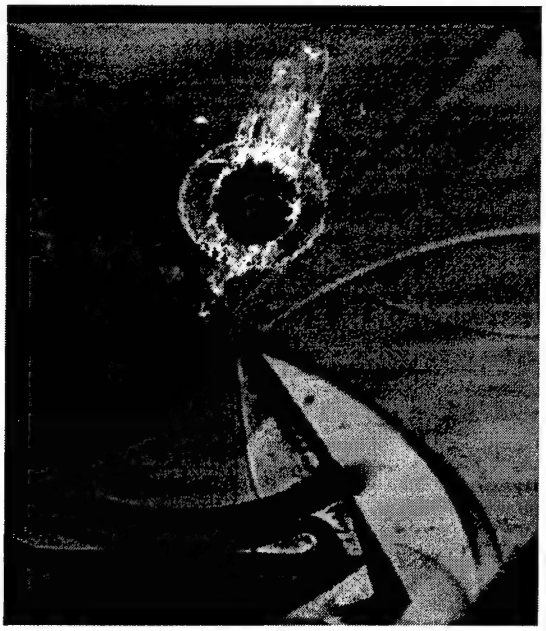

Figure A 12 Polycotton, No backing plate, M =1.422, $\theta_w$=60°, T=1590μs

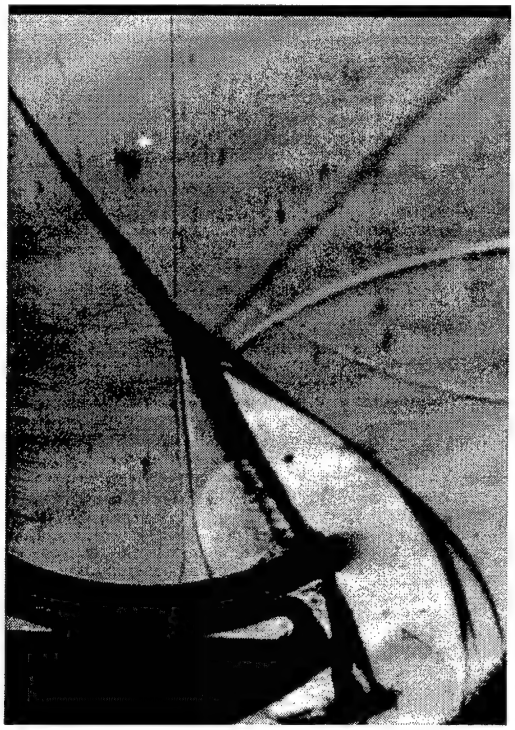

Figure A 13 Polycotton, No backing plate, M =1.424, $\theta_w$=60°, T=1600μs

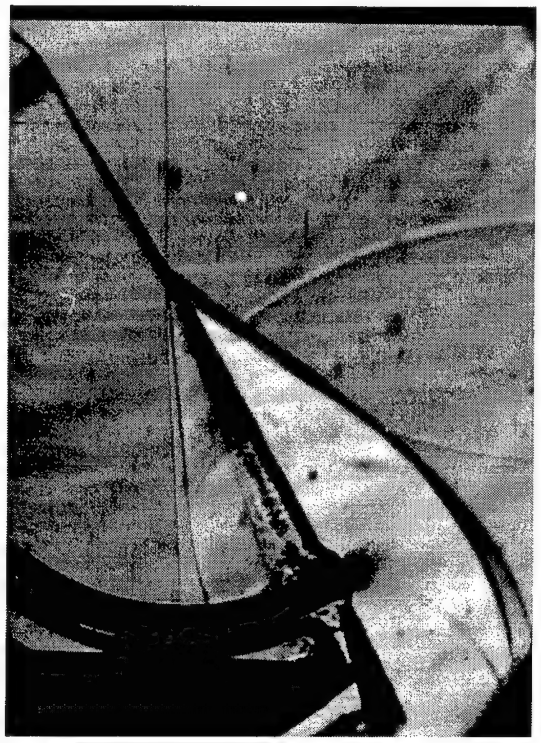

Figure A 14 Polycotton, No backing plate, M =1.422, $\theta_w$=60°, T=1620μs

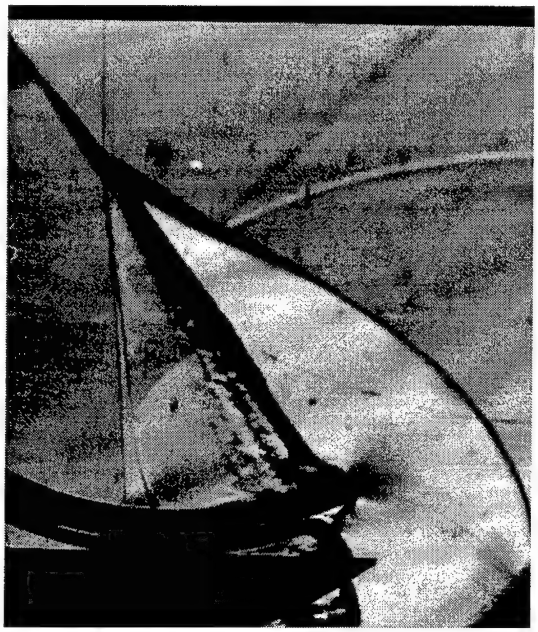

Figure A 15 Polycotton, No backing plate, M =1.413, $\theta_w$=60°, T=1650μs

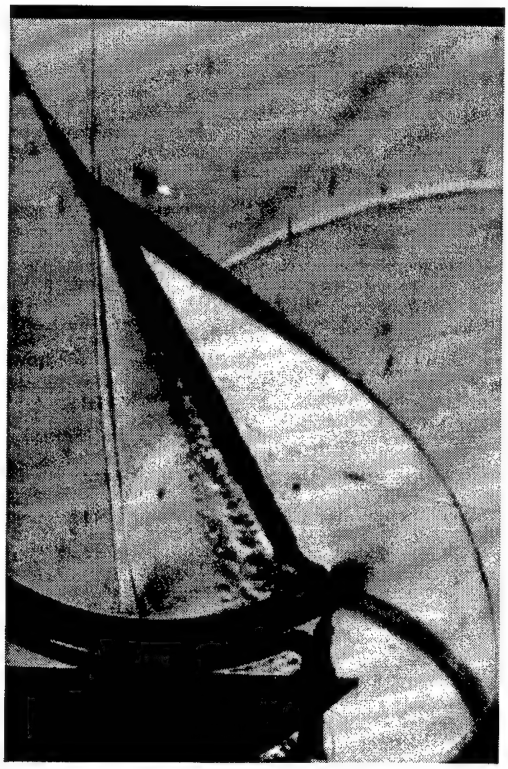

Figure A 16 Polycotton, No backing plate, M =1.412, $\theta_w$=60°, T=1650μs

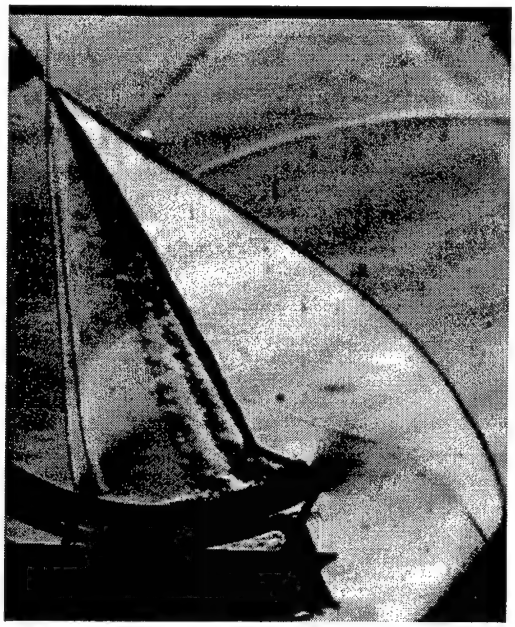

Figure A 17 Polycotton, No backing plate, M =1.415, $\theta_w$=60°, T=1675μs

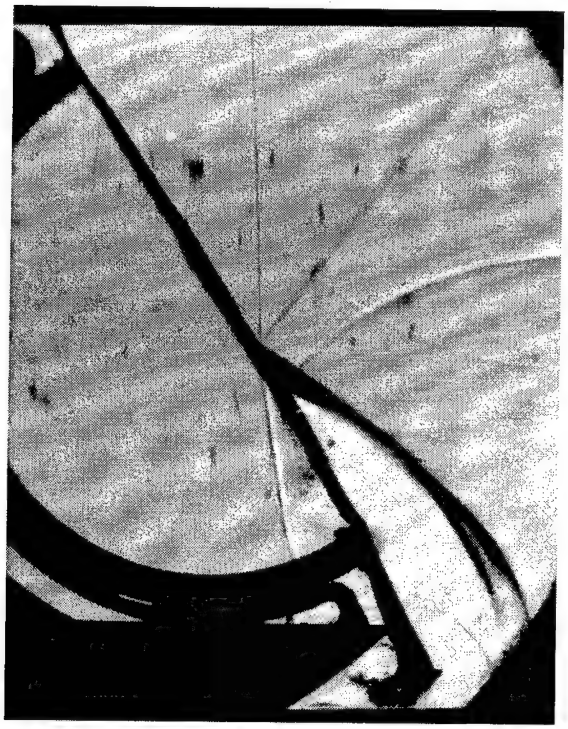

Figure A 18 Satin, No backing plate, M =1.419, $\theta_w$=60°, T=1590μs

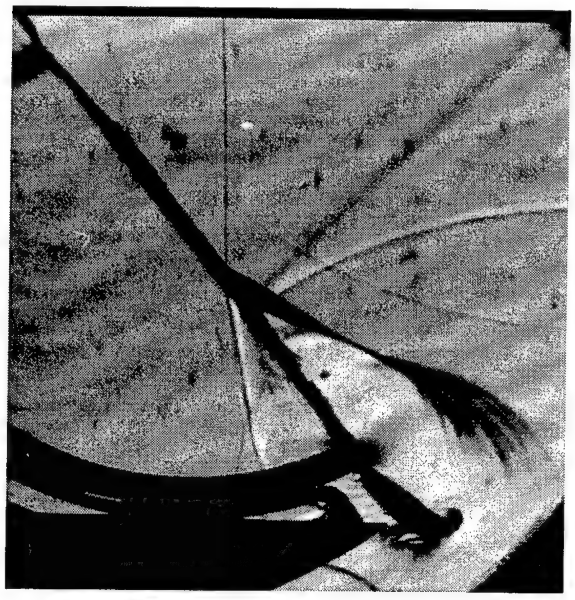

Figure A 19 Satin, No backing plate, M =1.422, $\theta_w$=60°, T=1600μs

Figure A 20 Satin, No backing plate, M =1.416, $\theta_w$=60°, T=1620μs

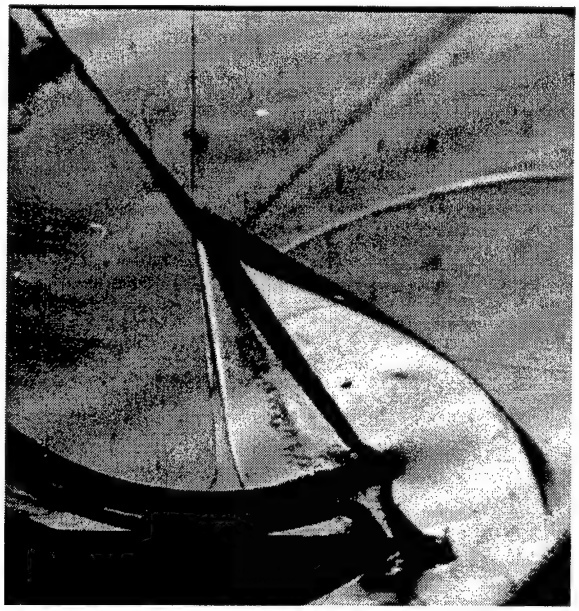

Figure A 21 Satin, No backing plate, M =1.416, $\theta_w$=60°, T=1630μs

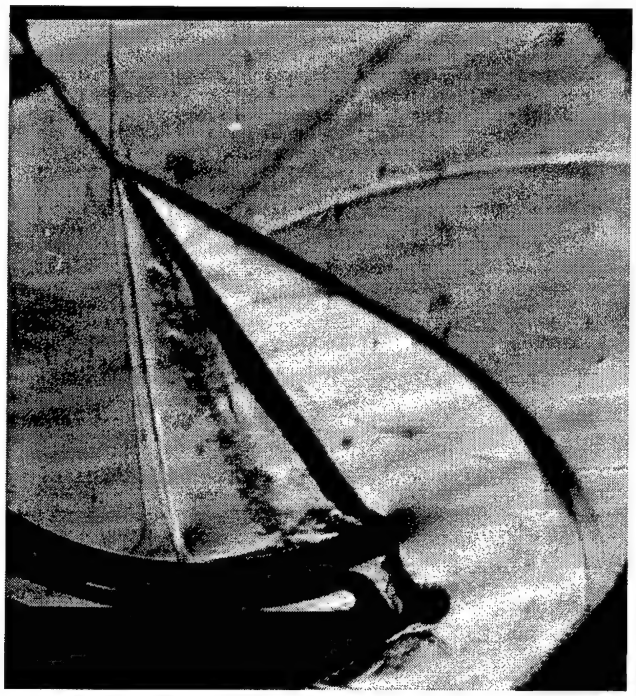

Figure A 22 Satin, No backing plate, M =1.421, $\theta_w$=60°, T=1650μs

Figure A 23 Satin, No backing plate, M =1.424, $\theta_w$=60°, T=1675μs

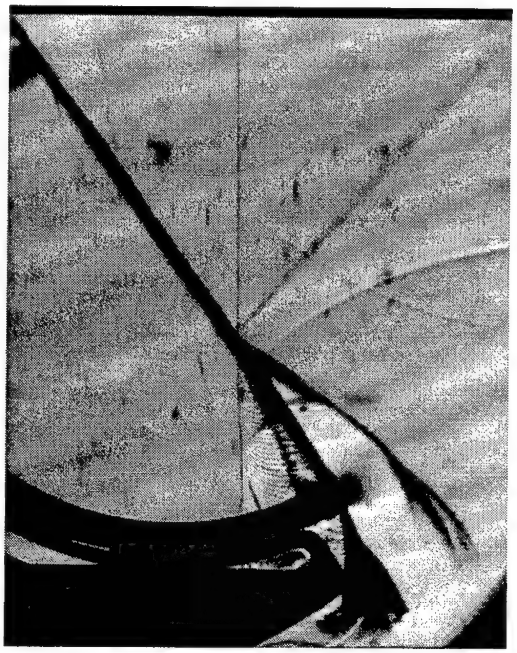

Figure A 24 Muslin, No backing plate, M =1.421, $\theta_w$=60°, T=1590μs

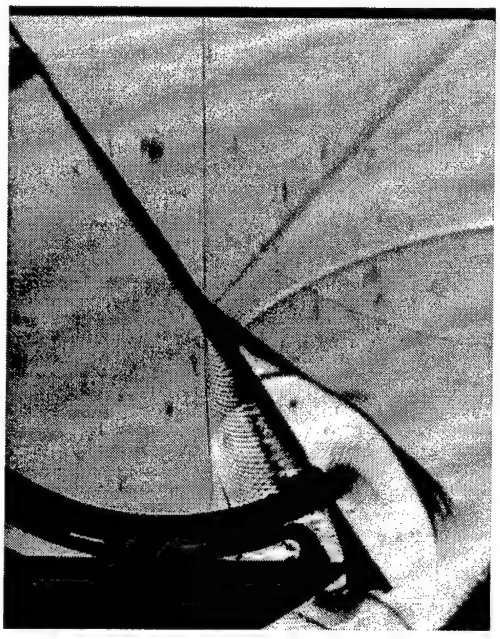

Figure A 25 Muslin, No backing plate, M =1.42, $\theta_w$=60°, T=1600μs

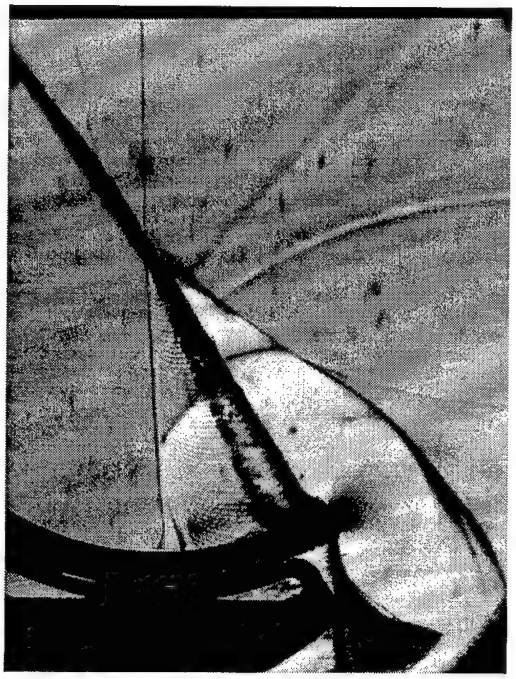

Figure A 26 Muslin, No backing plate, M =1.424, $\theta_w$=60°, T=1620μs

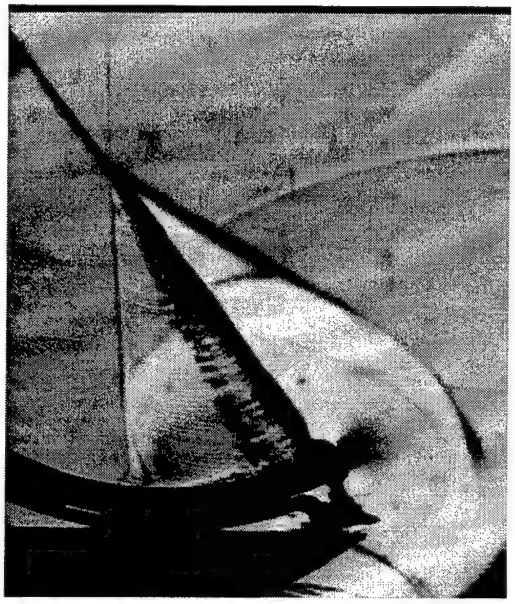

Figure A 27 Muslin, No backing plate, M =1.424, $\theta_w$=60°, T=1650μs

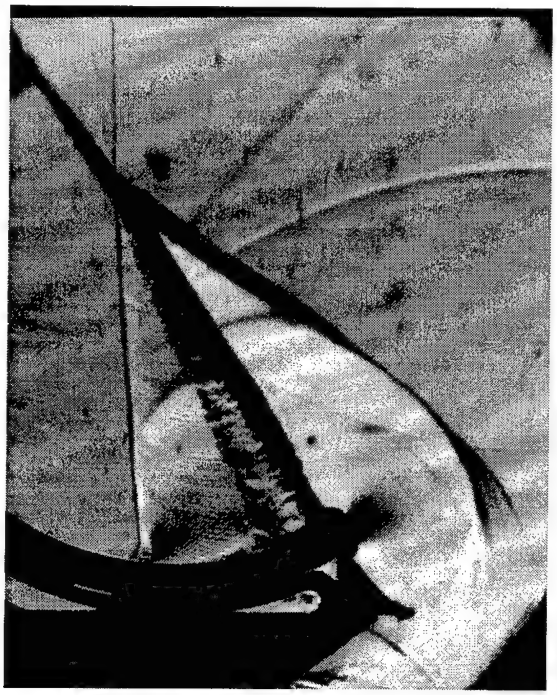

Figure A 28 Muslin, No backing plate, M =1.412, $\theta_w$=60°, T=1650μs

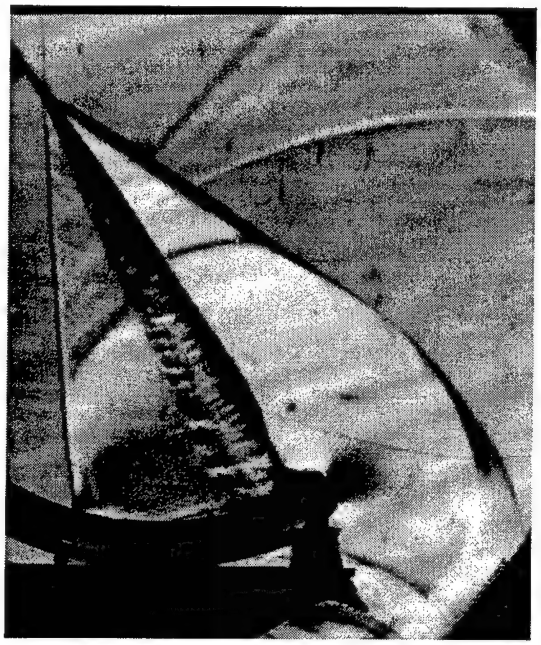

Figure A 29 Muslin, No backing plate, M =1.413, $\theta_w$=60°, T=1675μs

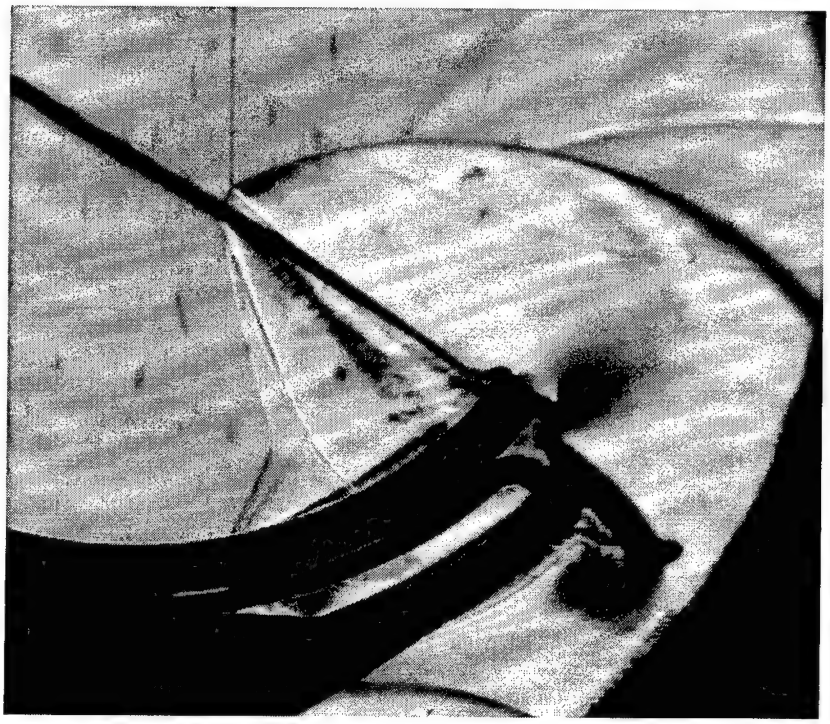

Figure A 30 Satin, No backing plate, M =1.42, $\theta_w$=35°, T=1585μs

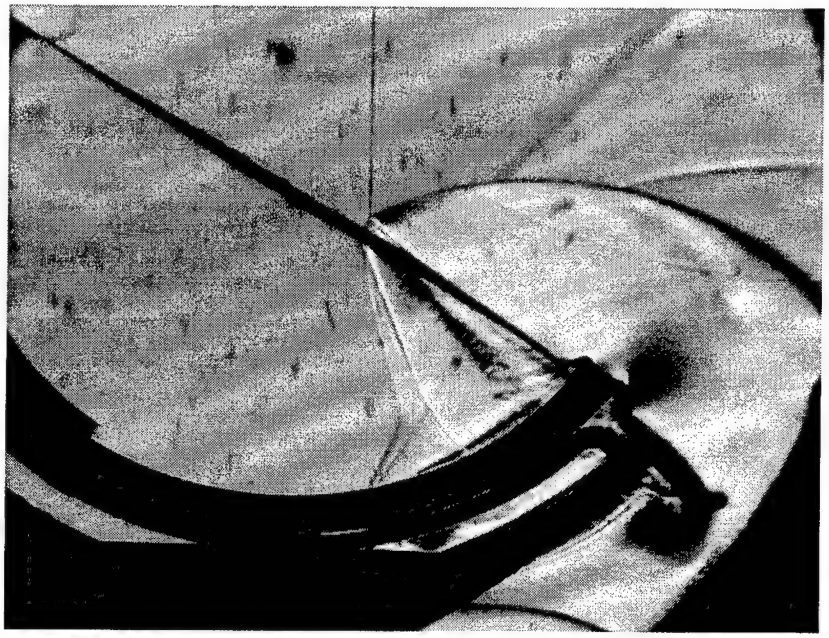

Figure A 31 Satin, No backing plate, M =1.42, $\theta_w$=35°, T=1585μs

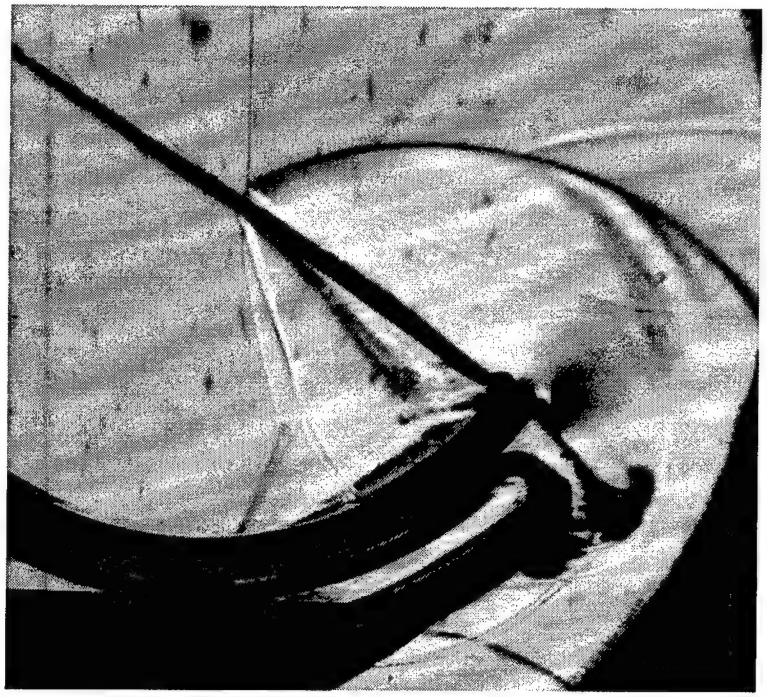

Figure A 32 Satin, No backing plate, M =1.413, $\theta_w$=35°, T=1600μs

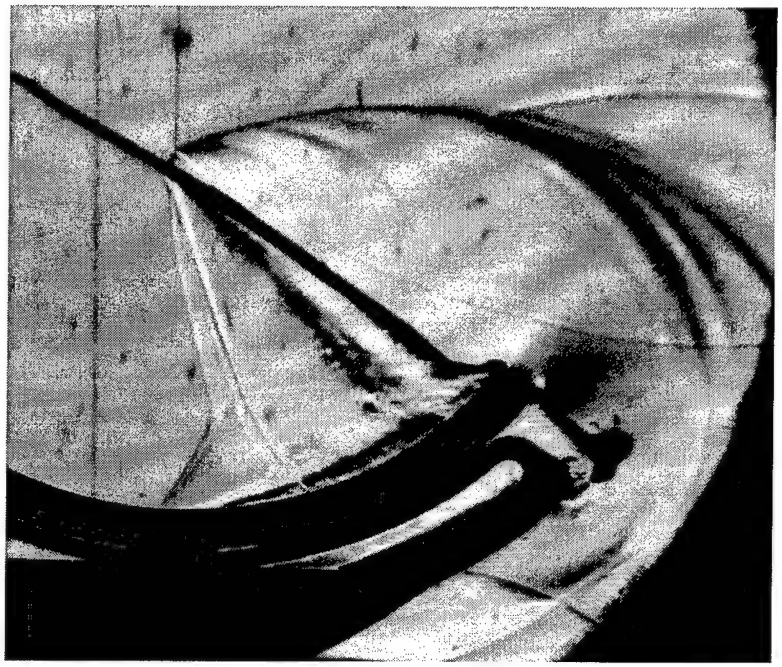

Figure A 33 Satin, No backing plate, M =1.413, $\theta_w$=35°, T=1620μs

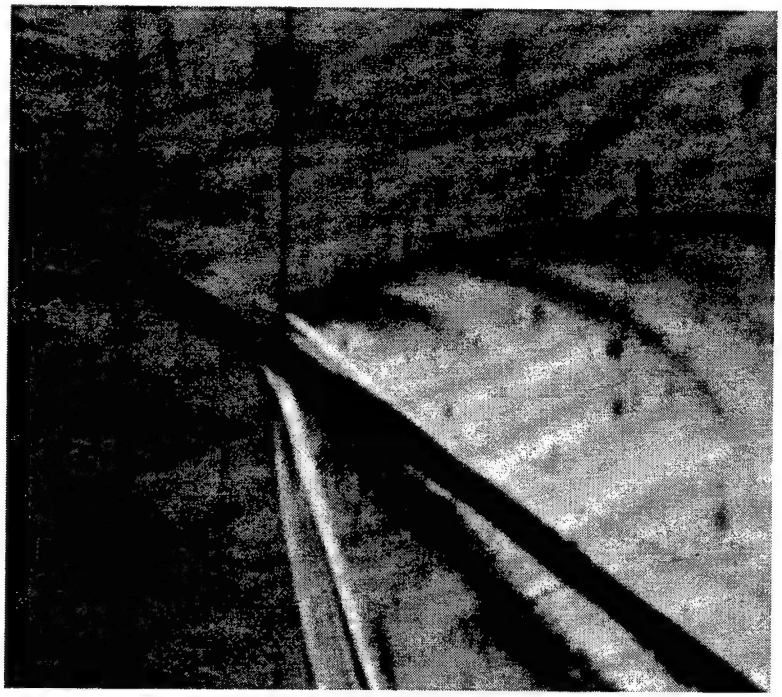

Figure A 34 Satin, No backing plate, M =1.413, $\theta_w$=35°, T=1620μs

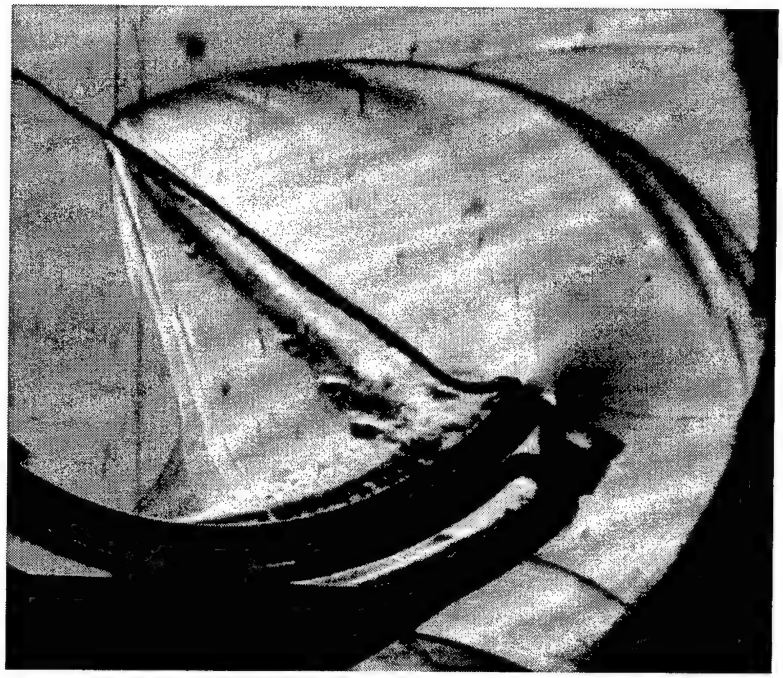

Figure A 35 Satin, No backing plate, M =1.413, $\theta_w$=35°, T=1650μs

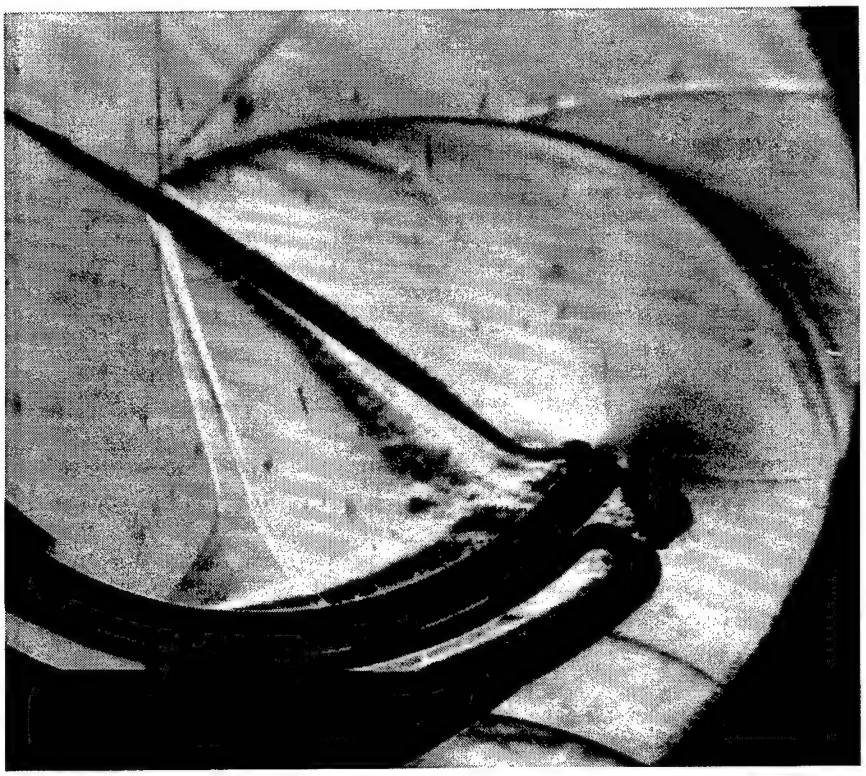

Figure A 36 Satin, No backing plate, M =1.416, $\theta_w$=35°, T=1650μs

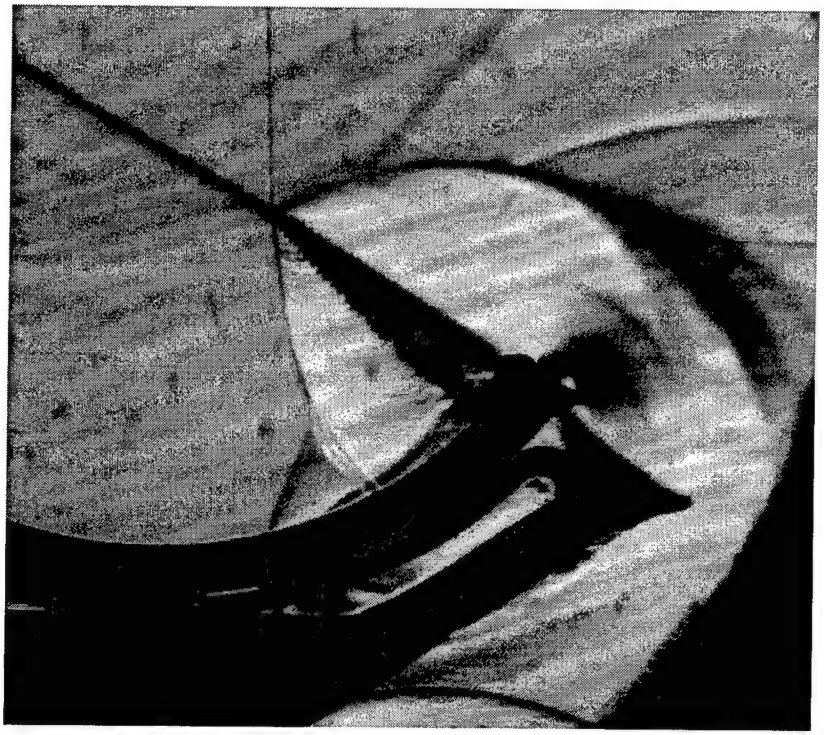

Figure A 37 Muslin, No backing plate, M =1.414, $\theta_w$=35°, T=1585μs

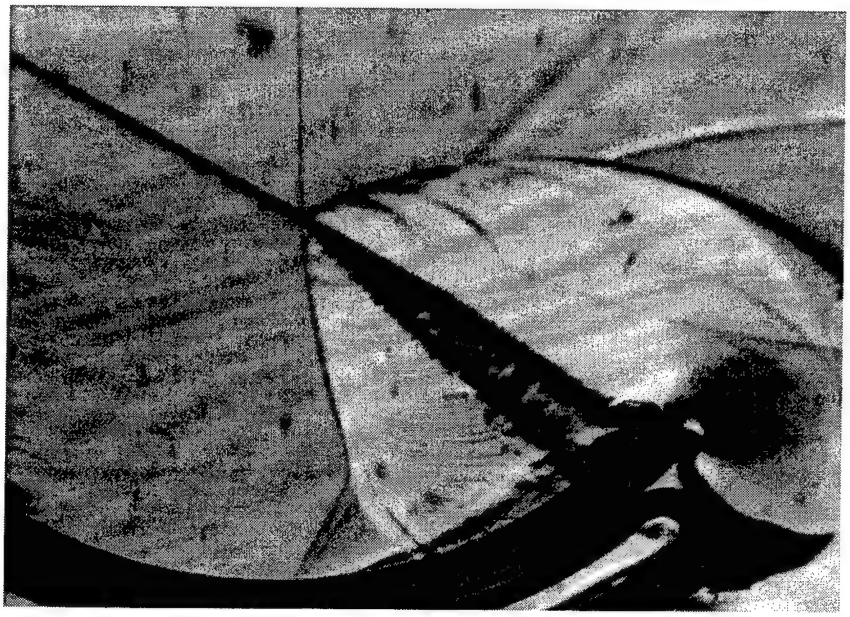

Figure A 38 Muslin, No backing plate, M =1.415, $\theta_w$=35°, T=1610μs

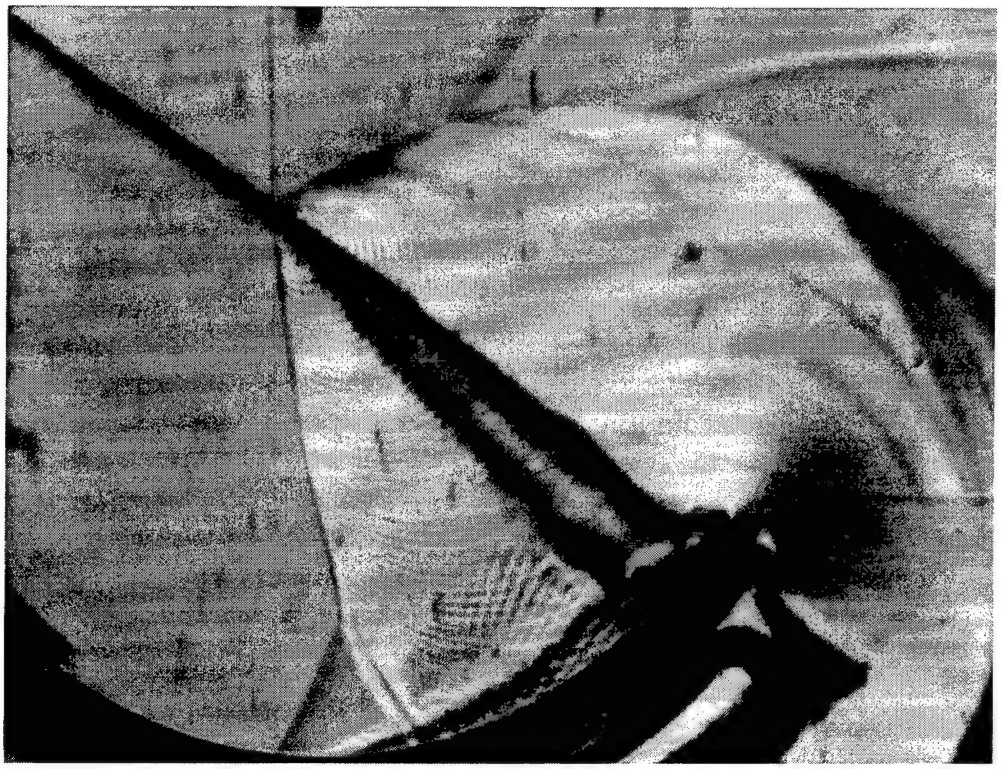

Figure A 39 Muslin, No backing plate, M =1.417, $\theta_w$=35°, T=1630μs

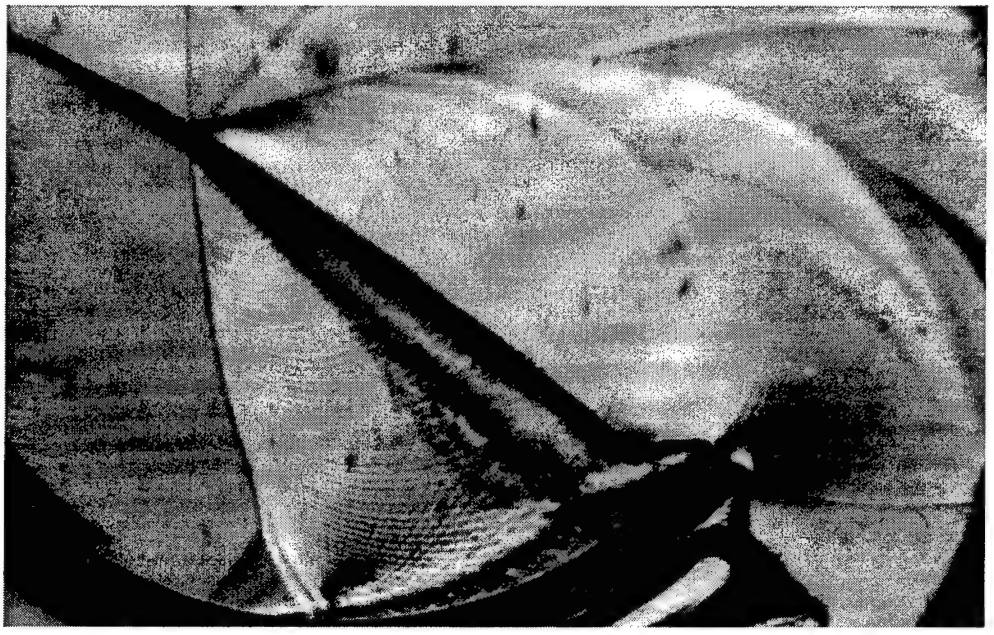

Figure A 40 Muslin, No backing plate, M =1.413, θw=35°, T=1660μs

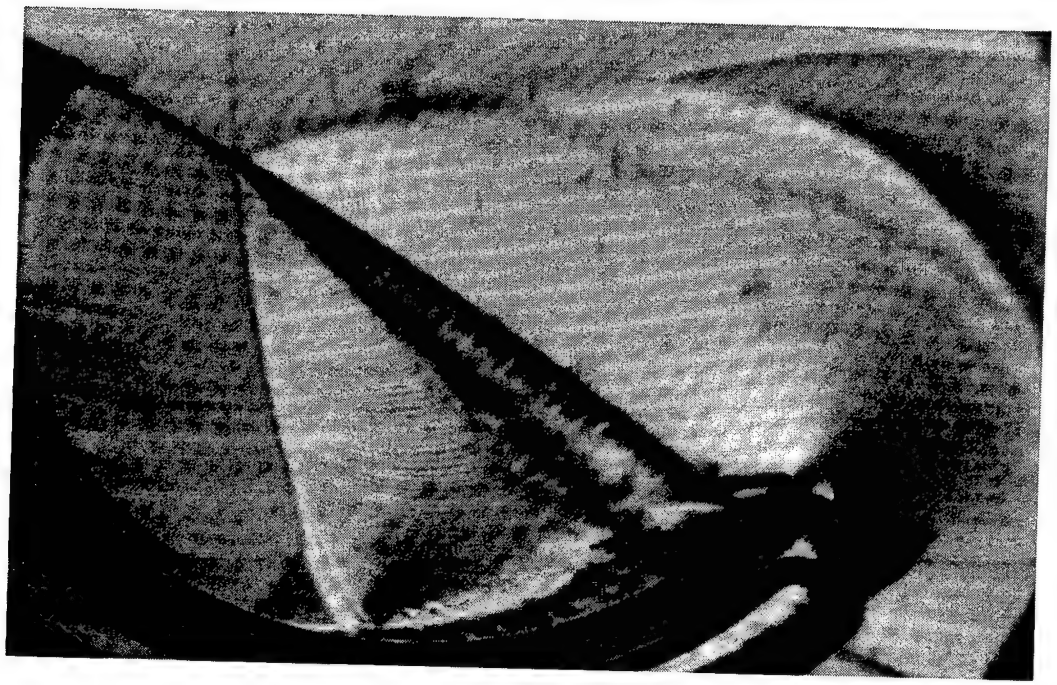

Figure A 41 Muslin, No backing plate, M =1.418, $\theta_w$=35°, T=1670μs

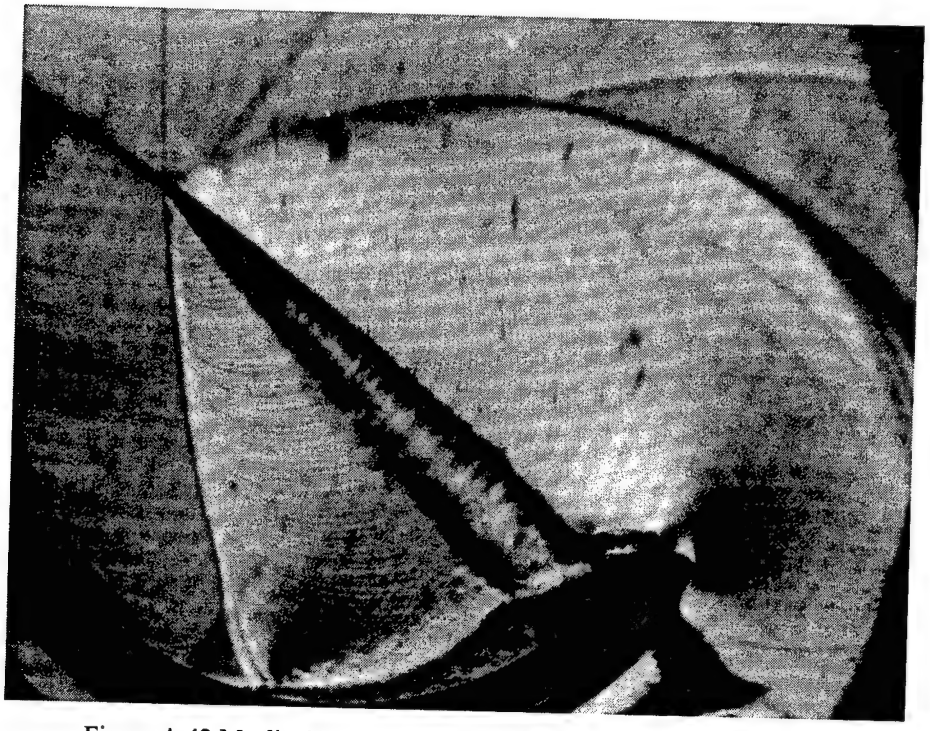

Figure A 42 Muslin, No backing plate, M =1.418, $\theta_w$=35°, T=1680μs

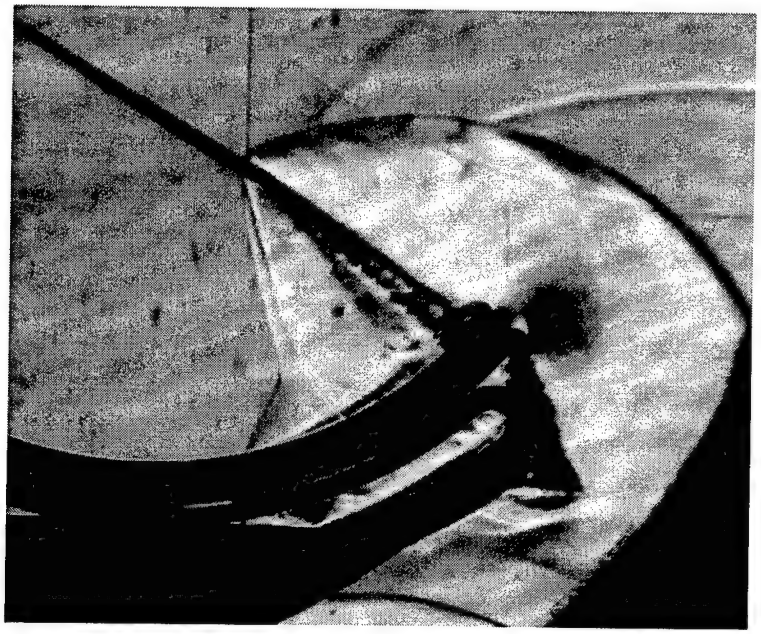

Figure A 43 Polycotton, No backing plate, M =1.417, $\theta_w$=35°, T=1585μs

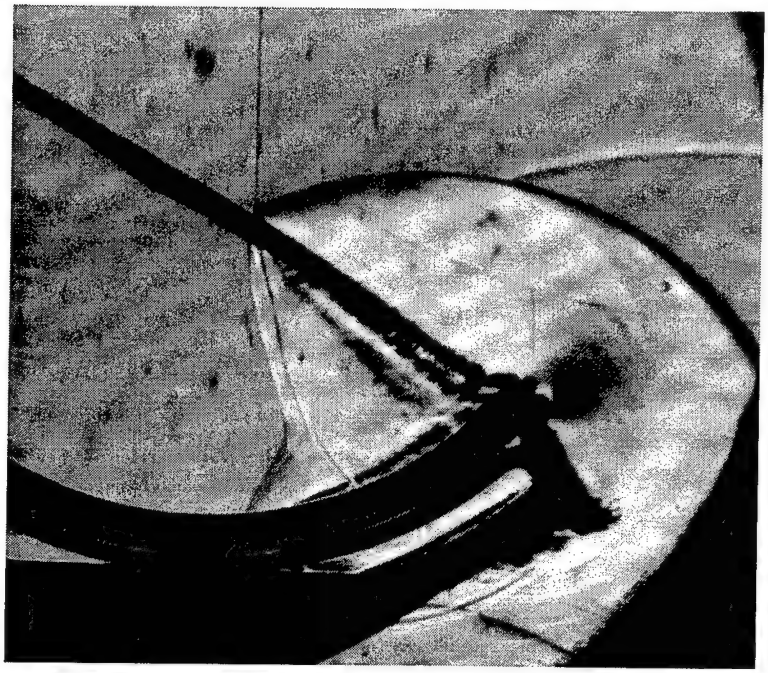

Figure A 44 Polycotton, No backing plate, M =1.414, $\theta_w$=35°, T=1600μs

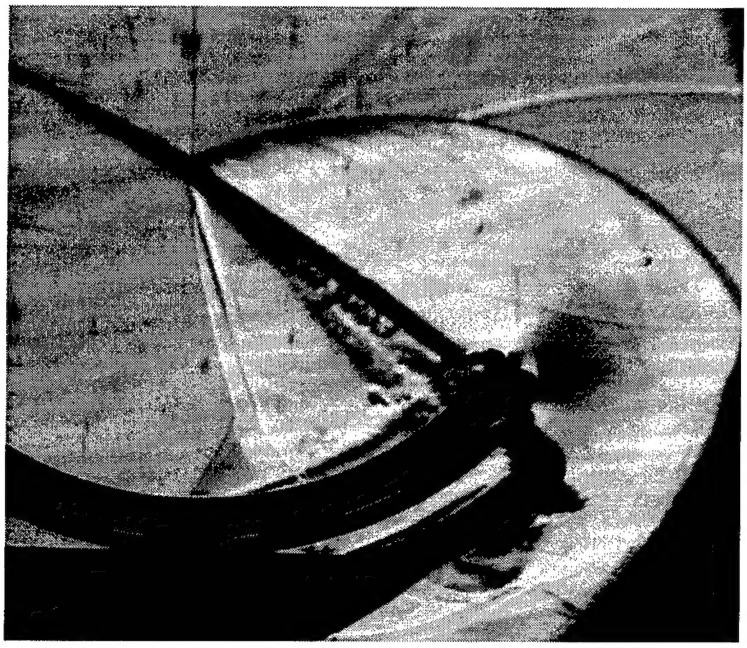

Figure A 45 Polycotton, No backing plate, M =1.414, $\theta_w$=35°, T=1620μs

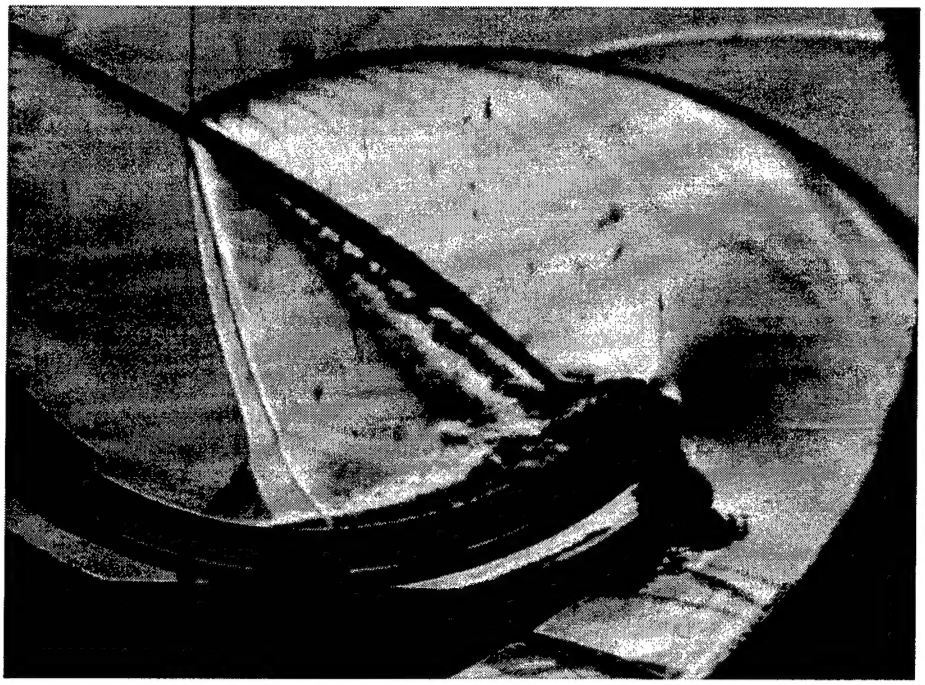

Figure A 46 Polycotton, No backing plate, M =1.418, $\theta_w$=35°, T=1650μs

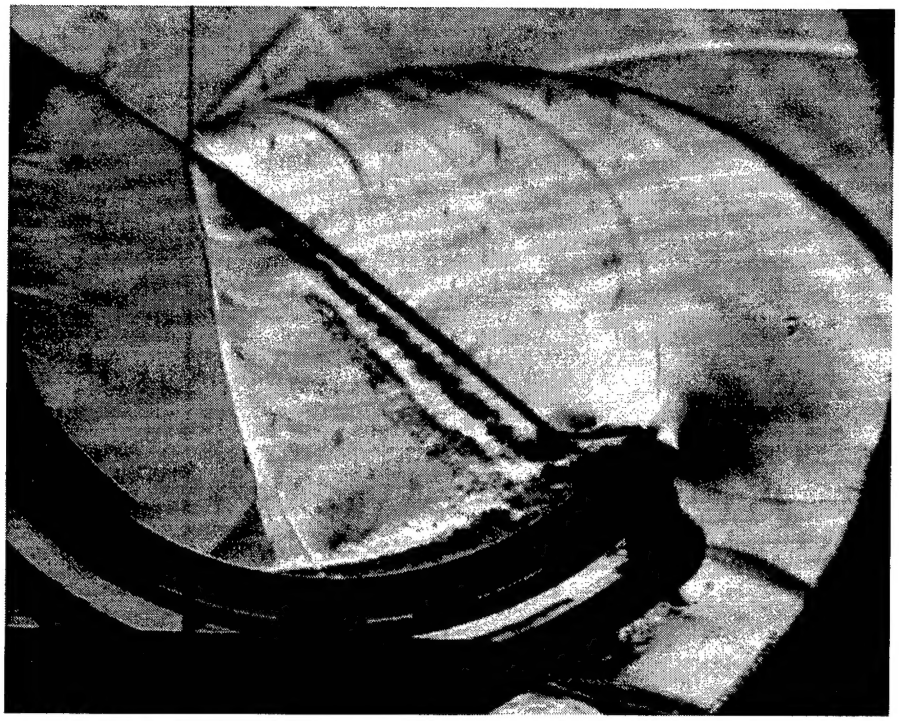

Figure A 47 Polycotton, No backing plate, M =1.409, $\theta_w$=35°, T=1670μs

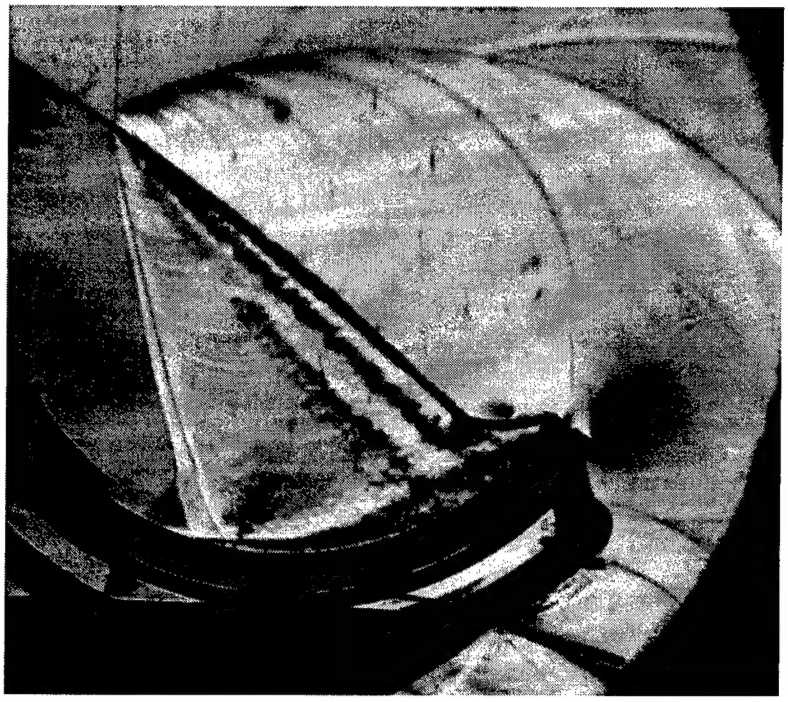

Figure A 48 Polycotton, No backing plate, M =1.421, $\theta_w$=35°, T=1680μs

# APPENDIX B

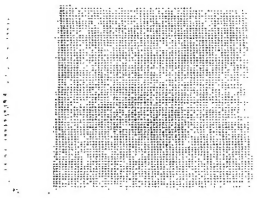

Sample 1

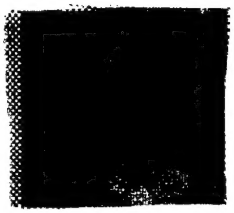

Sample 2

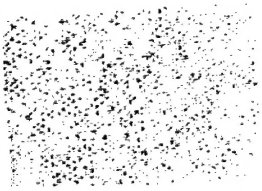

Sample 3

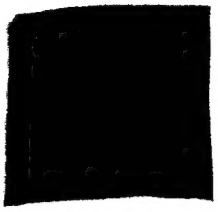

Sample 4

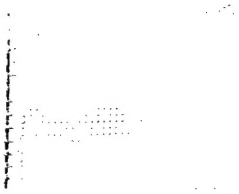

Sample 5

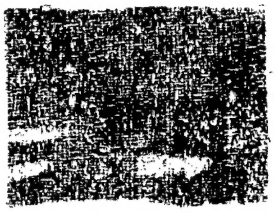

Sample 6

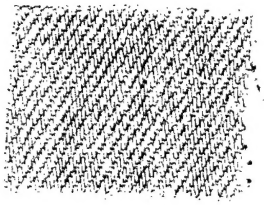

Sample 7